THE INFLUENCE OF THE EVAPOTRANSPIRATION PROCESS OF GREEN ROOF TOPS ON PV MODULES IN THE TROPICS

RELIGIANA HENDARTI

NATIONAL UNIVERSITY OF SINGAPORE

2013

THE INFLUENCE OF THE EVAPOTRANSPIRATION PROCESS OF GREEN ROOF TOPS ON PV MODULES IN THE TROPICS

RELIGIANA HENDARTI

((B.Eng), Trisakti University, Indonesia)
((M.Eng), Trisakti University, Indonesia)

**A THESIS SUBMITTED
FOR THE DEGREE OF DOCTOR OF PHYLOSOPHY**

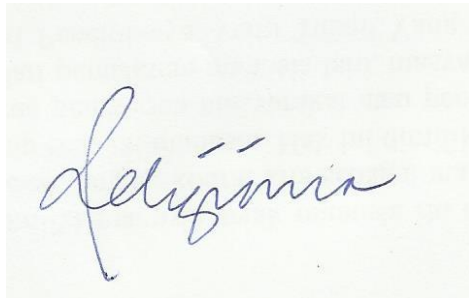**DEPARTMENT OF BUILDING
NATIONAL UNIVERSITY OF SINGAPORE**

2013

DECLARATION

I hereby declare that the thesis is my original work and it has been written by me in
its entirely.

I have duly acknowledge all the source of information which have been used I the
thesis.

This thesis has also not been submitted for any degree in any university previously

_____

Religiana Hendarti

20 August 2013

ACKNOWLEDGEMENT

cherishes me during the hard time. Finally, I dedicated this thesis to my big family (Arifin and Madjid family), especially my parents for their lasting and unconditional love.

TABLE OF CONTENTS

CHAPTER 1 INTRODUCTION

CHAPTER 2 LITERATURE REVIEW

CHAPTER 3 HYPOTHESES AND METHODOLOGY

CHAPTER 4 EVAPOTRANSPIRATION RATE PREDICTION MODEL FOR A SMALL GREEN ROOF

CHAPTER 5 MATHEMATICAL DEVELOPMENT TO PREDICT THE DYNAMIC TEMPERATURE OF PV MODULE INFLUENCED BY EVAPOTRANSPIRATION OF GREEN ROOF TOP

CHAPTER 6 EVAPOTRANSPIRATION EVALUATION

CHAPTER 7 THERMAL AND PERFORMANCE EVALUATION OF PV MODULE INTEGRATED WITH GREEN ROOF

CHAPTER 8 THE OVERAL EFFECT OF THE EVAPOTRANSPIRATION OF GREEN ROOF TOP ON PV MODULE TEMPERATURE

CHAPTER 9 SIMPLE LIFE CYCLE COST ANALYSIS OF THE PV MODULE INTEGRATED WITH GREEN ROOF IN SINGAPORE

CHAPTER 10 CONCLUDING REMARKS

SUMMARY

The performance of a solar cell is strongly influenced by its temperature. Environmental conditions, such as solar radiation and ambient temperature are the main influential factors for the solar cell temperature. Especially in tropical climates with constant high temperatures and humidity levels, result in increased solar cell temperature which in turn reduce the PV performance. A green roof was therefore proposed as the sub-layer for PV modules mounted on roof tops to improve the environmental condition by its evapotranspiration process in which a large amount of solar radiation is absorbed to convert water into vapor without generating a temperature rise. The objectives of this study were to examine the cooling effect of green roofs on PV modules and to develop a mathematical model for PV module temperature and evapotranspiration rate in an integrated PV system and green roof in the tropics.

In order to achieve the objectives of this research, the study was conducted in three steps: (1) study the energy balance mechanism in the integrated PV and green roof system with all the corresponding parameters to determine the predictive numerical model for the PV module temperature influenced by the evapotranspiration process; (2) study the measurement methods and current equation models of the evapotranspiration rate to develop the predictive numerical model for evapotranspiration rate for a small green roof, and (3) conduct field measurements to validate the proposed mathematical model. The field experiments used two PV modules mounted of different roof sub-layers: green roof and concrete roof. The PV module over the concrete roof was used as the reference for the comparative quantification of the green roof effect on the other PV module.

The results from the field measurements show that the green roof with its evapotranspiration process improves the environmental condition surrounding the PV module and hence reduces the PV module temperature. The influence of this process was significant on clear days, with an average reduction of the PV module temperature of 4 °C. On intermediate and overcast days the average module temperature reduction was 2.5 °C and 1 °C respectively. Subsequently, the calculated annual energy yield (kWh/kWp) of the PV module over green roof increases by 2% compared to that of the PV module over the concrete roof when the solar irradiance is within the range of 600 Wm^{-2} and >900 Wm^{-2}.

Numerical model to predict the evapotranspiration rate (ET rate) for a small green roof top has also been outlined using statistical methods. The results show that the ET rate calculated by the proposed numerical model could represent the ET rate measured by the Bowen Ratio Energy Balance method. They are also in accordance with other two current ET rate estimation models, the Penman Monteith and the Priestley Taylor equation. The coefficient determinant value (R^2) of the proposed model is above 0.9 with the RMSD of $5.74 \times 10^{-6} \, kgm^{-2}s^{-1}$.

In terms of the prediction model for estimating the dynamic change of the PV module temperature influenced by the evapotranspiration, the results show that the prediction model is in good agreement with the field measurement. The coefficient determinant value (R^2) is above 0.9 for clear and overcast sky conditions, and 0.8 for intermediate condition.

In conclusion, this study has confirmed that the evapotranspiration process reduces the temperature of the PV module over the green roof and subsequently improves its performance. Furthermore, the prediction model developed under the Energy Balance principle is in agreement with the experimental results. This prediction model could be used in practical applications to estimate the improvement of the electricity generation when mounted over green roofs.

List of tables

List of Figures

xiii

List of symbols

Symbol	Definition	Unit
m_{pv}	Mass of the PV module	kg
C_{pv}	Specific heat of PV module	$Jkg^{-1}K^{-1}$
A	Area of the PV module	m^2
I	Solar radiation	Wm^{-2}
T_{pv}	PV module temperature	K
T_{gr}	Green roof canopy temperature	K
T_{cr}	Concrete roof surface temperature	K
T_{apvtop}	Ambient temperature above PV module	K
$T_{apv\text{-}gr}$	Ambient temperature at 12 cm above the green roof and near the PV module	K
T_{apv_cr}	Ambient temperature at 15 cm above the concrete roof and near PV module	K
h_{cpv}	Heat convective coefficient over PV module	$Wm^{-2}K^{-1}$
h_{cgr}	Heat convective coefficient over green roof	$Wm^{-2}K^{-1}$
h_{cr}	Heat convective coefficient over concrete roof	$Wm^{-2}K^{-1}$
t	Time	
ET	Evapotranspiration rate	$kg\ m^{-2}\ s^{-1}$
P	Power output of a PV module	W
E	Irradiance	Wm^{-2}
E_{photon}	Photon energy	Joule
α	Green roof absorption coefficient (shortwave)	
ρ	Green roof reflection coefficient (shortwave)	
σ	Stefan-Boltzmann constant	$W\ m^{-2}K^{-4}$
$\varepsilon_{pvfront}$	Emissivity of the PV module.	
ε_{pvback}	Emissivity of the back surface of the PV module.	
ε_{sky}	Emissivity of the sky	
ε_{gr}	Emissivity of the green roof	
ε_{cr}	Emissivity of the concrete roof	
λ	Latent heat vaporization	$kJ\ kg^{-1}$
λET	Latent heat flux	Wm^{-2}
f	Fraction of energy released from PV module to air.	
V_w	Wind speed	(ms^{-1})
P	Air density	kgm^{-3}
c_p	Specific heat	$Jkg^{-1}K^{-1}$
$T_{in}\text{-}T_{out}$	Temperature difference between the one under the PV module and the one surrounding the PV module	K

CHAPTER 1 INTRODUCTION

1.1.   PV performance and its influencing factors

A photovoltaic (PV) module is an interconnection of solar cells (typically in series) with an encapsulation to protect the cells from environmental influences, such as humidity and dust. The solar cells are made of semiconductors and the most widely used ones today are made of silicon. Semiconductor materials have an energy gap between the so-called valence band (VB) and the conduction band (CB). If the photon energy is in the range of visible and near infra-red (IR) energy levels, the photon can excite electrons from VB into its CB, where they can freely move and generate electric power. This direct conversion of sunlight into electricity is called 'photovoltaic effect', and it was detected by Edmond Becquerel in 1839. The number of generated so-called electron-hole pairs depends on the number of incident photons either in per unit area, unit time or unit energy (Moller, 1993).

The performance of these semiconductor based solar cells under illumination, which is characterized by the open circuit voltage (V_{oc}) and the short circuit current (I_{oc}), is mostly influenced by optical losses and the cell temperature (Wysocky and Rappaport, 1960; Moller, 1993). These two factors lead to a deterioration of the solar cell efficiency.

The optical losses are caused by the light reflected from the surface or by light with too high or too little energy given the band gap of the semiconductor. This lack of optical absorption generates an electron-hole pair and results in decreasing of the short circuit current and the open-circuit voltage.

The rise of the solar cell temperature predominantly arises from absorbed infra-red light and heat from parasitic absorption process. A solar cell directly absorbs the photon which has higher energy than its energy band gap. However only a part of that incident lights is transferred into electricity. This conversion depends on the efficiency of the solar cell. Subsequently, the excess energy of that incident light is changed into heat. With increasing temperature, more energy remains in the band gap become occupied, effectively reducing the band gap and in consequence the maximum energy that can be generated from the solar cell. Even though the increase in irradiance slightly increases the generated electric current due to the increased light absorption, the open circuit voltage decreases significantly due to the exponential dependence of the saturation current on the temperature. The reduction of the open circuit voltage hence affects the overall performance of the solar cell, typically expressed by the efficiency and the maximum power point (MPP) (Singh et al, 2008; Yuki et al, 2009).

The increase of the electric current of the solar cell with higher solar radiation is shown in Fig. 1.1. As a reference point, the so-called Standard Test Conditions (STC) define irradiance (1000 Wm^{-2} in a AM 1.5 spectrum) and module temperature (25 ^{0}C) and are used for better comparison of individual products and devices. Higher temperatures, which are associated with higher irradiances in real-world applications, however, strongly reduce the voltage of the solar cell and therefore result in lower efficiencies. The temperature of the solar cell at a given irradiance is therefore the most critical loss factor in a performance assessment.
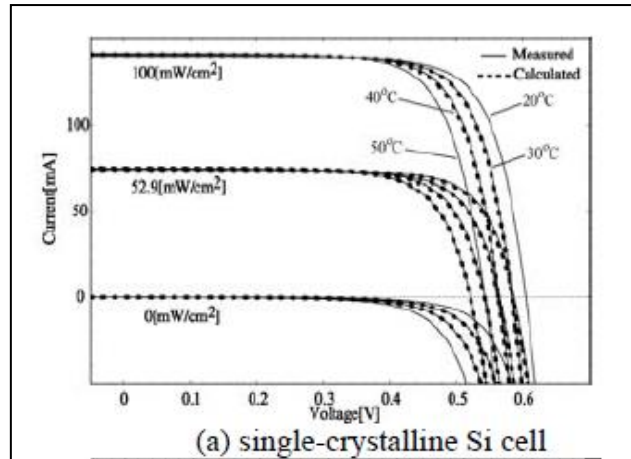
Figure 1.1. Influence of solar irradiance and cell temperature influence on the I-V characteristic of a single crystalline, wafer based solar cell
Source: Yuki et al. (2005)

The environmental conditions, particularly the ambient temperature, contribute to the rising operating temperature of the solar cell (Sabounchi, 1998; Garcia and Balenzategui, 2004; Skolapki and Palyvos, 2008). Ambient temperature, which is influenced by the surrounding environment, determines the degree of the heat intake of solar modules by convection. PV installation which is mounted on the flat concrete roof experiences a high temperature increase in mid-day. The concrete roof radiates high energy flux to the surrounding environment because of its low albedo coefficient (less than 0.1). Material with such low albedo will absorb large amounts of solar radiation and lead to a high surface temperature which then re-radiates the heat (as described in Energy balance theory) to the surrounding, including the ambient of the PV module.

There are some ways to minimize the effect of the outdoor thermal condition to the rise of PV module temperature. One of them is by combining PV systems with green roofs. Such hybrid system is designed to improve the thermal environment and in consequence, the performance of a PV module. The subsequent sections provide an overview of the approaches to reduce the PV module temperature and the use of energy balance theory to analyse the energy exchange for an integrated PV module

3

and green roof for tropical climates. A detailed discussion of previous and current research particularly on PV performance and the so-called evapotranspiration process will be given in Chapter 2.

1.2. **PV system application for minimizing its temperature increase**

Some ways to minimize the operating module temperatures are the combined Photovoltaic and thermal usage (PV/T) and the ventilated PV façade. A PV/T system is built from photovoltaic panels for the conversion of solar radiation into electricity and a solar thermal collector that absorbs excessive heat and hence effectively cools the PV modules, while generating hot water (Zondag, 2008; Hasan and Sumathy, 2010). There are four different PV/T categories (Hasan and Sumathy, 2010): Ligquid PV/T collector, Air PV/T collector, Ventilated PV with heat recovery and PV/T concentrator. This combination can reduce the PV module temperature between 3 °C and 20 °C and improve the PV module performance between 1 % and 20 % (Krauter et al.,1999; Chow, 2005; Naveed et al., 2006). According to those studies, PV/T significantly improves the PV module performance, however, these hybrid systems are a complex technology and expensive.

A ventilated PV façade is another way to reduce the PV module temperature by providing air circulation behind the PV modules to dissipate heat by convective heat transfer. According to Brinkworth (2000) this design application is effective to reduce the PV module temperature. Measurement of PV systems performance in a tropical region, Singapore, has shown that the PV module temperature and the associated losses of the PV systems can be reduced by providing a gap of around 0.5 meter between roof top and PV modules (Nobre, et al., 2012). This method is not only effective but also economical. However, it does not provide any additional impact to the surrounding thermal condition.

4

1.3. Green roofs and its cooling effect on the surrounding environment

The two previous methods are meant to reduce the PV module temperature by focusing on the PV module itself. The following method is applied in order to improve the surrounding thermal condition of PV module, and hence, indirectly reduce the PV module temperature. This approach was initially introduced by Kohler (2000). The basic principle is that green roofs can mitigate the increase of the ambient temperature because of their biological activities, especially evapotranspiration, where large amounts of solar radiation are absorbed and then used as energy to convert water into vapor (Jones, 1992; Smithsons et al., 2002), see Fig. 1.2. Furthermore, green roofs have higher albedo than asphalt concrete roof (see Table 1.1), so less solar radiation is absorbed by green roofs, resulting in a reduced surface temperature.
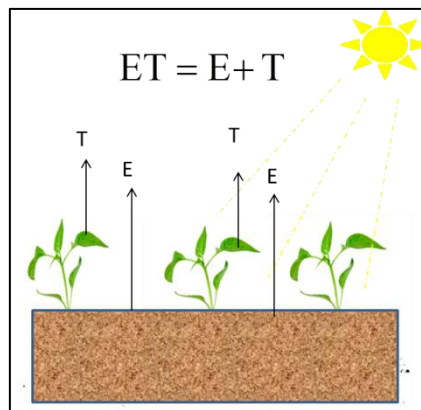
Figure 1.2 Evapotranspiration process
Source: http://wwwcimis.water.ca.gov

Several green roof measurements in Singapore conducted by Wong et al (2003a) showed that the evapotranspiration process over green roofs is effective in cooling the local environment compared to the thermal conditions over concrete roofs. The ambient temperature over green roofs can be reduced by 4 °C and the roof surface temperature can be reduced by as much as 30 °C when an extensive green roof is

5

installed. Another study conducted by Kohler (2006) proved that after a long period of investigation (1985-2005), green roofs were effective in providing a better thermal condition to the surrounding, when it was as compared to a bitumen roof. Green roofs indeed improve the thermal conditions in the surrounding of the PV modules and reduced its operating temperature. This result, however, is not easily transferable to tropical climates, which are characterized by constant high temperatures, a high fraction of diffuse light and high levels of humidity where the water vapor is nearly at the saturation level and to the best of our knowledge; no studies have been carried out in tropical regions.

Table 1.1. Albedo of different materials

Material	Albedo or reflection coefficient
Dark bitumen	0.066 (Scherba et al., 2011)
Green areas	0.25 (Jones, 1992)

1.4.   **Energy balance**

Analysis of the rooftop energy balance can be used to assess PV module temperatures influenced by the material of the roof top. The energy arriving at the surface must be equal to the energy leaving from the surface for the same period. All fluxes of energy should be considered when deriving an energy balance equation. The gradient of the PV module temperature can be assessed by utilizing the principle of heat transfer. Jones and Underwood (2001) and Amy (2009) stated that the principle of heat transfer through a PV module eventually breaks down into three heat transfer modes:

conduction, convection and radiation and another factor is the electrical power output. The evapotranspiration process of a green roof and the associated cooling effect can also be analysed through the heat transfer principle. The energy exchange governs the evapotranspiration process at the vegetation and is limited by the amount of energy available. The heat flux for the evaporative cooling is known as latent heat in which energy is transferred without the change of temperature (Smithsons et al. 2002). As a result, large amounts of solar radiation are used as latent heat without causing a rise in temperature over the green roof, effectively lowering the ambient temperature. Lower ambient temperatures in turn result in a lower convective heat flux from the green roof to the PV module, leading to a decrease in total heat storage of the PV module.

1.5. **Motivation of the study**

Singapore is an island located at the Southern tip of the Malaysian peninsula, approximately 137 km north of the equator. The typical climate is tropical with relatively high daily temperatures (around 28-32° C), strong but variable solar radiation and high relative humidity (around 85%) year round. These conditions cause PV module temperatures to rise far above the 25 °C as used in the standard test conditions. In consequence, the high operating temperatures are the single-largest loss factor for PV modules and systems (Nobre, 2012). An integrated PV system with green roof is therefore proposed here to reduce the rise of PV module temperatures by taking advantage of the evapotranspiration process of plants as the cooling mechanism. Owing to the high degree of urbanization and the scarcity of available free land in Singapore, rooftops will be the predominant installation area of the PV systems there. The main consideration for this study is hence to analyze to what extent green roofs can be beneficial to PV module installations in the tropics.

1.6.   Objectives and the scope of the study

This study addressed the effect of a green roof on PV module temperature and its performance with the following objectives:

1.   To determine the cooling effect of a green roof on PV module temperature and its impact on the module performance by conducting field measurements on two PV modules made of polycrystalline silicon wafer-based solar cell. They are installed over a green roof and a concrete roof respectively, where the one over concrete roof is the reference to evaluate the effect of the green roof.   The scope of this study is to assess the evapotranspiration rate of the green roof and its potential on the PV module temperature reduction as well as to evaluate the improvement of the PV electricity generation in tropical climates. The other biological acitvities of plants such as photosynthesis and respiration are not included in this study since these process only use a small portion of solar radiation (less than 10%).

2.   To develop a predictive model of evapotranspiration rate based on empirical data that allows for the prediction of the PV module temperature.

3.   To develop a mathematical model for the dynamic change of the PV module temperature influenced by evapotranspiration based on the energy balance principle.

1.7.   The significance of the study

The following potential contributions are expected :

1.   To reduce the rise of PV module temperatures in tropical PV systems, resulting in a higher electrical yield and hence increased utilization of scarce rooftops in an urban context.

2.   To provide a practical method of measuring the evapotranspiration rate for a small green roof top in tropical regions, particularly for Singapore condition.

3.   To provide a prediction model for determining the PV module temperature influenced by evapotranspiration in tropical regions, particularly for Singapore condition.

1.8.   **The structure of the thesis**

The structure of the thesis is as follows: Chapter one presents an overview of: (1) the factors that influence the increase of the PV module temperature, (2) several methods for mitigating the increase of PV module temperature, (3) the advantageous of green roof in mitigating the ambient temperature and (4) the energy balance theory, followed by the objectives, scope and significance of the study. Chapter two provides literature review on (1) the characteristics of PV cell and modules, particularly those cells made of silicon, (2) evapotranspiration process and (3) energy balance mechanism in the PV module systems, in the evapotranspiration process and between two gray surfaces. The hypothesis and methodology of the study are then formulated in Chapter three. The numerical model for a small green roof top and the dynamic PV module temperature influenced by evapotranspiration as well as the validation results are outlined in Chapter four and five respectively. The experimental results of the evapotranspiration rate and the effect of a green roof on the PV module temperature and its performance are presented in Chapters six and seven. The overall trend of the influence of the evapotranspiration of the green roof on PV module is summarized in Chapter eight. Additionally, the economic analysis of the life cycle cost (LCC) of the integrated PV module with green roof is presented in Chapter nine. The final Chapter presents the concluding remarks which consist of summary, the limitations of this work and recommendation for future studies.

CHAPTER 2 LITERATURE REVIEW

2.1. PV Performance Parameters

Photovoltaic (PV) is the direct conversion of sunlight into electricity, using a solar cell which is typically made from semiconductor materials such as silicon. Semiconductors become conductive when external energy (e.g. from sunlight) in case of photosensitive materials is large enough to lift electrons from the valence band (VB) to the conduction band (CB) through the so-called band gap (Fig 2.1).
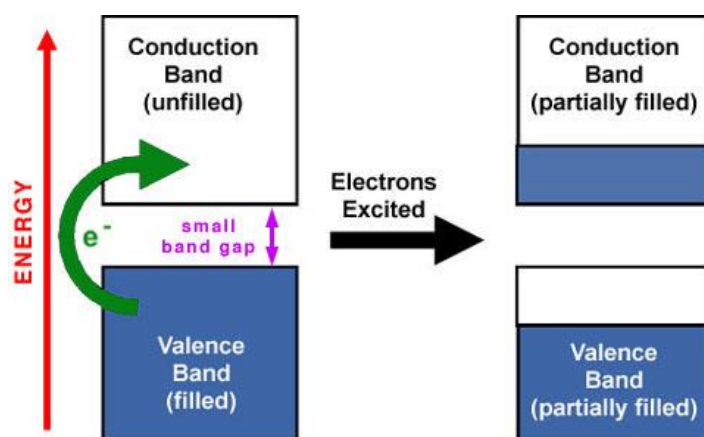
Figure 2.1. Energy from solar radiation excite electrons from VB to CB
Source http://www.chemistry.wustl.edu

The band gap determines the generated open-circuit voltage (V_{oc}), while the amount of irradiance determines the number of electrons excited into the conduction band and hence the generated short-circuit current (I_{sc}). Therefore, the current and voltage (or abbreviated as I-V) characteristics can be used to describe the performance of a solar cell. The generated power can be calculated by the following equation (Skoplaki and Palyvos, 2009):

$$P_{max} = FF \times V_{oc} \times I_{sc} \quad [W] \tag{2.1.}$$

where, P_{max} is the maximum power output defined by voltage and current. The Fill Factor or *FF* is a measure of the deviation of the real I–V characteristic from the ideal one. The same maximum power output curve can also be used to characterize PV modules (which consist of interconnected solar cells).

The open circuit voltage (V_{oc}) of PV cells and modules is significantly affected by the device (semiconductor) temperature. Heat is another form of external energy, which in case of a solar cell made from semiconductors narrows the energy gap between valence band and conduction band, effectively reducing V_{oc} and eventually P_{max}. In contrast, the short-circuit current (I_{sc}) slightly increases with the increase of PV module temperature due to higher conductivity of the semiconductor device. The effect of PV module temperature on the PV performance is illustrated in Fig. 2.2:
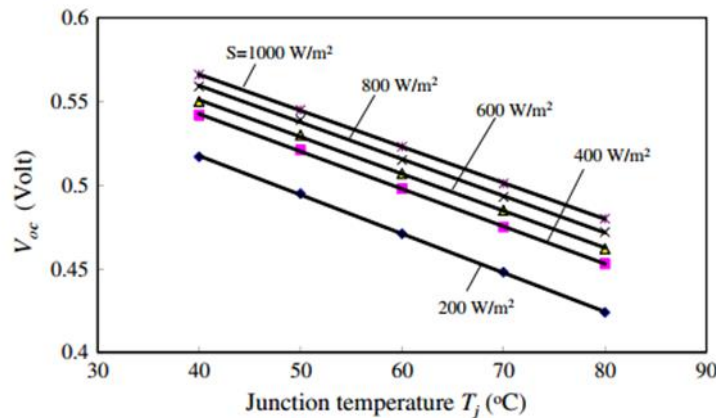
Figure 2.2 The effect of temperature increase on the open circuit voltage
Source: Huang et al., 2011

As an example, the study of Park et al (2009) revealed that the voltage reduction of the crystalline wafer-based module samples was about 0.49% per 1 °C increase of the PV module temperature while the current increase about 0.01% per 1 °C increase. These results were measured at standard test conditions (STC), and with the exception that the PV module temperature was varied from 25 °C to 65 °C in the test.

The higher PV module temperature reduced the maximum power output by 0.48% per 1 °C of module temperature rise above 25 °C as in STC. Clarke et al (1996) found that when the cell temperature increased, the electrical power output of silicon based cell linearly decreased from 32 W at 25 °C to 24 W at 80 °C, equivalent to cell efficiency drop from 15.8% at 25°C to 12% at 80°C, indicating 10.7% relative reduction in cell efficiency.

This effect is reduced for larger band gap materials, such as GaAs, where the sensitivity to increasing temperature is only about half compared to silicon (Moller, 1993). Those materials are not mass-produced as silicon and hence higher in cost.

In addition to those three parameters, the solar cell's energy conversion efficiency (η) also describes the performance of PV modules. It is the percentage of power converted from absorbed light to electrical energy. This term is calculated by using the ratio of the maximum power output, P_{max}, devided by the input light irradiance (E, in Wm^{-2}) and the surface area of the solar cell (A_c, in m^2):

$$\eta = \frac{P_{max}}{E \times A_c}$$

(2.2)

The cell efficiency (η_c) is also temperature dependent and decreases with the increasing of the cell temperature (T_c). It can be expressed in the following equation (Skoplaki and Palyvos, 2009):

$$\eta_c = \eta_{Tref}[1 - \beta_{ref}(T_c - T_{ref}) + \gamma \log_{10} G_T]$$

(2.3)

where, η_{Tref} is the module's efficiency at the reference temperature, T_{ref}, which is typically 25 ⁰C as defined in the STC. β_{ref} is the temperature coefficient and γ is a material property factor. According to Evans (1981), the latter part of the equation ($\gamma \log_{10} G_T$) is usually taken as zero. The temperature coefficient which is symbolized by β describes a rate of change with reference to temperature of different photovoltaic performance parameters. The change of rate can be determined for short-circuit current, maximum power current, open circuit voltage, maximum power voltage, maximum power, fill factor and efficiency (King et al., 1997).

Table 2.1 gives an example of the temperature coefficients of various types of solar cells. The relative temperature coefficient of crystalline silicon solar module is in the range between 0.4 and 0.6%C^{-1} according to Moshfeghe and Sandberg (1998). As for an amorphous Si, the temperature coefficient of the efficiency is typically lower at -0.1%C^{-1} as compared to -0.4% C^{-1} for c-Si and CIS (Photon international, 2004).

Table 2.1. Temperature coefficient of various PV technologies

Module type	c-Si	c-Si	c-Si	pc-Si	pc-Si	CIS	CdTe
% °C^{-1}	−0.496	−0.388	−0.427	−0.401	−0.431	−0.484	−0.035

c-Si: Crystalline Silicone; pc-Si: Polycrytalline Silicone; CIS: Copper Indium Selenida;
CdTe   : Cadmium Telluride
Source: Del Cueto (2002)

2.2. Outdoor Influence on PV module temperature

2.2.1. Solar radiation

The amount of solar radiation decrease when reaching the earth's surface due to the condition of the atmosphere, the position of the sun and local geographical features such as mountains or large water bodies (Jayarama, 2010). Solar radiation also depends on the latitude of the place, the time of day and the day of the year. At solar noon, the earth will receive maximum solar radiation as the sun is in zenith position. In the case of a location at the equator, this is referred to as air mass 1 (AM1).

The atmospheric conditions such as clouds or emerging particles like CO_2 and NO_2 will reflect, absorb and scatter the solar radiation. Sunlight that reaches the earth's surface without scattering is described as direct or beam radiation. Diffuse radiation is scattered sunlight and albedo radiation is reflected sunlight from the ground. The sum of all three components of sunlight is called global radiation.

The amount of solar radiation that arrives at a specific area of a surface during a specific time interval is called solar irradiance and it is defined in Wm^{-2}. The solar irradiance intensity affects the I-V characteristic in three ways which can be explained as follows:

- At low levels of irradiance, the short circuit current (I_{sc}) is proportional to the solar irradiance (neglecting the series resistance R_s).
- The short circuit current (I_{sc}) increases slightly with increasing irradiance.
- The optimal power of the PV module is proportional to the irradiance.

The effect of solar irradiance on the I-V curve and the maximum power output of a solar cell under various irradiances at 25° C and AM1.5 spectrum is illustrated in Fig. 2.3:
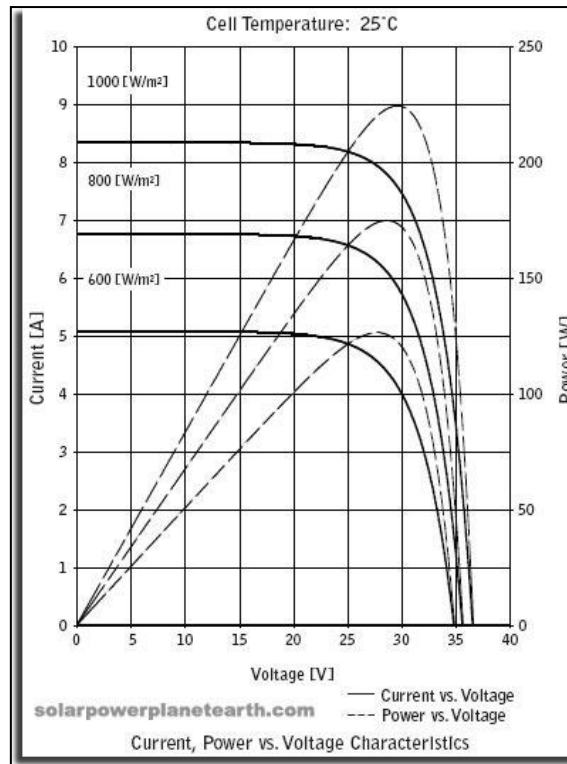
**Figure 2.3. The impact of different irradiance on current, voltage,
and PV power output at 25° C cell temperature
Source: http://solarpowerplanetearth.com**

These characteristics will be different when it is measured in outdoor condition, since

the solar radiation intensity strongly impacts the PV cell temperature condition.

Jones and Underwood (2001) stated that the response of the module temperature is

dynamic with changes in irradiance and wind. The role of solar radiation on PV

module temperature gradient is determined by its photon energy. This photon energy

is emmited by sun in the form of spectrum, namely optical frequency of light. There

are three basic levels of the optical frequency spectrum:

1. Infrared-Band of light wavelengths that are too long for response by the
   human eye.

2. Visible-Band of light wavelengths that the human eye responds to.

3. Ultraviolet-Band of light wavelengths that are too short for response by the
   human eye.

Based on the quantum theory, higher frequencies have higher photon energies. The photon energy (E_{photon}) can hence be expressed in terms of electromagnetic wavelength. It is described in the following equation:

$$E_{photon} = \frac{hc}{\lambda} \text{ [Joule]}$$

(2.4)

where, the wavelength is denoted by λ, h is the Planck's constant ($6.626068.10^{-34}$ m^2 kg s^{-1}), and c is the speed of light. This is an inverse relationship which means that light consisting of high energy photons, such as blue light, has a short wavelength. On the other hand, light consisting of low energy photons, such as red, has a long wavelength.

The photon energy must exceed the semiconductor band gap energy (E_g) to be absorbed by a PV cell for electricity generation. The band gap energy is the amount of energy, in electron volts (eV), required to stimulate an electron that is wedged in its bound state into a free state where it can participate in conduction. The energy level at where an electron can be considered free is named "conduction band" (E_c), while, the lower energy level of a semiconductor is called the "valence energy" (E_v). Thus, E_g is the required energy to excite the electron to participate in conduction (Fig. 2.4, the energy signed by the green arrow).
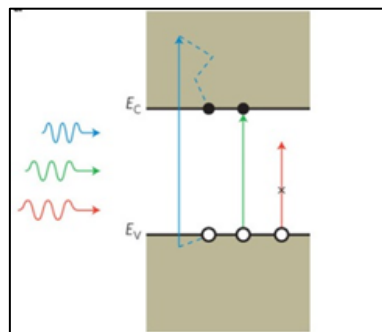
Figure 2.4 The schematic of the energy bands for electrons
Source: Chalabi and Brongersma (2013)

The band gap for solar cell made from crystalline silicon is 1.1eV. Photons with shorter wavelengths which have higher energy will be absorbed by the solar cell, however it will lost in the rapid thermalisation process (Fig. 2.4, the energy signed by the blue arrow). Meanwhile, photons with the wavelength of more than 1.2 microns do not have sufficient energy to elevate electrons from the valence band to the conduction band (Fig. 2.4, the energy signed by the red arrow).
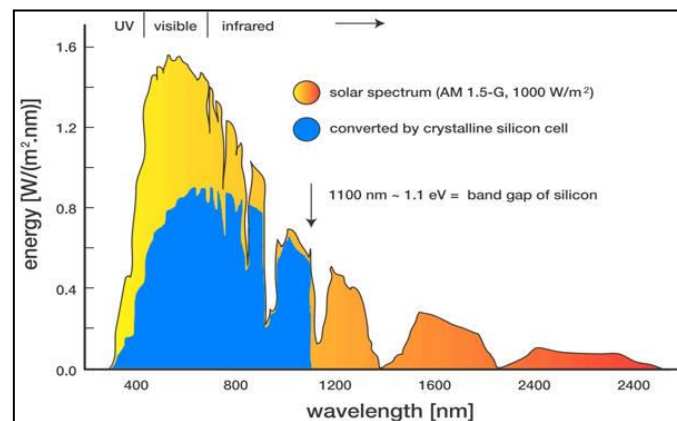
Figure 2.5. Spectrum converted by crystalline silicon cell
Source: http://www.sdstate.edu

Since the energy band gap of silicon is only 1.1 eV, and not all energy above is fully converted, can only produce a single electron-hole-pair, the remainder of the photon energy is converted or absorbed as heat. Figure 2.5 shows the spectral absorption by a crystalline silicon solar cell. It is also stated by Mavromatakis et al (2010), that one of the major factors leading to the reduction of the power produced by a PV module or array is the increase in its temperature due to excess photon energy. Therefore, only the spectral energy amount to E_g is sufficient to be converted into electricity and the rest of the spectrum contribute to produce heat.

According to a study conducted in Singapore (Reindl et al, 2012), the peak efficiency of a solar cell made from silicon is in the range of between 200 Wm-2 and 500 Wm^{-2},

far away from the STC irradiance of 1,000 Wm^{-2}, which is mostly due to the impact of the high module temperature at higher irradiance especially in a constantly hot climate.

In summary, a considerable amount of solar radiation absorbed by a PV module is not converted into electricity, but heat.   Therefore, it contributes to the rise of the PV module temperature, and subsequently affects the current, the voltage and the efficiency.   The current will increase slightly when the value of solar radiation increases.   On the other hand, the voltage decreases significantly and in consequence the cell efficiency.   This results in the deterioration of the electrical generation of the PV module performance.

2.2.2. Ambient temperature

The effect of ambient temperature on PV module temperature can be seen from the two following equation models:

(1). Equation using the NOCT (Nominal Operating Cell Temperature)

$$T_{pv} = T_{amb} + (NOCT - 20)\frac{E}{800} \; [°C] \tag{2.5}$$

where, T_{pv} is the module temperature, T_{amb} is the an environmental ambient temperature and E is the irradiance level in Wm^{-2}. Calculated NOCT is the module temperature under the following condition: Irradiance on cell surface is 800 Wm^{-2}, air

temperature is 20º C, wind velocity is 1 ms^{-1} and the mounting is with open back side (Garcia and Balenzategui, 2004).

This equation model uses NOCT values and other parameter such as the amount of irradiance and ambient temperature at other environmental conditions to predict the PV module temperature. The NOCT value is usually available in the module's data sheet.

2. Equation using the Ross coefficient (k)

$$T_{pv} = T_{amb} + kE \ [°C] \tag{2.6}$$

where, T_{pv} is the module temperature, T_{amb} is the ambient temperature, E is the irradiance level and k is the "Ross coefficient". Equation 2.6 shows that the PV module temperature is linearly proportional to the ambient temperature and the value of k.

The k coefficient defines the temperature rise above ambient with increasing irradiance and also by the influence of wind speed. However, the coefficient is less influenced by the wind direction and practically insensitive to the ambient temperature level (Griffith et al, 1981).

A study of k coefficient has also been conducted in Singapore (Ye et al, 2013). The value k is varies, based on the local condition and the distance between the PV module and the material of the PV module. Data of module temperature and ambient temperature from field measurement of 16 different PV systems were evaluated to determine the k value. The results showed that the variance of the PV module

temperatures was between 5.9 ° C and 27.9 ° C, while, the variance of the ambient temperatures was only between 0.9 °C and 3.1 °C (Fig. 2.6), which means that the ambient temperature influences the module temperature only to a smaller extent and the other factors such as the distance between the roof top and the PV module as well as the roofing material contribute significantly to the rise of the module temperature. The k value varies by a factor of 3 between the 'hottest' (fixed on metal roof) and the 'coolest' (well ventilated system) module temperature.
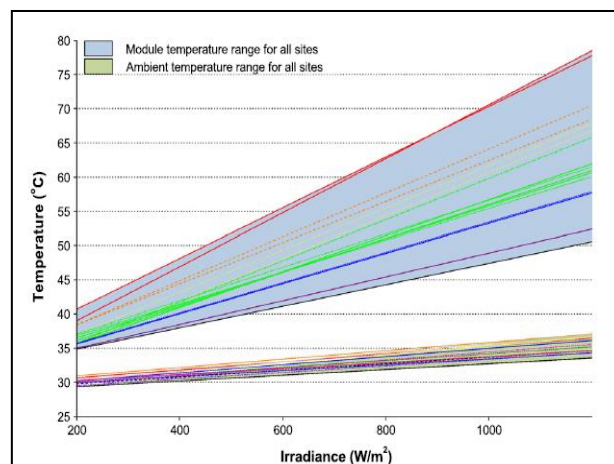
Figure 2.6 The comparison of the influence between irradiance and ambient temperature on PV module temperature.
Source: Ye et al (2013)

The effect of the ambient temperature has also been analysed in a simulation study conducted by Kim et al (2011) through a thermal analysis program. The study showed that the V_{oc} decreased by around 55 % and the I_{sc} increased by around 104 % when the ambient temperature was increased from -25 ℃ to 50 ℃. Those results lead to a significant drop in PV module performance.

2.3. Evapotransporation process and its impact to the ambient temperature

Evapotranspiration is a process in which water vapor moves into the atmosphere through plants and soil. More specifically, evapotranspiration is the loss of water

from a vegetated surface through the combined processes of water evaporation from the soil and the transpiration of the plants.
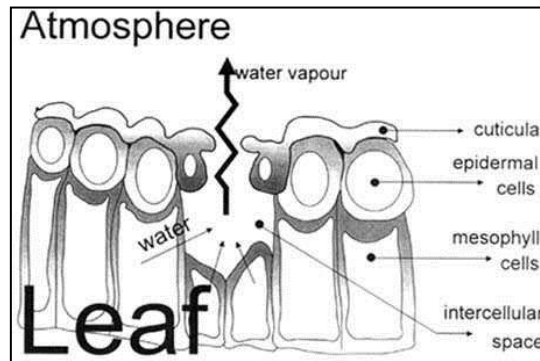
Figure 2.7. Process of transpiration through stomata
Source: Allen et al (1998)

Figure 2.7 shows the transpiration process where water from the plants' leaf is converted into vapor and then transferred to the surface by diffusion or convection. Most of the water in plants is lost by transpiration through the stomata, which are small pores in the leaf that also allow gases needed for photosynthesis such as CO_2 to enter and the release of O_2 and water vapor. Plants can control their transpiration rate by opening and closing their stomata (Allen et al, 1998).

Evaporation and transpiration occur simultaneously. Apart from the water availability in the top soil, the evaporation from a cropped soil is mainly determined by the fraction of the solar radiation reaching the soil surface. This fraction decreases over the growing period as the crop develops and the crop canopy shades more ground area. Figure 2.8 illustrates the separation of evapotranspiration rate (ET) into evaporation and transpiration which is plotted in correspondence to leaf area per unit surface of soil below it. At sowing period, nearly 100% of ET comes from evaporation, while when the crop is well develop and fully cover the soil more than 90% of ET comes from transpiration.
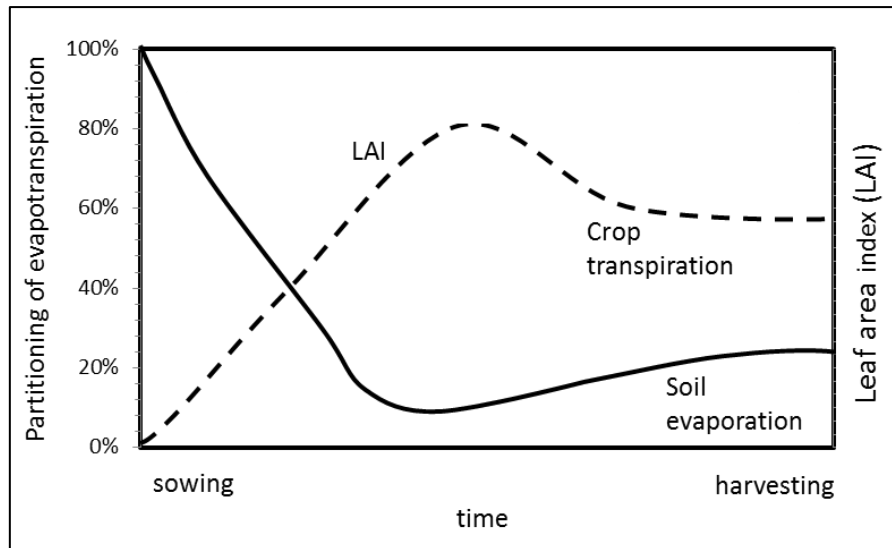
Figure 2.8. Evapotranspiration rate and plants development
Source: Allen et al (1998)

Energy is required to change the state of the molecules of water from liquid to vapor. This energy is provided by solar radiation. The cooling effect of green roof on the surrounding condition is the result of an energy balance mechanism in which the evapotranspiration process of green roof is in used. The detail description of this energy balance mechanism will be presented in sub chapter 2.4.2. It is also stated by Takebayashi and Moriyama (2007) that the sensible heat flux on a green surface becomes smaller due to the larger latent heat flux as a result of evaporation and transpiration process.

The ambient temperature, therefore, can be mitigated through these processes. According to a study on green roof top in Singapore conducted by Chen and Wong (2006), the ambient temperature could be reduced between 2 °C and 3 °C. This reduction was measured at 300 mm above the intensive green roof, and when an extensive green roof was installed, the roof top surface temperature was lower by even 30 °C. The difference between the intensive and extensive green roof are the soil depth, loading capacity and function. Extensive green roofs have thin soil depth, less

weight and are usually planted only with grass or shrubs. While, intensive green roofs have deep soil layers and are planted with a variety of vegetation, therefore, its weight is heavier and it requires high maintenance.

2.3.1. Types of evapotranspiration

Smithson et al (2002) differentiates the definition of evapotranspiration into:

1.   Potential evapotranspiration (PE)

It defines the ability of the atmosphere to remove water from the surface where water supply is assumed to be unlimited or the maximum meteorologically evaporative power on land surface (Zhou et al, 2006). Furthermore, Kirkham (2005) summarised from Rosenberg, that potential evapotranspiration is the evapotranspiration from an extended surface of (a) short green crop which fully shades the ground, (b) exerts little or negligible resistance to the flow of water, and (c) is always well supplied with water.

2.   Actual evapotranspiration (AE).

It defines the amount of water which is actually removed. Smithsons et al (2002) explained that the actual evapotranspiration process equals potential evapotranspiration process when there is a constant and sufficient amount of water to fill the demand of atmospheric condition. Thus, the limitation of water over a surface area can cause the declining rate of the actual evapotranspiration below the potential evapotranspiration. However, in a particular case such as an open water surface like the ocean, the rate of evaporation falls when the air temperature is warm relative to the sea. This condition resists moisture and subsequently causes low humidity gradient. The open water also not always evaporates since the absorbed solar radiation is expended in heating the water and is circulated through the water body. Evaporation from water body is large when the water body is warm compared to the

air. Regarding the actual evapotranspiration from a land surface, the requirement is similar with the case of open waters, i.e. the water supply of the soil should be adequate to supply enough water for the plants. The rate falls below PE when the soil experiences dry condition and causes a moisture deficit over the soil. Subsequently the plants suffer from moisture stress and nutrients deficiencies.

2.3.2. Energy and Parameters in Evapotranspiration Process

As mentioned in the previous section, the evapotranspiration process is a combined process of evaporation and transpiration by which water goes through a phase change both at plants and soil level. This process requires energy to convert water into vapor. Besides that, wind also plays an important role to mix the water molecules with the air and to transport them away from the surface. Additionally, the conditions of the surface also determine the pressure gradient between the ground and air. Dry surfaces and a lack of moisture will consequently affect the evapotranspiration rate.

According to Smithson et al (2002), there are three influencing energy sources for ET:

1. Solar radiation

Solar radiation is one component of the total radiant energy balance of vegetation and referred to as net radiation. Radiant energy is more effectively utilised for evapotranspiration when air temperature is high. The maximum evapotranspiration rate occurs under clear skies and hot days of tropical oceans, with the minimum rate happen under colder and cloudy conditions. Additionally, location, latitude, the angle of the sun as well as aerosols (e.g. haze) will determine the amount of radiant energy.

2. Wind

Wind maintains the vapor pressure gradients above the surface by removing the water molecules from the canopy. The wind has two major roles, as a heat transport medium and serves to accelerate evaporation by enhancing turbulence transfer of water vapor from moist vegetation to the dry atmosphere. Wind has more impact on evapotranspiration rate when the air temperature is low.

3.   Vapor pressure gradient.

This gradient determines the state of the surface. The dry ground surface leads to a lack of moisture above the surface and hence limits the continuity of the evapotranspiration process.

The following parameters also determine the evapotranspiration process (Allen et al., 1998):

- Humidity and air temperature

 Humidity and air temperature together determine the dryness or drying power of the atmosphere.   Air temperature impacts on the relative effectiveness of the radiant energy and wind in evaporating water.

- Crop characteristic.

Evapotranspiration levels will be different, depending on the crop characteristics such as its type, variety, resistance to transpiration, height, roughness and rooting even when other conditions are maintained identical.

- Management and environmental aspects

Evapotranspiration process and crop development may decrease when the soil management and land fertility are poor. Other factors to be considered when assessing evapotranspiration rate (*ET*) are ground cover, plant density and the soil water content. The effect of soil water content on *ET* is conditioned primarily by the

magnitude of the water deficit and the type of soil. Nevertheless, excessive water will result in water logging which might damage the root and limit root water uptake by inhibiting respiration.

Besides the energy source, Jones (1992) stated resistance and conductance also determine the rate of evapotranspiration. The concept of resistance and conductance to evapotranspiration are summarized as follows:

- The basic principle of evapotranspiration is equal to the total conductance between the evaporating sites and the bulk air and the difference of water vapor deficit between the pathway of the canopy and the bulk air. Therefore, the transpiration is less when the canopy conductance value low. Furthermore, the canopy conductance affects the vapor pressure term where it is different for each type of greenery, such as the conductance is more sensitive to forest compared to short grass. The *ET* for forest is more sensitive to the vapor pressure difference, while short grass is more sensitive to the value of the net radiant. The value of the leaf conductance itself is strongly influenced by the growth conditions and the age of the leaf.

- In terms of resistance, the soil resistance increase when its condition is lack of water. The soil evaporation depends on the wetness of the soil and plant cover. However, the soil water condition affects the physiological stress of the plants and resulted in the *ET* reduction because of the stomatal closure.

In relation to the stomata closure, the stomatal aperture is affected by the environment, such as light, water status, humidity, temperature and carbons dioxide and other pollutant gasses. The central role of the stomata is important in the process of regulating water vapor and CO_2 exchange. In terms of photosynthesis, there is a

pigment near the stomata (located on the grana and stroma lamella membranes of the chloroplasts) that absorb the incoming solar radiation. The stomata particularly for CAM plants works inversely compared to C_3 and C_4 plants. The stomata of CAM plants open during the night and close during the day. Therefore, CAM has an advantageous for water conservation.

2.3.3. The measurement and estimation of evapotranspiration rate

There are three approaches for evapotranspiration rate (ET) measurements:

1. Hydrology approaches

    *   Soil water balance

        Soil water balance is an indirect method. ET is obtained as a residual term in the water balance equation. This equation is based on the principle of conservation of mass in one dimension applied to the soil. The average rate of ET is determined in the water balance method by noting the change in soil water content over time. ET is calculated from the change in total soil water between sampling dates plus rainfall minus any upward movement of water from a lower water zone into the zone sampled. This calculation can be explained by the following equation (Rana and Katerji, 2000):

$$P + I + W - ET - R - D = \pm[\Delta S]_0^r \, [\text{kgm}^{-2}\text{s}^{-1}] \tag{2.8}$$

        where, P is precipitation, I is irrigation, W is contribution from water table upward, R is surface runoff, D is drainage and ΔS is the change in soil moisture content. The precipitation and the irrigation as well as the surface run off can easily be measured, but for the drainage and the soil moisture

27

content is difficult, therefore this method can be used only on a large scale, long-term basis where it can be assumed that drainage to bedrock is balanced by release from spring seepage and where the change in soil moisture content can be neglected (Smithson et al., 2002).

- Weighing lysimeters

A weighing lysimeter is a direct measurement. In principle, it is a device, a tank or a container, to define the water movement across a boundary. It can directly determine *ET* by the mass balance of the water, in contrast to a non-weighing lysimeter, which indirectly determines *ET* by volume balance (Howell et al., 1991). Lysimeters can be grouped into three categories (Allen et al, 2011): (1) non-weighing, constant water-table types that provide reliable data for weekly or longer time periods in areas where a high water table normally exists and where the water table level is maintained essentially at the same level inside and outside the lysimeter; (2) non-weighing, percolation types, where changes in water stored in the soil are determined by sampling or by precision measurement of inputs, and the rainfall and percolate are measured; (3) weighing types, in which changes in soil water are determined either by weighing the entire unit with a mechanical scale, counter-balance scale and load cell, directly suspended by load cell, or by supporting the lysimeter hydraulically.

The last type, if well managed, will provide the most accurate data for short time periods and the *ET* rate can be determined accurately over periods as short as 30 minutes. However, the data from lysimeter may only represent the ET of just one point in the field (Grebet and Cuenca, 1991) due to differences in vegetation density, soil and height. Especially in arid environments, the surrounding crop may also affect the measurement in the area of interest (Allen et al., 1991).

28

2. Micrometeorological approaches

This approach considers evapotranspiration as the heat usage for changing the water inside the vegetation into vapor. That heat changes is called as latent heat and is measured as energy flux density (Wm^{-2}). There are three approaches to calculate the latent heat flux (Rana and Katerji, 2000):

- The Bowen ratio and energy balance (BREB) method

  The latent heat flux is obtained from measurements of the heat budget or radiation balance of the surface covered with an active growing crop. However, the latent heat flux cannot be measured directly, but calculated by the method of Bowen ratio energy balance. Further details of this principle and equation can be found in sub chapter 2.4.2.

- Aerodynamic method

  This is a method that assumes a flux density that can be related to the gradient of the concentration in the atmospheric surface layer (ASL). The latent heat flux (λET) in the aerodynamic technique can be determined directly by means of the scaling factor q (specific air humidity) and u (friction velocity) which is explained by the following equation (Rana and Katerji, 2000):

$$\lambda ET = -\lambda \rho u \cdot q \,[\text{Wm}^{-2}] \tag{2.9}$$

  where ρ is the specific heat of air. Another approach conducted by Pieri and Fuchs (Pieri and Fuchs, 1990) to avoid the difficulties of measuring the water vapor gradients is by determining the sensible heat flux (H) by the flux-gradient relation (Eq 2.10). Then, the latent heat flux can be derived directly through the energy balance.

$$H = -\rho c_p u \cdot T \text{ [Wm}^{-2}] \tag{2.10}$$

where, c_p is the specific heat of air and T is deduced by the temperature profile. The friction of velocity is derived from the wind profile measurement. The calculation of stability function is made by iterative processes and needs at least three or four levels (Webb, 1965).

- Eddy covariance

This method measures and calculates turbulent fluxes within the atmospheric boundary layer. The fluxes measurement is to estimate heat, water, CO_2 exchange and other gases. The measurement takes instantaneous vertical airspeed, air temperature and water vapour density together with statistical covariance (correlation) calculations to yield values of fluxes, especially for sensible heat and evapotranspiration measurement (Uddin et al., 2013). To gain the required data such as temperature (T), vertical wind velocity (W), mean vapor pressure (e) and specific humidity (q) requires a high speed measurement system, usually at frequencies of 5-20 Hz, by using quick response sensors (Allen et al., 2011).

The statistical relationship for evaporation rate is as follows (Swibank, 1951):

$$ET = \rho_a \overline{W'q'} = \frac{0.622}{P} \rho_a \overline{W'e'} \text{ [kgm}^{-2}\text{s}^{-1}] \tag{2.11}$$

where, ρ_a is the density of moist air, P is the atmospheric pressure, q' is the instantaneous deviation of the specific humidity from the mean specific humidity, e' is the instantaneous deviation of the vapor pressure from the

mean vapor pressure and W' is the instantaneous deviation of the vertical wind velocity from the mean vertical wind velocity. ET is the evaporation rate with units of mass per unit surface area per time (kgm^{-2}s^{-1}).

The statistical relationship for sensible heat flux density (H) is as followed (Allen et al., 2011):

$$H = \rho_a C_p \overline{W'T'} \, [\text{Wm}^{-2}] \tag{2.12}$$

where, T' is the instantaneous deviation of air temperature from mean temperature (T). The evaporation rate can be computed as a residual from the energy balance equation.

The main difficulty for this method is to establish an equilibrium boundary layer deeper than the instrument height, therefore, an adequate distance or fetch is required (Allen et al, 2011). A minimum ratio of fetch to height of 100 are usually considered sufficient, however, extended fetches are desirable (Wieringa, 1993). The other requirements for this method are: (1) the need of fast hygrometer at typical frequencies of 10-20 Hz, (2) a number of corrections, such as air density correction, are needed and (3) good knowledge of the physics of turbulences (Rana and Katerji, 2000; Allen et al., 2011). The complexity of the equipment is illustrated in Fig. 2.9.
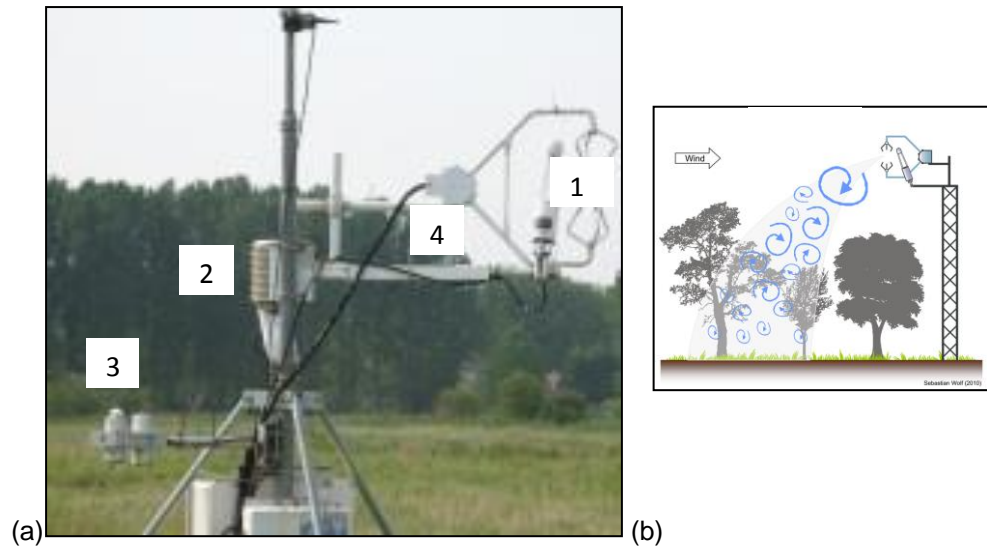
Figure 2.9 (a) The instrument of Eddy covariance which consists of (1) sonic anemometer , (2) fast hygrometer sensors, (3) net radiant sensors and (4) infrared gas analyser; (b) The concept of the Eddy covariance estimation. Source: (a) http://www.zalf.de; (b) http://homepage.usys.ethz.ch

3. Plant physiology approaches

- Sap flow method

  Sap flow is only applicable to plant transpiration as it measures the flow of water in the xylem by either the velocity of a heat pulse carried away from the heat source in the transpiration stream or by the dissipation of heat energy in the stem due to convection in the transpiration stream (Allen et al., 2011). However, this method only measures the plant transpiration component not the whole evapotranspiration component of ET since it does not measure the evaporation over a heterogeneous surface. Sap flow can be measured by two basic methods: heat pulse and heat balance (Rana and Karteji, 2002). The heat pulse velocity measurements are appropriate for measuring the transpiration in forests and orchards. The velocity of the heat pulse is due to conduction as well as convection. Cohen et al (1988) applied this method by measuring the heat velocity, stem area and xylem conductive area but this

32

method seems to be inaccurate at a low transpiration rates and requires separate calibration for every crop species.

The heat balance method measures the conductive losses upstream (q_u), downstream (q_d) and radially (q_r) away from the heat source. The heat source is gained by thermocouples referenced to the temperature at the heating wire and the differences in temperatures are used to calculate conductive heat losses, as well as convective heat losses. The transpiration is then calculated as the total heat input minus conductive heat losses. It can be expressed by the following equation (Allen at al., 2011):

$$q_f = P_w - q_u - q_d - q_r \,[\text{W}] \tag{2.13}$$

where P_w is power applied to the heater, and q_u, q_d and q_r are the conductive heat away from the heat source. All terms are in units of power (W). According to Grime et al (1995), this method can only be implemented for the branches under 50 mm diameter, since the heat source must be able to uniformly heat the entire segment of branch around which it is wrapped to produce valid results.

(a)   (b)
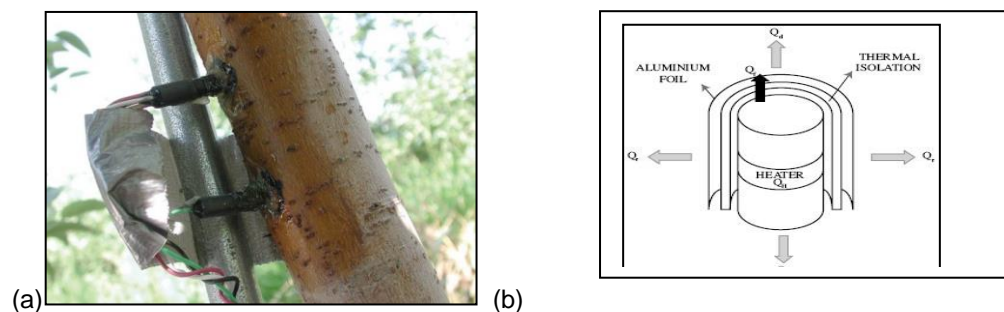
Figure 2.10 (a) The sap flow gauges; (b) Sap flow thermal balance principle
Source:(a) http://www.goodfruit.com; (b) http://www.scielo.cl

- Chamber Systems

Chamber systems were firstly described by Reicosky and Peters (1977) where latent heat flux (λET) is calculated from the slope of vapor density, change as a function of time, chamber volume, soil surface area and latent heat of vaporisation (Dugas et al., 1991). The chamber was made from a clear plastic (Lexan) and was covered by a square metal frame, but then it was modified by a clear glass to reduce the irradiance level (Reicosky, 1983). An infrared gas analyzer was operated in the differential mode with a range of $\pm$ 5 mmol mol^{-1} and calibrated for a 5 °C dew point to measure the difference of the vapor density. The air within the chamber was mixed continuously with fans which strategically located and the psychometer is also applied to measure both temperature and humidity.

Stannard (1988) has constructed a chamber for a small area with different types of vegetation which also has been studied and implemented by Mc Jannet et al (1996) and (McLeod et al., 2004). Figure 2.11 is one example of a portable chamber constructed by McLeod et al (2004) which follow from that of Stannard (1988) only the scale of the hemispherical dome was smaller, 0.67 m in diameter compared with 1.06 m originally.

(a) (b)
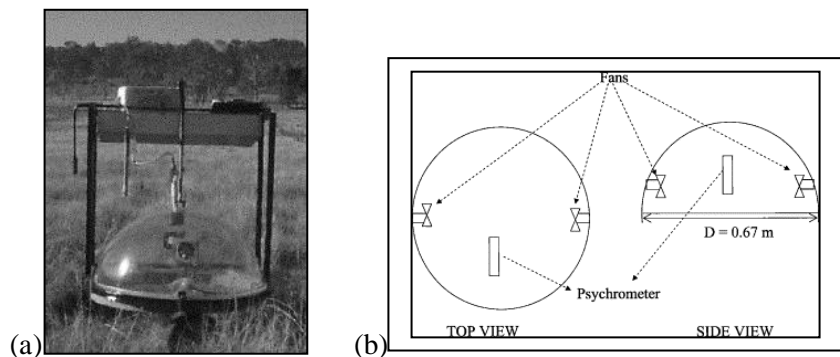
Figure 2.11. (a) The enclosed portable chamber for measuring ET;
(b) The schematic diagram of the chamber from above which was redrawn from
Stannard(1988)
Source: McLeod et al., 2004

The shortcoming of this method is the sensitivity of this chamber with the surrounding conditions, as the modification of the microclimate of the chamber needs an accurate manufacturing. The major environmental condition affecting the measurement is the wind speed inside the chamber which could be significantly reduced and the rapid increase of temperature inside the chamber which could alter the biological control of leaves transpiration process (Rana and Karteji, 2000).

The estimation models for the evapotranspiration rate (ET) based on analytical approach are as follows:

1. Penman-Monteith (PM) model

   This estimation model was developed by Penman (1948) and is described as follows:

$$ET = \frac{\{s(Rn-G) + \rho_a c_p g_H \delta_e\}}{\lambda[s + (\gamma g_H / g_W)]} \ [\text{kgm}^{-2}\text{s}^{-1}] \tag{2.14}$$

where s is the slope of the curve relating saturation vapor pressure to temperature (the values can be found in Appendix 5), R_n is the net radiant, G is the soil heat flux, ρ_a is the air density, c_p is the specific heat capacity, g_H is the heat conductance, δ_e is water vapor deficit, γ is the psychrometer constant, g_W is the water conductance and λ is the latent heat of vaporization.

This equation can also be expressed in different forms, such as by using the value of the resistance and is described as follows (Zhang et al., 2008):

$$\lambda ET = \frac{s(Rn - G) + (\rho_a c_p D / r_a)}{s + \gamma[1 + (r_c / r_a)]} \; [\text{kgm}^{-2}\text{s}^{-1}] \tag{2.15}$$

where r_a is the aerodynamic resistance and r_c is the surface canopy resistance. The surface canopy resistance depends on climatic factors and the availability of soil water. Further details are provided in Chapter 4.

2. Priestley-Taylor (PT) model

The model, which is the simplification of the Penman Monteith, is expressed as follows (Priestley and Taylor, 1972):

$$ET = \alpha_{PT} \frac{s(Rn - G)}{s + \gamma} \; [\text{kgm}^{-2}\text{s}^{-1}] \tag{2.16}$$

where, α_{PT} is termed a Priestly-Taylor coefficient with the value of 1.26, s is the slope of the curve relating saturation vapor pressure to temperature, ϕ_n is the net radiant , G is the soil heat flux and γ is the psychrometer constant.

In practice, the PT coefficient varies depending on the vegetation types, soil moisture condition and strength of advection (Nicholas et al., 2004; Flint and Childs, 1991).

Regarding to tropical climates, Gunston and Batchelor (1983) reported that both PM and PT models offer a satisfactory equation for estimating the evapotranspiration rate. The PT coefficient, 1.26, was confirmed to be suitable for this type of climate as long as the conditions remain homogeneous or free from the advection influence, relatively high humidity and low wind speed.

While Li et al (2011) reported that this model with the coefficient of 1.26 is not suitable for a desert region since the results overestimated the Eddy covariance observation by a factor of 5. For arid conditions, the modified PT model by Ding et al (2013) showed a good agreement with their observation using the Eddy covariance methodology under different mulching fractions. That modification of the coefficient was made by considering the effects of leaf area, soil moisture, ground mulch and leaf senescence on ET.

2.3.4. Evaluation of ET measurement for a small green roof in tropical region

The choice of both measurement and estimation method for potential evapotranspiration (PE) should consider the typical condition of where green roofs are located. Tropical climates are characterized by low wind speed, high temperatures and humidity level. Additionally, since the green roof does not generally fully cover the total area of the roof top, the surrounding condition may also cause an advection and hence influence the ambient condition over the green roof portion. Itier et al (1994) stated that advective flux depends on the following conditions: (1) the fetch or the distance between the rear sides of the greenery area to the measurement points; (2) the roughness length of the crop; (3) the wind speed through the friction velocity and (4) the temperature difference between the dry and irrigated fields.

Based on the statements above and in order to obtain a sufficient representativeness of PE for a small green roof, the choice of the measurement methods and estimation is based on the following conditions:

-   It is necessary to do a correction for the measurement by applying a so-called Advection Index (AI).

- The Bowen ratio (BR) measurement method may be appropriate to measure a green roof which is surrounded by concrete roof, even if it is affected by advection over the surface since it has been proven for an advective regime as reported by Rana and Karteji (2000) and the ratio of fetch-to-height can be as low as 20:1 (Heilman and Brittin, 1989). Furthermore, Yeh and Brutsaert (1971) reported that the BR method is not sensitive to imperfect fetch conditions as long as the Bowen ratio is small.

- The Priestley Taylor and the Penman Monteith equation model could be used to estimate the Potential Evapotranspiration, however it is necessary to conduct a sensitivity analysis to determine the most appropriate PT coefficient.

2.4. The mechanism of Energy Balance

2.4.1. PV module temperature

The decisive parameter for the performance of a PV module in this study is the solar cell temperature. However the solar cell is not accessible anymore after the lamination process. Further, the packaging also plays a role for heat distribution. Therefore, the PV module is considered here for the heat exchange consideration with its surrounding.

Jones and Underwood (2001) stated that PV module temperature can be estimated by considering the thermal energy exchange of a PV module with its environment through three main heat transfer paths. The heat transfers paths are in the form of conduction, convection and radiation respectively. Another factor is the electrical power output. The convection and radiation heat transfer are on the front and back

surfaces of PV module and are considered significant (Amy, 2009). Meanwhile, the conduction heat transfer from the array can be considered negligible when the contact point area is small, which is typically the case for standard rail mounting structures. Figure 2.12 illustrates the thermal energy exchange and the electrical power output of a PV module.
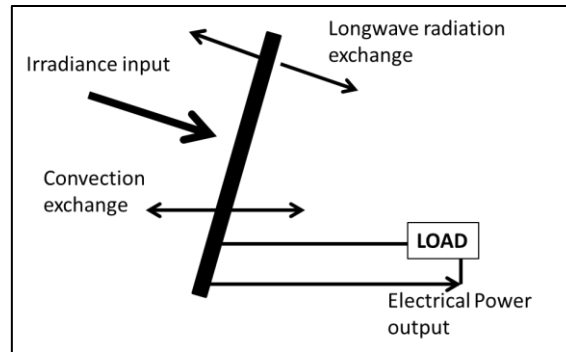
Figure 2.12. Thermal energy exchanges of a PV module, including electric power output
Source: Jones and Underwood (2001).

The rate of the PV module temperature exchange (dT) as a factor of time (dt) is expressed by the sum of the individual contributions (Jones and Underwood, 2001):

$$C_{PV}\frac{dT}{dt} = q_{lw} + q_{sw} + q_{conv} - P_{out} \text{ [W]}$$
(2.17)

Equation 2.17 is explained as follows:

1. Module heat capacity (C_{PV})

The module heat capacity is the sum of the heat capacities of the individual elements of the module.

$$C_{PV} = \sum_{m} A \times d_m \times \rho_m \times C_m \text{ [W]}$$
(2.18)

where, A is the PV module area, d_m is the thickness of the PV module, ρ_m is the density of a typical solar cell, C_m is the specific heat capacity and m denotes the type of solar cell such as multicyrstalline silicon.

2.   Short wave radiation heat transfer (q_{sw})

The effective radiation reaching the front surface of the cell is a function of the intensity of the direct and diffuse short wave radiation inputs, and the absorption coefficient of the cell face.

$$q_{sw} = \alpha \times E \times A \,[\text{W}] \tag{2.19}$$

where, α is the absorption coefficient of cell surface, E is the total irradiance intensity and A is the area of PV module.

3.   Long wave radiation heat transfer (q_{lw})

The rate of long wave electromagnetic energy radiation per unit area of a body at surface temperature (T) is given by the Stefan Boltzmann law:

$$q_{lw} = \sigma \times \varepsilon \times T_{pv}{}^4 \,[\text{W}] \tag{2.20}$$

where, σ is the Stefan Boltzmann constant (5.6703x10^{-8} Wm^{-2}K^{-4}) and ε is the emissivity of material.

4.   Convection heat transfer (q_{conv})

The total convection energy exchange from a module surface is:

$$q_{conv} = h_c \times A \times (T_{pv} - T_a) \,\text{W}] \tag{2.21}$$

where, h_c is the convective heat transfer coefficient, A is the area of PV module, T_{pv} is the surface temperature of PV module and T_a is the ambient temperature. The value

of the convective heat transfer coefficient h_c depends on the physical situation. Convection might be a combination of free and forced convection effects. On a calm day and on the sheltered rear side of the array, free convection will be the major form of cooling. Forced convection will predominate when the exposed front of the array experiences wind.

5. Electrical power generation

The power output is modeled by a fill factor model, which may be concisely written as:

$$P_{out} = C_{FF} \times \frac{E \ln(k_1 E)}{T_{pv}} \text{[Watt]} \tag{2.22}$$

where, P_{out} is the DC electrical generation, C_{FF} is the fill factor constant (1.22 K m^2), E is incident irradiance, k_1 is a constant (K/I$_0$, 106 m^{2}W^{-1}) and T_{pv} is the module temperature.

Krauter (2006) determines the module temperature by carrying out a balance of heat flow inputs and heat flow outputs. For a stationary case, heat flow input is equal to heat flow dissipation to the environment. Heat flow output is driven by convection and by thermal radiation exchange with the sky (for the front side of PV module) and with the ground (for the back side of PV module).

$$Q_{in} = Q_{nc} + Q_{rad} \text{[W]} \tag{2.23}$$

$$Q_{nc} = h_{ncf} \times A_f \times (T_f - T_a) + h_{ncb} \times A_b \times (T_b - T_a) \text{[W]} \tag{2.24}$$

$$Q_{rad} = \sigma \times \varepsilon_f \times A_f \times (T_f^4 - T_s^4) + \sigma \times \varepsilon_b \times A_b \times (T_b^4 - T_g^4) \text{[W]} \tag{2.25}$$

where,

Q_{nc} = heat flow by natural convection (W)

Q_{rad} = heat flow by thermal radiation (W)

h_{ncf} = heat transfer coefficient for natural convection at the frontside

(Wm^{-2}K^{-1})

h_{ncb} = heat transfer coefficient for natural convection at the backside

(Wm^{-2}K^{-1})

ε_f = emissivity of the front side of the module surface

ε_b = emissivity of the backside of the module surface

A_b = surface of area of the front of the module (m^2).

A_f = surface of area of the back side of the module (m^2).

T_a = ambient temperature (K)

T_f = temperature at the front side of the module (K).

T_b = temperature at the backside of the module (K).

T_s = sky temperature (K)

T_g = ground temperature (K)

In terms of PV module efficiency, Mattei et al (2006) stated that the effect of temperature on the module efficiency (η) under energy balance is given by the following equation:

$$\eta = \eta_r \times [1 - \beta \times (T_c - T_{ref}) + \gamma LogE]\ [\text{dimensionless}] \qquad (2.26)$$

where, η_r is the reference module efficiency at a PV cell temperature (T_{ref}) of 25 °C and at a solar irradiance (E) on the module equal to 1000 W/m2. γ and β are the solar irradiance and temperature coefficients for the PV module respectively. γ is assumed to be zero in most often of the equation. T_c is the PV cell temperature which

depends on the environmental conditions. Generally, the temperature coefficient (β) is given by photovoltaic manufacturer.

Another way of expressing the temperature dependence of the efficiency is the linear relationship with the temperature and with the function of temperature coefficient (β) by Sandnes and Rekstad (Mattei et al., 2006):

$$\eta = \eta_r \times [1 - \beta \times (T_c - T_{ref})] \text{ [dimensionless]} \tag{2.27}$$

In summary, heat dissipation of the heated module consists of the following components:

- Heat transfers by thermal radiation exchange with the sky and the ground.
- Heat transfer by convection. It occurs when the surface temperature of the PV module (T_{pv}) is higher than the ambient temperature.
- Heat transfer by thermal conduction towards an object with a certain heat capacity.

The total energy from radiation is partly reflected by the module encapsulation and the solar cell, and partly converted into electricity and subtracted from the system as electric power. The remaining energy balance can be described by heat flow considerations.

2.4.2. Evapotranspiration process

The energy exchange governing the evapotranspiration process at the vegetation is limited by the amount of energy available. Therefore, the principle of energy conservation can be applied to predict the evapotranspiration rate. The energy arriving at the surface must be equal to the energy leaving the surface for the same period. All fluxes of energy should be considered when deriving an energy balance equation.

Jones (1992) and Allen et al (1998) stated that all the heat transfer taking place on a green roof can be combined in the energy balance, as follows:

$$R_n = ET + Q_s + Q_c + S_t + M \ [\text{Wm}^{-2}] \tag{2.28}$$

Where, R_n is the sum of all incoming radiation fluxes minus all outgoing radiation. Incoming radiation includes all incident direct and diffuse solar radiation and that reflected from the surroundings as well as longwave radiation emitted by the sky and the surrounding. Radiation losses include the thermal radiation emitted as well as any incident radiation that is reflected or transmitted by the green roof. ET is the latent heat flux or heat converted in the evapotranspiration process. Q_s is the convective heat flux and Q_c is the conduction heat flux from green into the building roof. S_t is the thermal storage for substrate and plants. M is the metabolic storage of photosynthesis and respiration.

The heat stored or released in the plant, or the energy used in metabolic activities, can be assumed to be negligible when compared with the other four components. These terms account for a small fraction of the daily net radiation (Jones, 1992). Therefore, the equation for an evaporating surface can be written as:

$$Q = LE + H + G \ \ or \ \ R_n \ = \ \lambda ET + H + \ G \ \ [\text{Wm}^{-2}] \tag{2.29}$$

$$\lambda ET = R_n - H - G \ \ \ [\text{Wm}^{-2}] \tag{2.30}$$

where Q is the net radiation, H is the sensible heat, G is the soil heat flux and λET is the latent heat flux. The various terms can be either positive or negative. Positive R_n supplies energy to the surface, positive G supplies energy from surface to the surface underneath, and positive λET and H remove energy from the surface, as illustrated in Fig. 2.13.
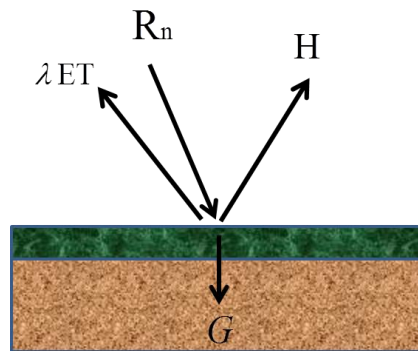
Figure 2.13. The mechanism of Energy balance at the vegetated surface
Source: Velasco and Srebric (2011)

Equation 2.28 also explains that the net flux of radiation entering the crop environment is distributed and consumed for soil heating, air heating and evaporating water. These three processes account for nearly all of the energy entering and leaving the crop environment. Other processes such as photosynthesis and respiration are assumed to be negligible. Further details on the evapotranspiration in terms of energy balance can be found in Chapter 4.

2.4.3. Energy balance between gray surfaces

Friling et al (2009) has developed a numerical model for the heat dynamics of PV module over a wooden wall with an air gap in between. The numerical model was constructed based on the following heat transfers:

- Radiant heat from the vertical solar radiation.

- Infra-red radiation from the PV module and the wooden surface to the surroundings.

- Infra-red radiation from the PV module to the wooden wall.

- Convection heat transfer from the surface of the PV module and the wooden wall to the ambient air.

- Convection heat transfer from the PV module to the air gap.

This numerical model ignores the conduction heat transfer, as the thickness of the module is small. The results showed that a high convective heat transfer resulted from a high forced velocity in the air gap lead to an increase of heat transfer from the PV module, and thus improve the production of electricity.

Duffie and Beckman (2006) summarized the basic assumptions for the infrared radiant exchange between gray surfaces having different temperatures:

1. The surface is gray where radiation properties are independent of wavelength.

2. The surface is diffuse or specular diffuse.

3. The surface temperature is uniform.

4. The incident energy over the surface is uniform.

Furthermore, they also describe radiation exchange between two surfaces in terms of solar energy application. The following equation is the equation for diffuse surfaces which have equal area and the view factors are unity:

$$\frac{Q}{A} = \frac{\sigma(T_2^4 - T_1^4)}{\frac{1}{\varepsilon_1} + \frac{1}{\varepsilon_2} - 1} [\text{Wm}^{-2}]$$
(2.31)

where, Q is the infra-red radiant heat, σ is the Stefan-Boltzmann constant, T is the temperature, A is the area and ε is the emissivity of the objects.

For two parallel plates with different area, where the other one is a large enclosure, so that the ratio between the two approaches zero, and the equation can be written as:

$$Q_1 = \varepsilon_1 A_1 \sigma(T_2^4 - T_1^4) \, [\text{Wm}^{-2}]$$
(2.32)

The equation illustrates that the large enclosure absorbs all radiation from the small object and acts like a blackbody.

A numerical model for two parallel plates is also constructed for EnergyPlus. EnergyPlus is a building simulation program, released by the U.S. Department of Energy (DOE). It has built-in features such as the building loads analysis and system thermodynamics (BLAST) and DOE-2 program. It is also designed for modeling buildings with associated heating, cooling, lighting, ventilating and other energy flows. The heat transfer for this condition is named "Exterior vented cavity". This type of model allows to calculate a special case for the outside boundary conditions of a heat transfer surface, here: that of a multi-skin exterior that is opaque. This exterior cavity acts as a radiation and convection baffle located between the exterior

47

environment and the outside face of the underlying heat transfer surface. The actual outer surface is referred to as the underlying surfaces.

The baffle is assumed to have a single temperature for both sides and along its area, and to completely cover the underlying surface. The heat balance diagram is shown in Fig 2.14 :
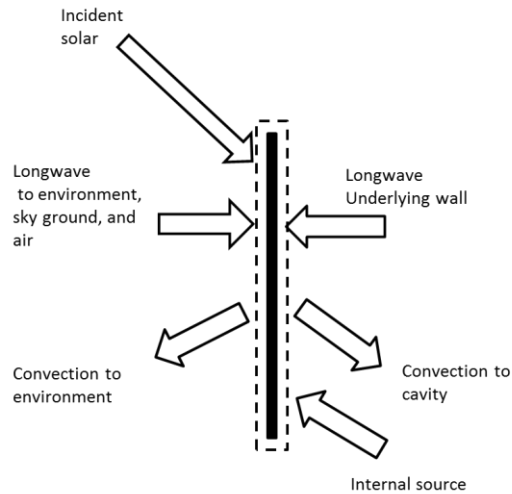
Figure 2.14 Heat balance in a baffle
Source: Engineering reference, EnergyPlus documentation

The heat balance on the baffle surface's control volume is:

$$q''_{sol} + q''_{LWR, Env} + q''_{conv, Env} + q''_{LWR, cav} + q''_{source} = 0 \,[\text{Wm}^{-2}]\qquad(2.33)$$

where,

q''_{sol} is the absorbed direct and diffuse solar (short wavelength) radiant heat flux from the front side, $q''_{LWR, Env}$ is the net long wavelength (thermal) radiation flux exchange with the air and surroundings, $q''_{conv, Env}$ is the surface convection flux exchange with the outside air. $q''_{LWR, cav}$ is the long wavelength (thermal) radiation flux exchange with the outside face of the underlying surface and q''_{source} is a

source/sink term that accounts for energy exported out of the control volume when the baffle is a hybrid device such as a photovoltaic panel. The cavity convection coefficient is obtained from correlation used for window gaps from ISO (2003) standard 15099.

The cavity heat balance is diagrammed in Fig 2.15. The cavity is the volume of air located between the baffle and the underlying heat transfer surface. The heat balance on the cavity air control volume is:

$$Q_{vent} + Q_{co} + Q_{c,baff} = 0 \,[\text{W}] \qquad\qquad (2.34)$$

where,

Q_{vent} is the net rate of energy added from natural ventilation, where the outdoor ambient air exchanges with the cavity air. Q_{co} is the net rate of energy added by surface convection heat transfer with the underlying surface. $Q_{c,baff}$ is the net rate of energy added by surface convective heat transfer with the collector.
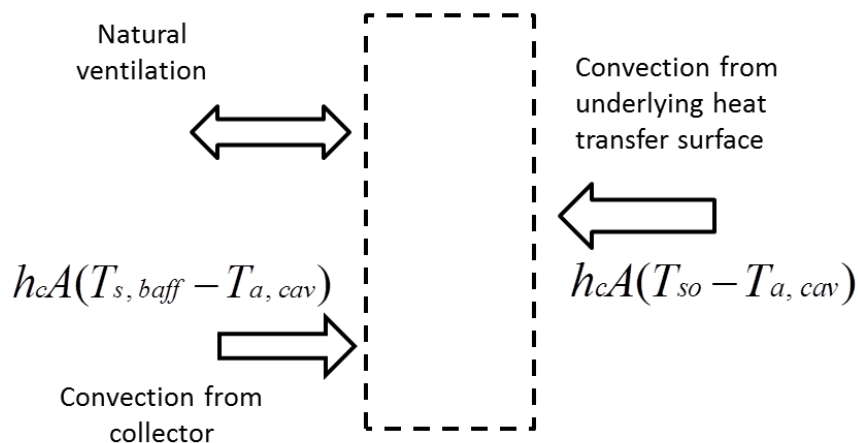
Figure 2.15 Heat balance in a cavity
Source: Engineering reference, Energyplus documentation

Based on the concept above and the use of "Integrated exterior vented cavity" as the simulation model, the temperature of the exterior cavity is used for the cell temperature and the energy exported from the baffle surface as electricity is deducted using a source term in the baffle's temperature modeling.

2.5. Researches on PV and greenery

Kohler et al (2002) reported that crystalline silicon wafer based PV modules shared higher voltage as a result of installation over a green roof (see Fig. 2.16) when compared to the conventional bituminous roofs. In consequence, the electricity generation of the PV modules on the green roofs was higher than that on conventional roofs. He also stated the positive interactions between the green roof and the photovoltaic panels such as the efficiency increase of the PV modules due to the cooling effect, but also the impact on the vegetation (of *'Sedum'* type) that showed growth improvement and the number of species increased (Table 2.2).

Figure 2.16. PV arrays on green roof in Germany
Source: Kohler (2002)

Table 2.2 Extensively greened roofs before and after installation of PV panels

	Before PV-Panel-installation (1992–1999)	Northern part of the roof without PV-panels	Southern part with PV-panels (2001)
Av. number of plant species	41	41	43
Av. cover of all higher plant species (%)	89	85	97
Max. height of plants (cm)	65	110	118
Av. height of all plant species (cm)	22	15	38
Av. cover of the genus "*Sedum*" (typical for greened roofs) (%)		48	27
No. of plant species benefited by the shade of PV-panels			7

Source: Kohler (2002)

Another research on integrated PV and green roof is being conducted in Portland State University (USA), however also in a temperate climate zone. The research there started in early 2009. The main objective of the study is to assess how combining various green technologies might boost the overall photovoltaic energy production and the green roof functionality. This research utilizes the native plants of the Pacific Northwest for the green roofs.

Figure 2.17. Integration PV and eco roof in Portland State University
Source: Solar Seed

2.6. Identification of knowledge gap

From the literature review, there are three main aspects that should be considered:

1. The performance of a solar cell (and eventually the PV module) is mainly influenced by its cell temperature. Any increase in temperature can be attributed to the fact that the PV module cannot convert all the absorbed sun light into electricity, but only the spectral energy that is equal or slightly larger than the band gap energy. Therefore, there is an excess photon energy which is transformed into heat. The rise of temperature causes variations of the open circuit voltage and to a lesser extent to the short circuit current. The voltage decreases strongly with increasing module temperature and leads to a reduction in electrical power output, in spite of a small increase in the short circuit current.

2. Green roofs have been shown to be beneficial to mitigate the ambient temperature through their biological activities, especially the evapotranspiration process. This biological activity absorbs energy from solar radiation and uses it to convert water into vapor (larger portion) and to transport the nutrient from the soil to the whole part of vegetation (smaller portion).

3. Singapore is an island located at the Southern tip of the Malaysian peninsula, approximately 137 km north of the equator. The typical climate is tropical with relatively high daily temperatures (around 28-32° C), strong but variable solar radiation and high relative humidity (around 85%) year round. These conditions cause PV module temperatures to rise far above the 25 °C as used in the standard test conditions under which the maximum power output is rated.

Based on the above facts, the research gap can be identified as follows:

- To what degree are green roofs able to provide a thermal impact on the PV module temperature and possibly increase the performance of PV modules in tropical climates, especially in Singapore?

- How to predict the evapotranspiration rate for a small green roof under tropical climates conditions?

- How to predict the reduction of the PV module temperature through the evapotranspiration process in an integrated PV and green roof environment in the tropics?

CHAPTER 3 HYPOTHESES AND METHODOLOGY

3.1.   The Development of Hypotheses

Based on the literature review, it is found that:

1) Solar cells which are made from semiconductors (here: made of crystalline silicon), have the Power out that is inversely proportional to the temperature or have a negative temperature coefficient of its power output, i.e. the power generated goes down when the temperature rises.

2) The effect is driven by the reduction of the open circuit voltage (V_{oc}) with increasing temperatures.

3) Plants absorb large amounts of solar radiation for the evapotranspiration process and convert it into latent heat without generating a temperature rise in their surroundings. As a result, the ambient temperature and the net radiation can be reduced.

4) Evapotranspiration rate is determined by the amount of net radiation, soil heat flux, ambient temperature and water vapor pressure deficit. Another parameter is the conductance of the plants. The advective heat transfer from the surrounding can also increase the evapotranspiration rate.

5) The potential evapotranspiration rate (PE) is equal to the actual evapotranspiration rate (AE) when there is constant and sufficient water over the vegetation.

6) In order to minimize the error in the evapotranspriation measurement and estimation, the sensors should be located within the homogeneous region above the green roof.

7) The heat absorbed by a PV module, which determines the PV module temperature, is influenced by the solar radiation intensity and the surrounding

conditions. Energy balance equation can be used to predict that energy absorption.

Hypothesis 1 can be summarized as follows:

The rise of the PV module temperature could be minimized through mitigating the surrounding temperature or the ambient temperature. Evapotranspiration process of plants can reduce that surrounding temperature and consequently also reduce the PV module temperature.

Hypothesis 2 can be summarized as follows:

The evapotranspiration rate could be determined by the net radiation, ambient temperature near green roof, relative humidity, soil heat flux, air temperature and wind speed. The estimation requires to consider the homogeneous region over the green roof.

Hence the variables are as follows:

- Dependent variable: evapotranspiration rate
- Independent variables: net radiation, ambient temperature near the green roof, relative humidity near the green roof, soil heat flux, air temperature and wind speed.

Hypothesis 3 can be summarized as follows:

According to the energy balance principle, all the incoming energy must be equal to all the outgoing energy. Therefore, the dynamic temperature of a PV module affected by the evapotranspiration process within certain boundary conditions is determined by the level of latent heat flux .

The variables to determine the dynamic temperature of PV modules are:

1. Solar radiation intensity

2. Net long wave exchange flux from the PV module

3. Net convective exchange flux from the PV module

4. Electricity generation of the PV module

5. Sensible heat flux from the green roof

6. Latent heat flux from the green roof

3.2.   Methodology

The general framework of this study is illustrated in Fig. 3.1. It can be seen that the final deliverables are a numerical model for predicting the PV module temperature influenced by the evapotranspiration process and a numerical model for predicting the evapotranspiration rate for a green roof. The later part of this study is to investigate the influence of the evapotranspiration process on the PV module temperature and its performance, where the analysis was generally divided into three categories based on the amount of solar radiation: clear ($> 5,000 \text{Whm}^{-2}$), intermediate ($2,500\text{-}5,000 \text{ Whm}^{-2}$) and overcast ($<2,500 \text{ Whm}^{-2}$) sky condition (Wittkopf et al, 2012). Additionally, an initial economic analysis was also conducted to investigate the impact of the integrated PV module and green roof on the life cycle cost (LCC) of the PV system.
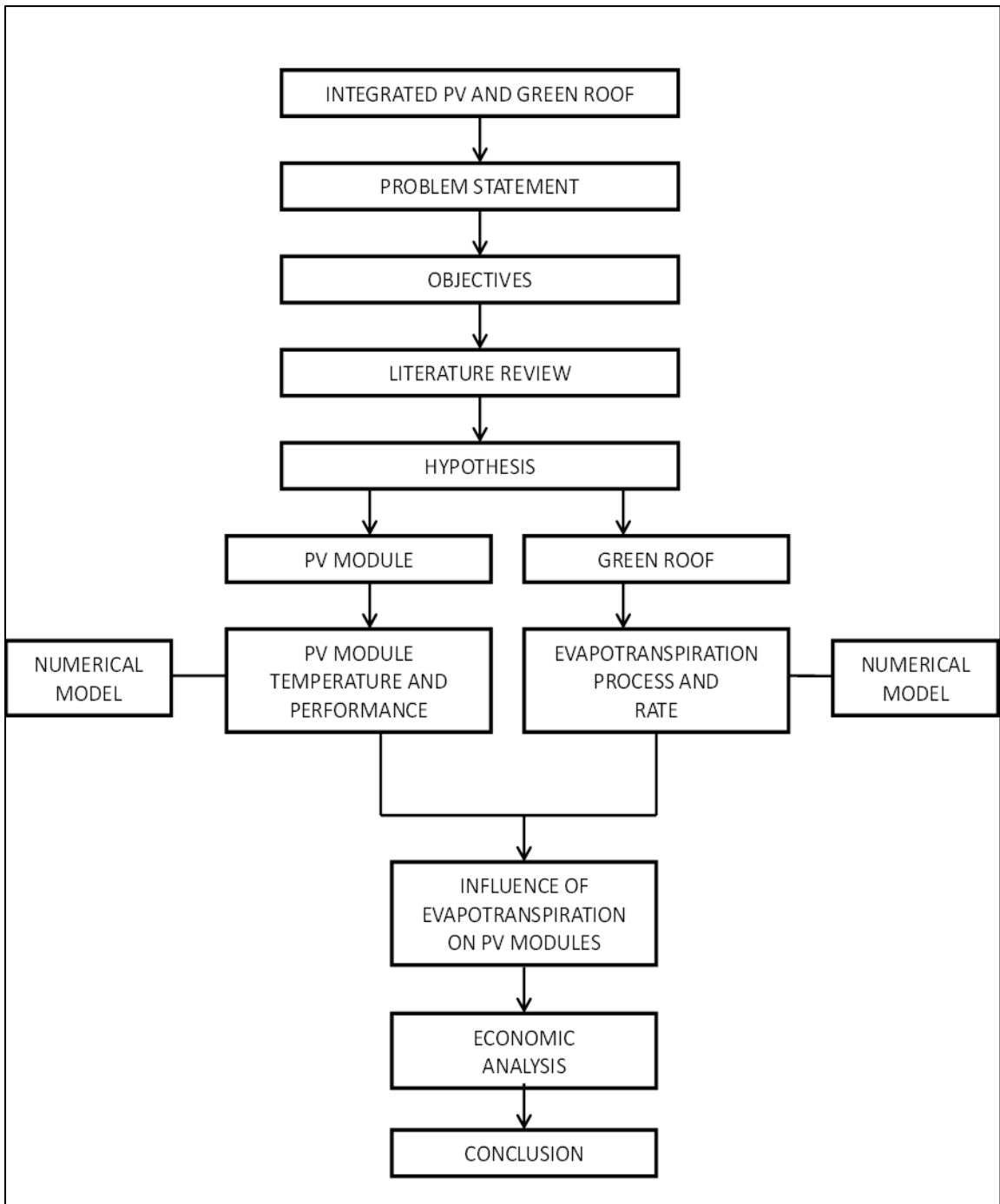
Fig. 3.1 The general framework of the research

Figure 3.2 presents the research approach to develop the two numerical models, which are achieved in three main steps:

1. Study the energy balance in the integrated PV module and green roof.

   The study includes: (1) the energy exchange mechanisms of the PV system and of the green roof (particularly the evapotranspiration process) by investigating the essential physics in the integrated PV and green roof, and (2) the current equation models of evapotranspiration rate, namely the Penman Monteith and the Priestley Taylor, in order to develop the proposed numerical model of evapotranspiration rate.

2. Governing equation

   - The evapotranspiration rate numerical model: Independent and dependent variables are outlined based on the literature review. These variables are then measured in the field experiment.

   - The PV module temperature numerical model: an initial numerical model is constructed based on the Energy Balance theory particularly for energy balance between two grey surfaces and Euler method is used to calculate the initial numerical model. Subsequently, the initial numerical model is validated by field measurement

3. Field measurement.

   - The evapotranspiration rate numerical model: the field experiment is conducted to obtain empirical data, and these data are then computed using statistical analysis to build a regression model for evapotranspiration rate. The applications of the statistical analyses are: correlation, Analysis of variance (ANOVA) and regression.

   - The PV module temperature numerical model: field measurement is conducted to validate the predictive numerical model of the PV module temperature influenced by the evapotranspiration process.

58
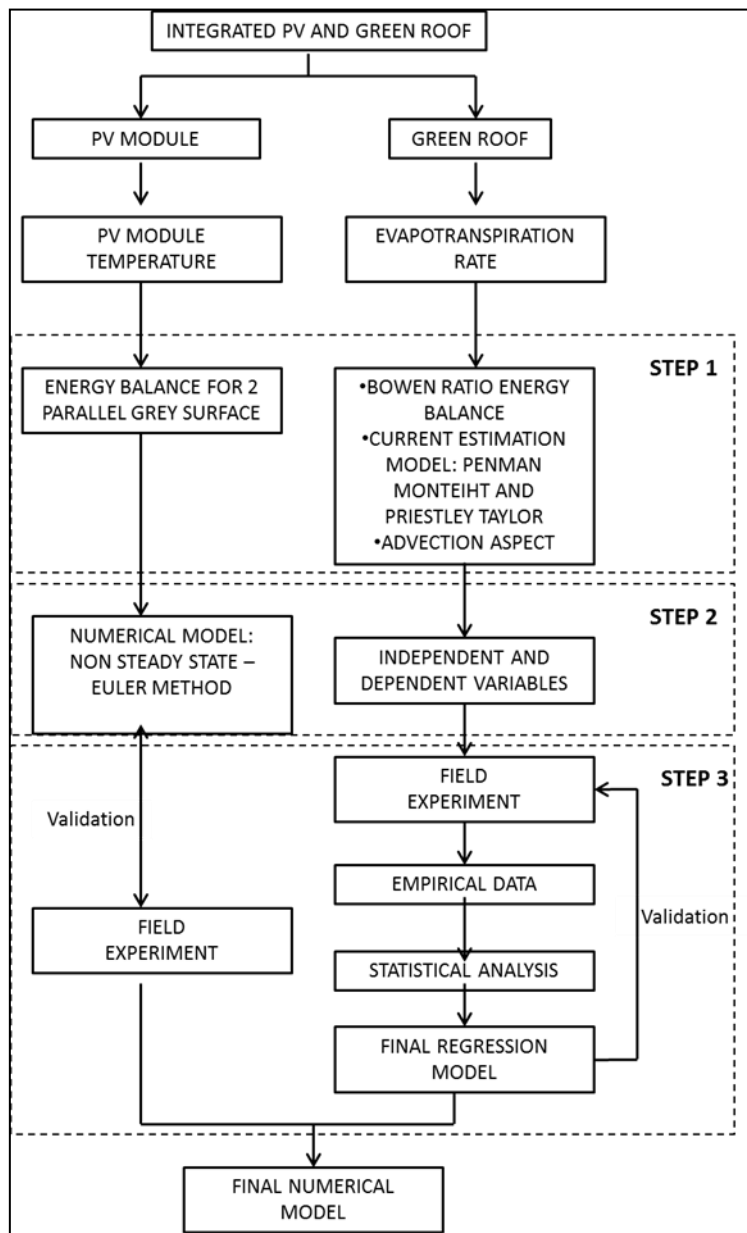
Figure 3.2 The schematic of the research approach

CHAPTER 4 EVAPOTRANSPIRATION RATE PREDICTION MODEL FOR A SMALL GREEN ROOF

This section describes the development of the proposed prediction model of the evapotranspiration rate for a small green roof for tropical Singapore climate. The prediction model was developed from the principle of Bowen ratio, Penman Monteith (PM) equation and Priestley Taylor (PT) equation. Additionally, the advective effect and the role of wind were also examined. A field experiment was conducted to obtain all the required data, which were eventually computed to construct a final equation. Statistical analysis was used for the computation process.

4.1. Methodology

In order to construct a mathematical model for a small green roof under the tropical climate of Singapore based on statistical analysis, the following steps were conducted:

1. Study the evapotranspiration rate measurement methods as well as various estimation models.

2. Investigate the influence of the advective heat from the surrounding environment

3. Conduct a field measurement to obtain the required data

4. Conduct a statistical analysis: regression, Analysis of variance (ANOVA) and correlation in order to verify and validate the influence of the independent parameters on the dependent variable (evapotranspiration rate).

5. Examine the results of the predicted evapotranspiration rate with the root mean square deviation (RMSD) to identify the suitability of the proposed equation model for estimating the evapotranspiration rate of the green roof.

Figure 4.1 illustrates the stages of this study.
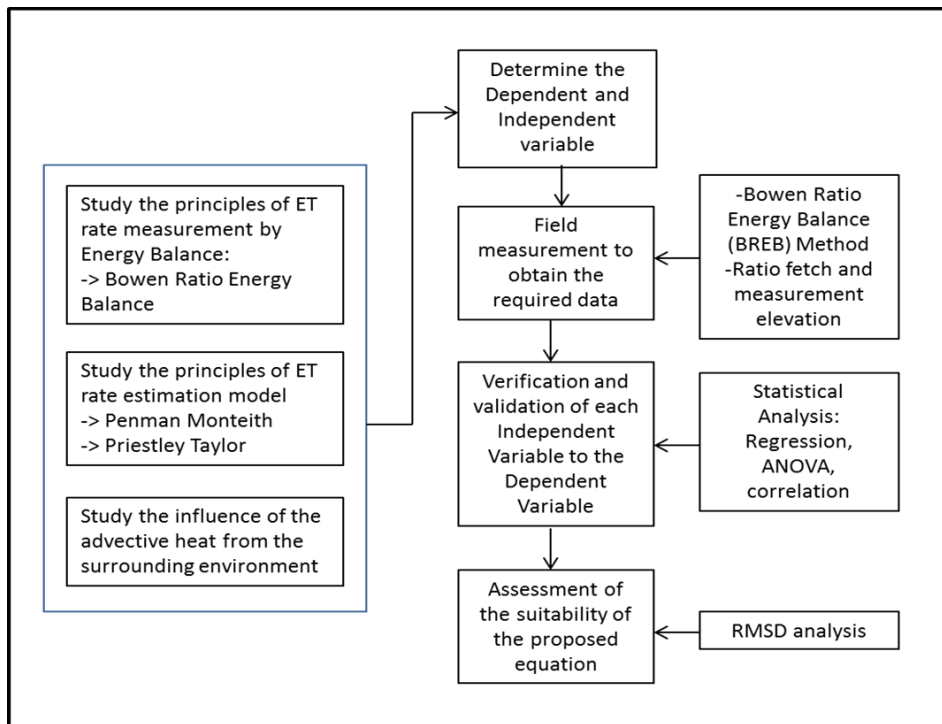
Figure 4.1 The stages of the study of the evapotranspiration (ET) rate prediction model

4.2. The evapotranspiration rate estimation principles and the influencing factors

This chapter outlines the principles of Bowen Ratio Energy Balance (BREB) method and other numerical models for estimating evapotranspiration process as well as the influencing factors on evapotranspiration rate, such as wind and advection from the surrounding.

4.2.1. Bowen ratio energy balance (BREB) method

As stated previously, evapotranspiration is a process of energy changes in a system containing plants and its substrate, where energy from the sun is used to convert liquid water into vapor. The heat consumed or absorbed by this conversion is called latent heat. To describe the process, the principle of energy balance is utilized to account for all changes of energy fluxes into and out of the system. The difference between the rate of ingoing and outgoing energy fluxes is equal to the rate of change in the total energy in the system (Jones, 1992).

$$R_n - H - \lambda ET = M + S \; [\mathrm{Wm^{-2}}] \tag{4.1}$$

where, R_n the net is radiant heat, H is the sensible heat, λET is the latent heat (λ is the latent heat vaporization and ET is the evapotranspiration rate), M is the net heat stored in biochemical reactions and S is the heat storage.

The latent heat flux (λET) that represents the evapotranspiration fraction can be derived from the energy balance equation if all other components are known. Net radiation (R_n) and soil heat fluxes (G) can be measured or estimated from climatic parameters. However, the λET cannot be measured directly but through an estimation so-called Bowen ratio (BR) calculation. Bowen ratio is the ratio of sensible to latent heat flux ($H/\lambda ET$). It is proportional to the ratio of the air temperature gradient (ΔT) to the vapor pressure gradient (Δe) over a specified vertical distance above the crop canopy (Jones, 1992). In calculating the Bowen ratio for

small plant or grass, the psychrometric constant (γ) can be assumed as 1 (Grattan et al., 1998). Mathematically, the λET term can be calculated as follows:

$$\beta = \frac{H}{\lambda ET} = \gamma \frac{\Delta T}{\Delta e} \text{ [dimensionless]} \tag{4.2}$$

$$\lambda ET = \frac{R_n - G}{1 + \beta} \text{ [Wm}^{-2}] \tag{4.3}$$

The net radiant (R_n) is calculated by the following equation:

$$R_n = I\alpha_{leaf} + \sigma\varepsilon_{sky}(T_{sky})^4 - \sigma\varepsilon_{gr}(T_{gr})^4 \text{ [Wm}^{-2}] \tag{4.4}$$

where, I is the solar radiation, α_{leaf} is the leaf absorption coefficient, T_{sky} is the sky temperature, ε_{sky} is the emissivity of the sky and ε_{leaf} is the emissivity of the leaf. σ is the Stefan Boltzmann constant and T_{gr} is the surface temperature of the green roof. The sky temperature is calculated by Eq. 5.9 and the value of the emissivity can be found in Appendix 3.

The soil heat flux can be calculated from the following equation:

$$G = \frac{k \times \Delta T}{x} \text{ [Wm}^{-2}] \tag{4.5}$$

where, k is the soil conductivity, ΔT is the difference of the soil temperature whereas the first sensor was located on the soil surface and the second sensor was located around 50 mm down from the first sensor. Therefore the distance (x) was defined as

50 mm. The soil was constructed from the non-organic soilless volcanic ejecta substrate which is mixed with sand, whereas the soil conductivity for volcanic rocks with the porosity of between 50 and 60% is between 0.3 and 0.6 $Wm^{-1}K^{-1}$ (Clauser and Huenges, 1995), and as for the moist sand is $0.25 - 2.00$ $Wm^{-1}K^{-1}$. Therefore the soil conductivity for the proposed numerical model was defined as 0.45 $Wm^{-1}K^{-1}$.

Equation 4.2 and 4.3 express the Evapotranspiration rate (ET) as a function of net radiation and soil heat flux together with the gradients of temperature between the two sensors (ΔT) and water vapor pressure (Δe) in the boundary layer. The value for the psychrometric constant and water vapor pressure deficit is derived from Jones (1992) as shown in Appendix 4 and 5. The vapor pressure is then determined by saturation water vapor (e_s) with the associated parameters of humidity and temperature. The relative humidity is attained at the same point as the ambient temperature.

The Bowen ratio energy balance (BREB) measurement method is used to collect the required data for the Bowen ratio calculation. Details of measurement including the definition of the sensors allocation to satisfy the homogeneous conditions requirement are provided in Chapter 6.

4.2.2. Evapotranspiration estimation model : Penman Monteith and Priestley Taylor

Evaporation is a transfer of mass where water change phases from liquid to vapor by some amounts of energy to supply the latent heat for the evaporation (Jones, 1992). In order to estimate this mass transfer, basically, it is defined by the Energy Balance

principle and is proportional to the total conductance and a concentration difference which is described in the following equation (Jones, 1992):

$$ET = g_w * \Delta c_w \ [\text{kgm}^{-2}\text{s}^{-1}] \tag{4.6}$$

where, g_w is the total conductance of the pathway between the evaporating sites and the bulk air, and Δc_w is the water vapor concentration difference between the surface and the bulk air. The last parameter is derived from:

$$\Delta c_w = (0.662 \rho_a / P)(e_{s(Ts)} - e_a) \ [\text{gm}^{-3}] \tag{4.7}$$

where, $e_{s(Ts)}$ is the saturation vapor pressure at surface temperature and e_a is the water vapor pressure.

The following subchapter describes the development of the above equation.

4.2.2.1. Penman-Monteith (PM) model

This model was originally suggested by Penman in 1948 to eliminate the measurement of surface temperature difference, so that it is possible to write an equivalent expression for the sensible heat flux between the surface and the air with the volumetric heat capacity of dry air used to approximate the heat capacity of air.

The value of the surface to air vapor pressure difference $(e_{s(Ts)} - e_a)$ can be substituted by the saturation water vapor pressure of the ambient temperature and a term that depends on the temperature difference between the surface and the air (Jones, 1992). The term is named as the slope of the curve relating saturation vapor pressure to temperature (s) (Fig. 4.2). It can be observed that the slope (s) estimates the surface temperature (T_s) to ambient temperature (T_a) by its straight line (signed by point A), and the difference between the vapor pressure deficit of ambient temperature (δe) and the saturation vapor pressures at T_a and T_s (approximated by s (T_s-T_a)).
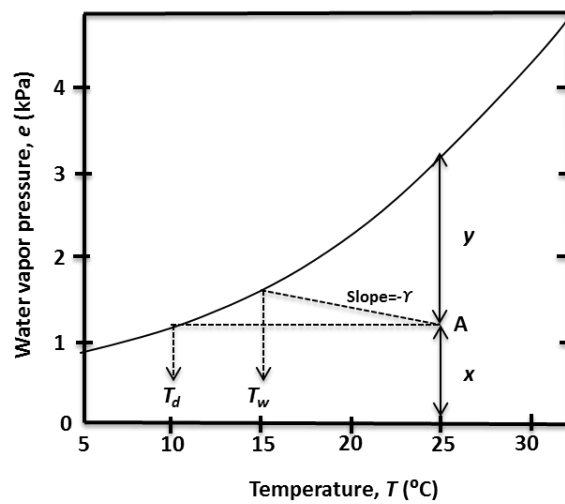
Figure 4.2. The curve relating saturation vapor pressure to temperature (s)
Source: Jones, 1992

In summary the Penman-Monteith model for determining the Evapotranspiration rate can be explained as follows (Jones, 1992):

$$ET = \frac{\{s(R_n - G) + \rho_a c_p g_H \delta_e\}}{\lambda[s + (\gamma g_H / g_W)]} \; [\text{kgm}^{-2}\text{s}^{-1}] \tag{4.8}$$

Or it can also be expressed by the following equation:

$$ET = \frac{\{s/\gamma(R_n - G) + g_H \delta c_w\}}{\lambda(s/\gamma + g_H/g_w)} \text{ [kgm}^{-2}\text{s}^{-1}]$$ (4.9)

where, s is the slope of the curve relating saturation vapor pressure to temperature (the values can be found in Appendix 4), R_n is the net radiation, G is the soil heat flux, ρ_a is the air density, c_p is the water specific heat capacity, g_H is the water heat conductance, δ_e is water vapor deficit, γ is the psychrometer constant, g_w is the water conductance, δc_w is the absolute humidity deficit of the air and λ is the latent heat of vaporisation.

Furthermore, Jones (1992) explained that the original derivation was to describe evaporation from a free water surface, where there is no surface resistance to water loss; therefore the denominator can be simplified using the approximation of $g_H \simeq g_w$. Hence, this free water calculation can be applied as a basis for estimating evaporation from well-watered crops which completely cover the ground. Monteith has applied this equation to plant canopies in 1965.

Thus, the main parameter for estimating evapotranspiration rate based on Penman Monteith equation are as follows: Net radiation, soil heat flux, aerodynamic data or the total conductance of total leaves (canopies), psychrometric constant (γ), water vapor deficit and slope (s). The last three parameters are obtained from the measurement of the ambient temperature and the relative humidity.

4.2.2.2. Priestley-Taylor (PT) model

Basically the PT model is the simplification of the PM model. This equation does not require aerodynamic data and is derived based on the concept of equilibrium evaporation from moist surface (Pereira, 2004). The concept of the equilibrium evaporation is applicable under the condition of a large homogeneous and thoroughly moist surface with steady condition; hence, the vapor pressure (e) tends to the saturation vapor pressure at air temperature (e_s) or the evaporation rate become equilibrium evaporation.

The model can be expressed as follows (Priestley and Taylor, 1972):

$$ET = \alpha_{PT} \frac{s(R_n - G)}{\lambda(s + \gamma)} \, [\text{kgm}^{-2}\text{s}^{-1}] \tag{4.10}$$

where, α_{PT} is termed as a Priestly-Taylor coefficient with the value of 1.26, s is the slope of the curve relating saturation vapor pressure to temperature, R_n is the net radiation, G is the soil heat flux, λ is the latent heat of vaporisation and γ is the psychrometer constant.

Hence, the main parameter for the Priestley Taylor equation can be defined as follows: net radiation, soil heat flux, the Priestley Taylor (PT) coefficient, the slope (s) and the psychrometric constant. The last two parameters are obtained from the ambient temperature measurement.

4.2.3. Influence of advective heat from the surrounding environment

Referring to Kirkham (2005), advection is described as the exchange of energy, moisture, or momentum resulting from the horizontal heterogeneity, e.g. in an area with hot and dry upwind over an irrigated field, sensible heat will be transferred to the air above the irrigated field and its evapotranspiration rate will be increased. This condition also applies to urban areas with high building density like Singapore. The urban morphology with many buildings and pavements made of hard materials radiates heat in a significant amount and eventually increases the air temperature.

4.2.3.1. Air temperature

Green roofs in Singapore are generally constructed on roof tops of tall buildings and are surrounded by unvegetated areas such as blocks of buildings with concrete roofs. In this urban context, the ambient air temperature will be substantially higher, providing additional energy for plants to evaporate more water beyond radiative gain. Advection or transfer heat from the surroundings and its effect on the air temperature of a particular area in Singapore has also been studied by Wong et al (2011). The study revealed that the level of air temperature is determined by two factors: solar radiation and urban morphology. The urban morphology includes: percentage of pavement area, average height of building, total wall surface area, green plot ratio, sky view factor and average albedo.

Hence, this study also took air temperature level at 2 meters above the green roof into consideration.

4.2.3.2. The role of wind

Beside radiative heat from the surrounding, wind also plays important role in transferring heat to and from the surrounding area by convection. In terms of evapotranspiration process, wind is also one of the energy sources and it works by enhancing turbulence transfer of water vapor from moist vegetation to the dry atmosphere. In order to investigate the role of wind, particularly for a small green roof particularly for Singapore climate, the influence of wind speed on evapotranspiration rate was examined in the statistical analysis.

4.3. The proposed equation for determining the ET rate for a small green roof in tropical climate

Based on the key principles of Bowen Ratio (BR), Penman Monteith (PM) and Priestley Taylor (PT) equation, there are several important points that can be used as the fundamental knowledge for governing the proposed equation for a small green roof in tropical climates:

1. The three equations are suitable for estimating a vegetated area which fully covers its ground surface and rich with water. These two requirements have to be considered when designing the experimental set up.

2. The main parameters for determining the evapotranspiration rate are ambient temperature, relative humidity and solar radiation.

3. The ambient temperature and relative humidity above green roof are used to obtain the level of saturation water vapor pressure (e_s) and water vapor pressure (e), and subsequently to determine the deficit saturation water vapor (δe).

4. Solar radiation is measured to determine the net radiation of the green roof surface by applying other parameters such as air temperature, sky temperature, surface temperature and emissivity of the surface material. As stated by Jones (1992), the estimation of evapotranspiration is based on the

70

knowledge of net radiation and soil heat flux together with the gradient of temperature and water vapor pressure in the boundary layer.

5. The data of ambient temperature and relative humidity are best obtained over a homogeneous layer. This layer is defined as the ratio between fetch and the highest location of the sensor.

6. The slope of the curve (s) represents the relationship between saturation vapor pressure and temperature

7. The psychrometric constant (γ) value is used to determine the water vapor pressure (e) from dry bulb (T_a) and wet bulb (T_w) temperatures.

8. The dependence of the canopy evaporation on the humidity deficit (δe) on small plants (grass) is less compared to the available energy from net radiant and soil heat flux (R_n-G) (Jones, 1992).

Hence, the main parameters for the proposed equation for estimating ET rate for a small green roof surrounded by concrete roof are as follows:

- Net radiation (R_n) which is derived from the amount of solar radiation, surface temperature, air temperature, the sky temperature, the emissivity of the plants, the emissivity of the sky which depends on the sky condition and the Stefan-Boltzmann constant.

- Soil heat flux (G)

- Ambient temperature (T_a) at one point above green roof

- Relative humidity (Rh) at one point above green roof

- Wind speed

- Air temperature

Figure 4.3 schematically illustrates the concept for the proposed equation:

71
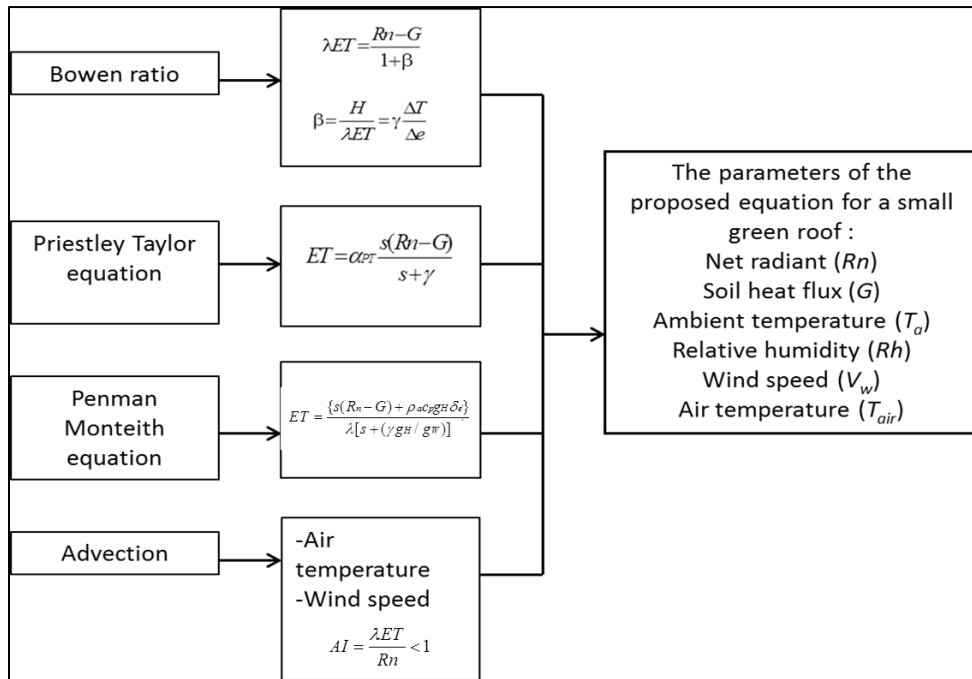
Figure 4.3. The schematic of the parameters derivation

Based on Fig 4.3, the independent variable and dependent variables are as follows:

- Dependent variable: evapotranspiration (*ET*) rate

- Independent variables are net radiation, soil heat flux, ambient temperature, relative humidity, wind speed and air temperature.

4.4. Boundary condition

The boundary layer for estimating the evapotranspiration rate for a small green roof is defined in the following figure (Fig. 4. 4):
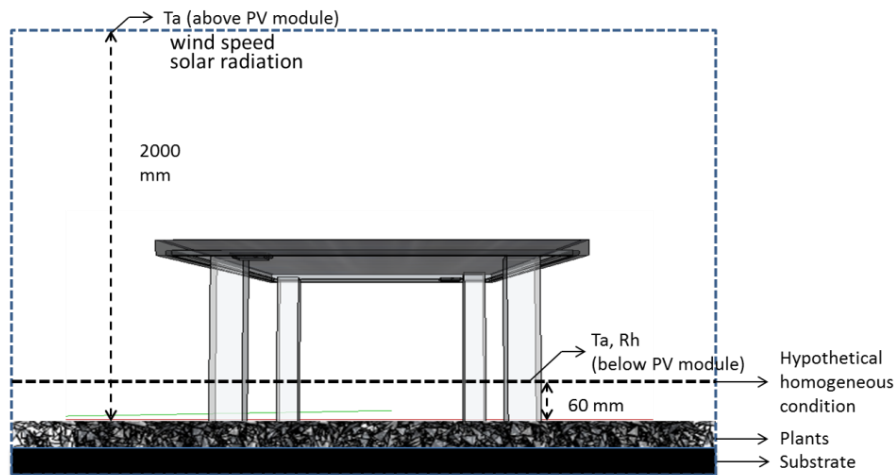
Figure 4.4. Definition of the boundary layer for a small green roof

The measured point of the ambient temperature and the relative humidity were defined by the ratio of the fetch to the highest location of equipment. The ratio was approximately defined as 20:1, whereas the minimum ratio can be 10:1. The green roof was a rectangle with the long side of 2500 mm. Hence, the measurement point was defined at 60 mm above the canopy of the green roof and was located in the middle of the green roof area (just beside the PV module) to ensure the sensors were in the homogeneous state. At this height, the condition between the measured point and the canopy was assumed to be homogeneous. The air temperature point was defined at 2000 mm above the canopy of the plants. This height was specified based on the standard climatological record of solar radiation, air temperature, humidity and wind speed (Food and Agricultural Organisation Document Respiratory).

4.5. Field Measurement to obtain the required data

The field measurement was conducted between June and October 2012. However, only the data which had the Advection Index (AI) lower than one, was validated with

the measured ET rate by BREB method and two other equation models (Penman-Monteith and the Priestley Taylor). The total data used in this validation were around 35% of the total data during June and October.   The measurement set up based on the boundary condition definition which is illustrated in Fig. 4.4. Note that the sensors of the ambient temperature and relative humidity (T/Rh) at the upper level (120 mm from the canopy) were used for the Bowen ratio energy balance measurement (the details are given in Chapter 6).   The data used for the proposed equation is derived from the sensor at the lower level (60 mm from the canopy layer). The data were read within 5 minute interval. The details of the equipment are summarized in Table 6.1.

4.6.   Validation and verification procedure

The proposed model was verified and validated through statistical analysis namely Toolpak and it is provided in Excel. Data of each independent variable obtained from the field experiment were computed to investigate their correlation to the dependent variable (here: evapotranspiration rate).   The computation was done by correlation analysis. The independent variables which have correlation coefficient less than 0.5 were eliminated and were not further considered for the regression and the ANOVA analysis. The remaining variables were further investigated by the regression and the ANOVA analysis to determine their significance on the evapotranspiration rate. Within this analysis the final coefficient regression of each independent variable was obtained.

Additionally, root mean square deviation (RMSD) was applied to assess the suitability of the proposed equation for its applicability in estimating the

evapotranspiration rate of the small green roof under tropical climate conditions in Singapore.

4.7. Statistical results of the proposed equation

The dependent variable in this study is evapotranspiration rate (ET), while the Independent variables are the residual of net radiation and soil heat flux (R_n-G), ambient temperature (T_a), relative humidity (Rh), wind speed (V_w) and ambient temperature (T_{air}). The input data of ambient temperature and the relative humidity were obtained at height of 60 mm from the canopy of the green roof, while the data of wind speed and air temperature were obtained 2000 mm above the roof top.

The evapotranspiration rates measured by the Bowen ratio energy balance (BREB) method were used in order to examine the influence of the independent variables on the dependent variable.   The ET rates were obtained from five months measurement under three different sky conditions: clear, intermediate and overcast. The ET rates that are used for the analysis are the rates which have small Bowen Ratio (between -1 to 1) and the Advection Index are below or equal to 1 (more details on the field measurement methods, the range of the Bowen Ratio method and the Advection Index are provided in Chapter 6).

As stated previously, correlation analysis is conducted to investigate which of the independent variables have correlation coefficient below 0.5. As seen in Table 4.1, it can be seen that wind speed has relatively low influence on the rate of evapotranspiration of the green roof since its correlation coefficient is below 0.5. Hence, wind speed is eliminated for the further analyses (regression and ANOVA).

While, the highest correlation coefficient is the residual of net radiation and soil heat flux with the value of 0.99 and followed by the ambient temperature, relative humidity, air temperature and wind speed by 0.79, -0.71, 0.55 and 0.16 respectively.

Furthermore, the negative values of the relative humidity suggest that the relative humidity has a strong inverse relationship with the evapotranspiration rate. The evapotranspiration rate is high when the relative humidity is low. This result is in line with Eq. 4.6 and 4.7 which explain that evapotranpsiration occurs when there is a large deficit of water vapor resulting from the residual of saturation water vapor at surface temperature and water vapor pressure at ambient temperature ($e_s - e$) (Jones, 1992).

Table 4.1 Correlation analysis results

	Evapotranspiration rate	Ambient Temperature	Humidity	Net Radiant	wind speed	Air temperature
Evapotranspiration rate	1					
Ambient Temperature	0.791	1				
Humidity	-0.709	-0.962	1			
Net radiant – Soil heat flux	0.999	0.792	-0.709	1		
wind speed	0.163	0.271	-0.156	0.166	1	
Air temperature	0.557	0.630	-0.663	0.558	0.023	1

Table 4.2 shows the results from the ANOVA, and it can be seen that the significance, represented by the F value, is far below zero (0). This value indicates that all the independent variables significantly influence the evapotranspiration rate.

Table 4.2 ANOVA analysis

ANOVA		
	F	*Significance F*
Regression	146521.5038	3.1734E-207

This significance of all the independent variables is also demonstrated in the results of the regression analysis (Table 4.3). It can be seen from the table that the R Square for the regression model is 0.9998, whereas the Net Radiant is the most influenced variable to the evapotranspiration rate (Table 4.4).

Table 4.3 Regression Statistic Results

Regression Statistics	
Multiple R	0.999908
R Square	0.999816
Adjusted R Square	0.999808
Standard Error	6.34E-07
Observations	117

Hence the constant and the coefficient of each independent variable are shown in Table 4.4

Table 4.4 Regression results for the constant and the coefficient of the independent variables

	Coefficients	Standard Error	P-value
Intercept	4.20595E-06	3.10676E-06	0.178524312
Ambien Temperature	-7.90133E-08	6.4747E-08	0.224899671
Humidity	-1.37096E-08	1.22235E-08	0.26443841
Net Radiant	3.94549E-07	9.11484E-10	2.2218E-182
Air temperature	-3.22983E-08	3.45077E-08	0.351300661

Hence, based on Table 4.4, the complete equation model is constructed as follows:

$$ETrate = 4.2 \times 10^{-6} + 3.9 \times 10^{-7}(R_n - G) - 7.9 \times 10^{-8}T_a - 1.3 \times 10^{-8}Rh - 3.2 \times 10^{-8}T_{air}$$

(4.11)

4.8. Comparison of ET rate calculated by the proposed equation model, Penman Monteith (PM) and Priestley Taylor (PT) equation to the ET rate measured by Bowen ratio.

The purpose of this comparison study is to investigate the suitability of the proposed equation model for estimating the evapotranspiration rate of the green roof. The analysis uses the Root Mean Square Deviation (RMSD). Additionally, two current equation models (PM and PT) are included in the comparison in order to know which equation model has the closest trend with the proposed equation model. Sensitivity analysis for determining the most appropriate canopies conductance for the PM equation and for determining the most appropriate PT coefficient for the PT equation are conducted.

4.8.1. Sensitivity analysis for governing the canopy conductance for the PM equation.

The equation used for the ET calculation by the Penman Monteith equation is defined in Eq. 4.6. In order to determine the value of gw (canopy conductance) for canopies, this study uses the canopy conductivity value provided by Jones (1992). The selected value is the alfalfa canopy conductance, where the range of the value is between 0.4 mms^{-1} and 50 mms^{-1}. Alfalfa is chosen as this plant is also classified as a type of shrub, the same type of the plant used for the experiment (*Complaya trilobata*). A sensitivity analysis is conducted to obtain the most appropriate value for the *Complaya trilobata* with reference to Singapore climate.

The sensitivity analysis is conducted by applying "one set off" analysis where one parameter is varied while keeping all other parameters fixed. In this study, the

selected canopy conductivity values for the analysis are 0.4 mms^{-1}, 10 mms^{-1}, 30 mms^{-1}, 40 mms^{-1}and 50 mms^{-1}. The PM equation is run for 3 days under different sky condition. The ET rate calculated by PM corresponding to the selected canopy conductance is plotted along with the measured ET rate by the Bowen ratio method.

It can be observed from Fig. 4.5 that the canopies conductance of 20 mms^{-1} has the lowest RMSD for all the selected days. Nevertheless, the RMSD of the other three: 10 mms^{-1}, 30 mms^{-1}and 40 mms^{-1}are almost identical.
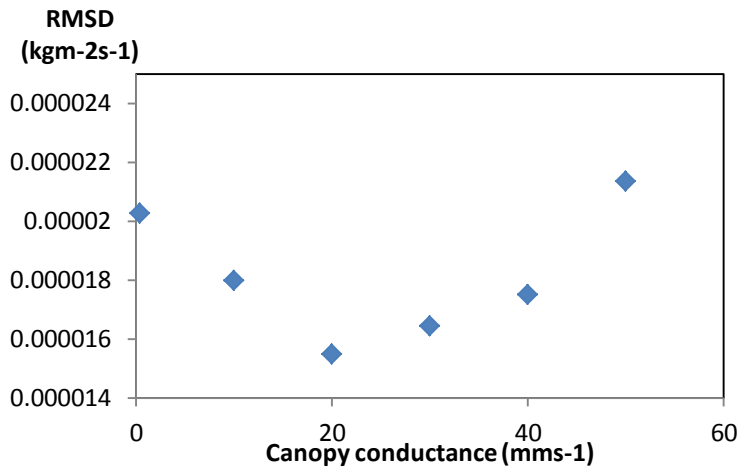
Figure 4.5 Sensitivity analysis: the canopy conductance

Fig 4.6 shows the comparison of the predicted ET rate calculated by PM equation with the selected canopy conductance with the measured ET rate by the BR method. In general, the diurnal trend is in a good agreement with the measured ET rate. Furthermore, it can be observed that, the predicted ET rate is always below the measured ET rate by BREB method. The maximum rate difference can be as high as 3%.
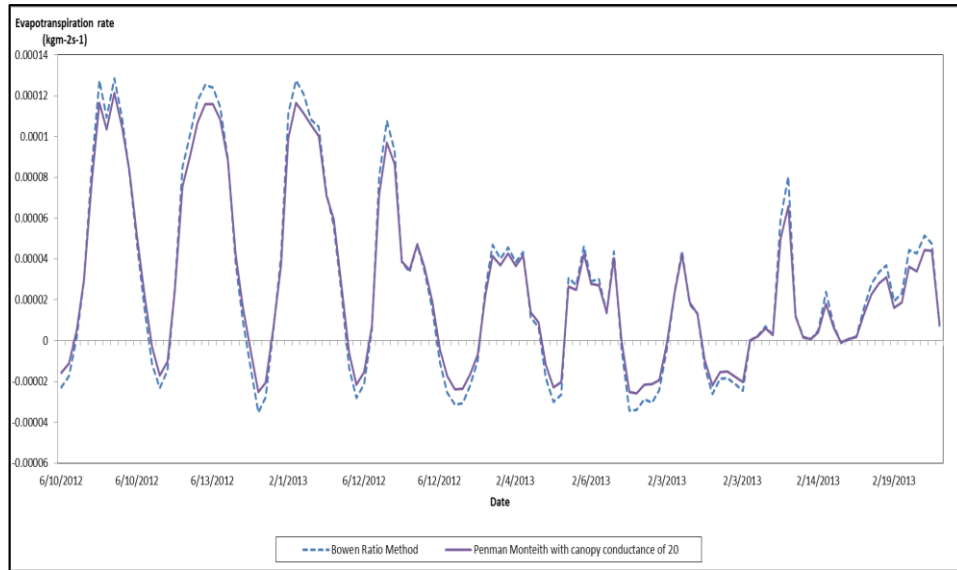
Figure 4.6 Comparison of the estimated ET rate by PM equation and measured ET rate by BREB method

These results may confirm that the canopy conductance of 20 mms^{-1} is the most appropriate conductivity coefficient for estimating ET rate for the small green roof under Singapore climate.

4.8.2. Sensitivity analysis for governing the Priestley Taylor coefficient for PT equation

This analysis is based on Eq. 4.8. In practice, the PT coefficient can be vary and the calculation depends on vegetation types, soil moisture condition and strength of advection (Flint and Childs, 1991).

Regarding to tropical climates, Gunston and Batchelor (1983) reported The PT coefficient of 1.26 was confirmed to be suitable for this type of climate as long as the conditions remain homogeneous or free from the advection influence, relatively high humidity and low wind speed. Furthermore, both PM and PT models offer a satisfactory equation for estimating the evapotranspiration rate over green areas in humid tropical climates.

Four values of PT coefficients are investigated to define the most appropriate coefficient for the calculation through sensitivity analysis, and the value are: 1.14, 1.18, 1.22 and 1.26. The analysis is also conducted by applying "one set off" analysis. Fig. 4.7 shows that the highest RMSD occurs at the lowest coefficient, while, the lowest RMSD occurs at the value of 1.22. As for the RMSD of the other two coefficients (1.18 and 1.26) are almost identical. This result is closest with the study of Gunston and Bachelor (1983) study, that the RMSD of PT coefficient of 1.22 is identical to that of 1.26. A slightly difference in values occurs might be caused by the difference area of greenery. This study used a small area for which the effect of advection from the surrounding gave relatively minor effects on the homogeneous condition, shown by the value of the Advection Index that almost reaches to 1 (Table 6.3, 6.5, and 6.7).
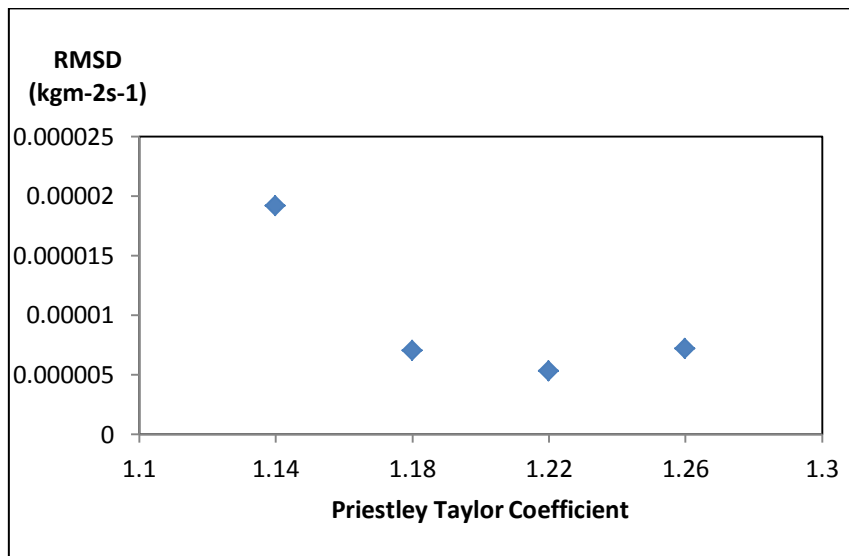
Figure 4.7 Sensitivity analysis: the Priestley Taylor coefficient

In line with Fig 4.7, Fig. 4.8 shows the comparison of the ET rate using the PT coefficient of 1.22 with the measured ET rate conducted by BR method for all three sky conditions. The estimated ET rates by PT equation, when using the coefficient of 1.22 are similar, only 1.5% difference . Thus, it may confirm that the PT coefficient

of 1.22 is suitable for estimating the evapotranspiration rate for small green roofs under tropical conditions.
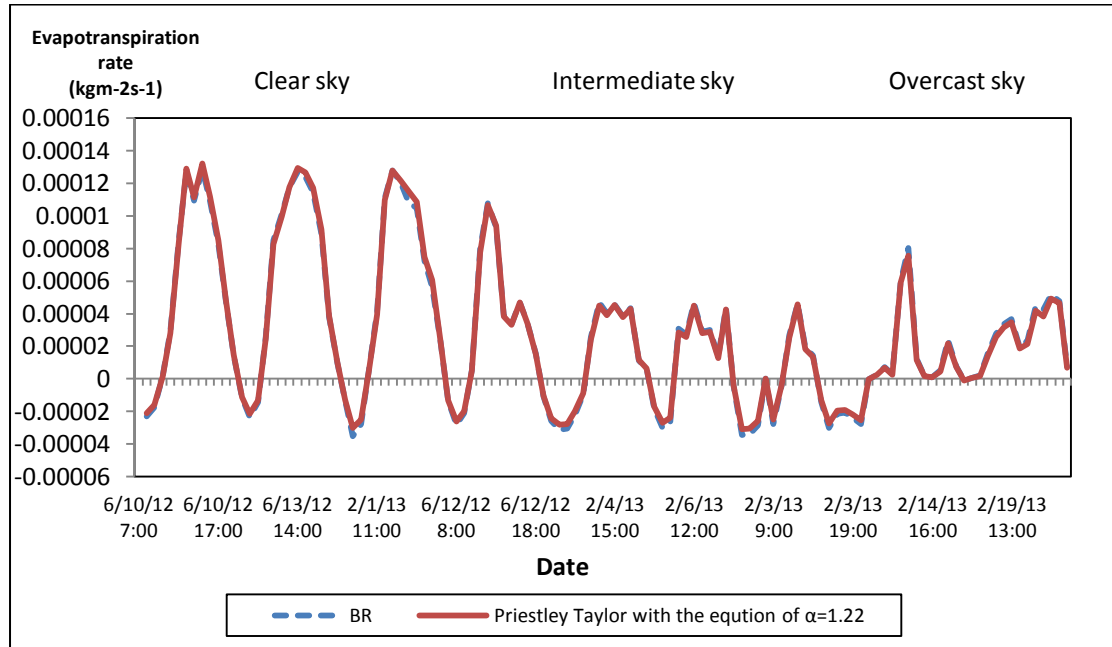
**Figure 4.8 Comparison of estimated ET rate by PT equation using α=1.22
and measured ET rate by BREB
Note: the lines of the measured ET rates by BREB and calculated ET rate by PT
equation are overlaying in most cases**

The following sub chapter presents the comparison analysis between the proposed ET rate model and the measured ET rate using BREB method, as well as the estimation of ET rate by PM and PT equation.

4.8.3. Results and Discussion

Figure 4.9 shows the calculated and measured evapotranspiration rate using the BR method, PM equation, PT equation and the proposed model. The analysis was divided into 3 parts based on three different sky condition: clear sky, intermediate sky and overcast sky respectively.
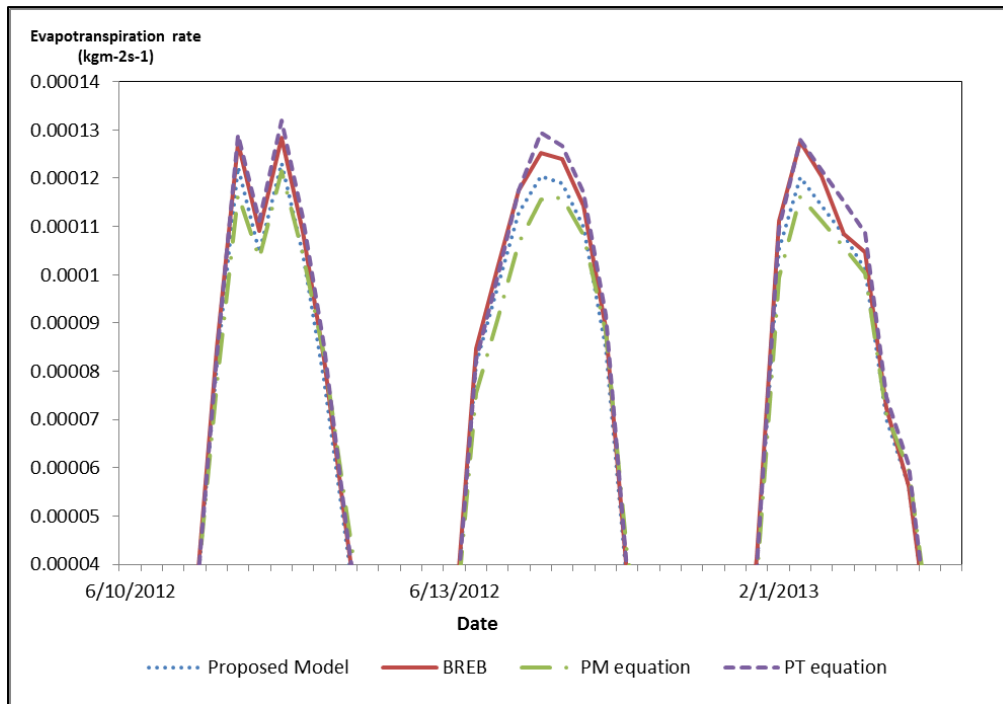
Figure 4.9 Measured and calculated evapotranspiration rate using BREB, PM, PT and the proposed equation on clear days

From Fig. 4.9, it can be seen that, in general, all the estimation methods are in a good agreement with the BREB measurement results, but there exist difference in the volume. It can also be observed that the measured ET rate by BREB method is similar with the calculated ET rate by PT equation in clear sky condition. While, the calculated ET rate by PM equation is similar with calculated ET rate by the proposed equation, in which the ET rate is reduced.

On intermediate and overcast days, there is no substantial difference between the measured ET rate by BR method and calculated ET rate by the three equation models (Fig. 4.10 and 4.11).
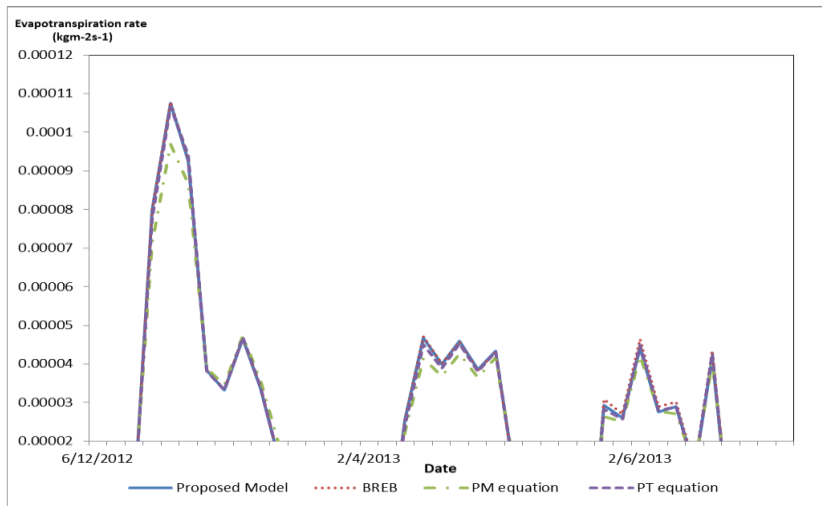
Figure 4.10 Measured and calculated evapotranspiration rate using BREB, PM, PT and the proposed equation on intermediate days
Note: the lines of BREB, proposed model and PT equation are overlaying
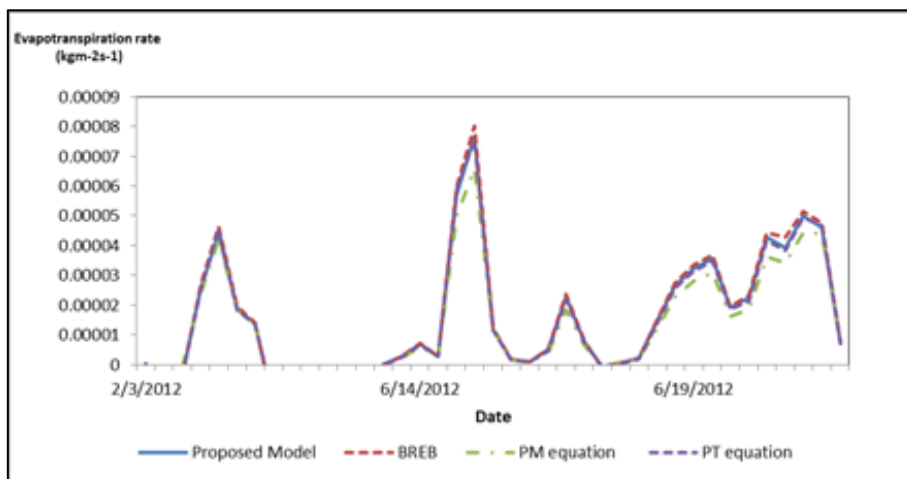
Figure 4.11 Measured and calculated evapotranspiration rate using BREB, PM, PT and the proposed equation on overcast days
Note: the lines of BREB, Proposed model and PT equation are overlaying each other

Fig. 4.9 to 4.12 indicate that the variation of ET rate estimation is potential to occur in a condition under high solar radiation (Fig. 4.12), where solar radiation may influence the moisture of humidity condition over the green roof, and there is a possibility that the value of the aerodynamic condition used in the PM calculation is not suitable. This potential is shown by a relatively larger error bars which occurs only on clear days.

84
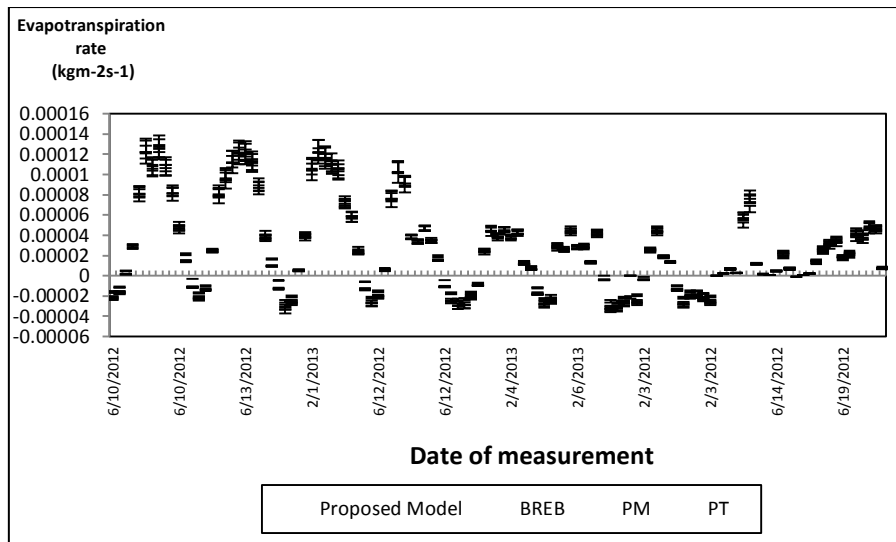
Figure 4.12. The error bars analysed by standard error from the estimation models (the proposed model, PM model and PT model) and the BREB measurement

Table 4.5 summarizes the maximum, the average and the minimum ET rate from each estimation methods as well as their RMSD when compared to the BREB measurement at all sky conditions.

Table 4.5 Summary of the ET rate calculation using different methodologies and the respective RMSD

Sky condition	ET rate $(kgm^{-2}s^{-1})$	BREB	PM Equation	PT Equation	Proposed Equation
Clear	Maximum	1.28E-04	1.21E-04	1.31E-04	1.23E-04
	Average	5.521E-05	5.421E-05	5.64E-05	5.30E-05
	Minimum	-3.51E-05	-2.50E-05	-3.01E-05	-3.19E-05
Intermediate	Maximum	1.07E-4	9.68E-05	1.06E-04	1.07E-04
	Average	1.47E-05	1.60E-05	1.62E-05	1.57E-05
	Minimum	-3.43E-05	-2.57E-05	-3.09E-05	-3.28E-05
Overcast	Maximum	8.02E-05	6.57E-05	7.54E-05	7.66E-05
	Average	1.26E-05	1.08E-05	1.23E-05	1.21E-05
	Minimum	-3.00E-05	-2.18E-05	-2.71E-05	-2.87E-05
RMSD			1.67E-05	5.31E-06	5.74E-06

85

It can be seen from Table 4.5 that the lowest RMSD occurs at the calculated ET rate by PT equation, followed by the calculated ET rate by the proposed model and the calculated ET rate by PM equation respectively. Furthermore, as seen on Table 4.5, in general the PM equation underestimates the ET rate as compared to the other two equation models. This results is in accordance with some studies (Kato et al., 2004; Stannard, 1993, Jarvis, 1976 and Shuttleworth and Wallace, 1985) which has been summarized by Zhang et al (2008). The possible reason for ET rate underestimated by PM model is generally caused by a high soil water content with a sparse canopy, so that it may decrease the soil surface resistance below the canopy resistance. On the other words, the surface canopy resistance will comprise the effect of soil evaporation. In contrast, the results of PM calculation is generally overestimate as compared to BREB in an advective regime (Zhang et al., 2008). The dryness over the soil surface leads to a higher soil surface resistance to the canopy resistance, because of the reduction of the wet area.

As for the PT equation and the proposed equation, the RMSDs show only a minor difference compared to the measured BREB values. The RMSD for PT equation and the proposed equation are 5.31E-06 $kgm^{-2}s^{-1}$ and 5.74E-06 $kgm^{-2}s^{-1}$ respectively. This result may indicates that all the independent parameters applied in the proposed equation are able to estimate the ET rate for small green roof in tropical regions, here in Singapore.

The suitability of the proposed equation is also shown in Figure 4.13, where the trend line of the PT equation and the proposed equation are identical. While, that of the PM equation is slightly lower.
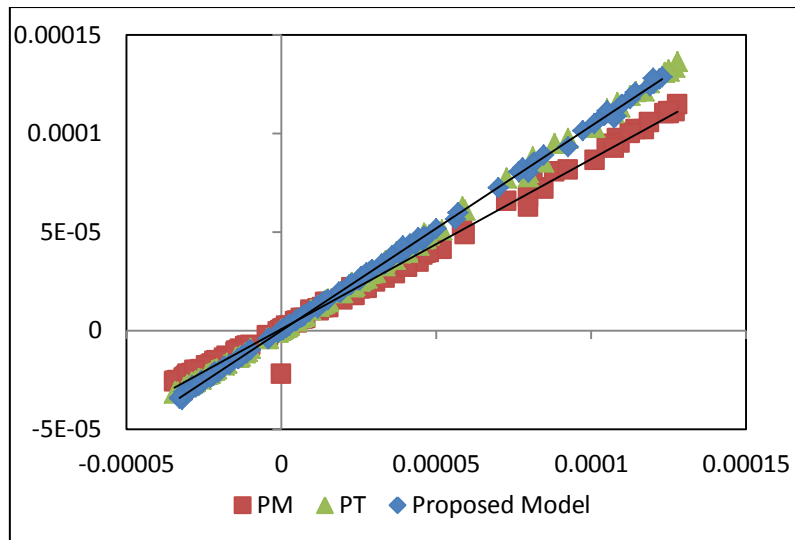
Figure 4.13 The regression model of PM, PT, Proposed model and BR method

4.9.   Conclusion

A new estimation model has been proposed using empirical data and were then scrutinised by statistical analysis. Furthermore, a comparison study of the modeled ET rate with the measured ET by the Bowen ratio energy balance (BREB) method and with two other equation models, the Penman Monteith (PT) and the Priestley Taylor (PT) equation, has been conducted. The following conclusions can be made:

1. The proposed equation have shown that the independent variables: (1) ambient temperature 60 mm above the canopy, (2) relative humidity 60 mm above the canopy, (3) air temperature 2000 mm above the canopy and (4) the residual of the net radiation and the soil heat flux, determine the value of evapotranspiration rate significantly. The determinant coefficient value (adjusted R^2) is 0.9998 as the result of the regression analysis.

2. The proposed equation has simplified the previous equation by eliminating: (1) the slope(s) that represents the interrelationship between ambient temperature and surface temperature, (2) aerodynamic data such as

87

conductance and (3) the psychometric coefficient (Υ) from the previous models.

3. The equation work well under the following conditions: the ground surface is fully covered by plants and is well watered.

4. The measured points for the input data, particularly the ambient temperature and relative humidity below the PV module, should be in line with the minimum required ratio between fetch and the highest elevation of sensors for those two parameters.

CHAPTER 5 MATHEMATICAL MODEL DEVELOPMENT TO PREDICT THE DYNAMIC TEMPERATURE OF PV MODULES INFLUENCED BY THE EVAPOTRANSPIRATION OF GREEN ROOFS

This chapter presents the development of the predictive numerical model of the PV module temperature influenced by the cooling effect of the evapotranspiration process. As reference, the comparative numerical model to predict the PV module temperature over concrete roof is also outlined.

5.1. Methodology

The predictive numerical model applies a non-steady state approach where the change of the module temperature is considered to be time dependent. The principle of Energy Balance is used as governing the modeling.

The model describes the following phenomena for local environment of the proposed integrated PV module and green roof (Fig 5.1):

1. Heat transfer

- The principle modes of heat transfer at the PV module are radiation and convection. The conductivity is neglected as the thickness of PV module is small (25 mm) and it is not thermally connected to a large heat capacitive body. The PV module specifications are given in Appendix 6.

- The principle modes of heat transfer at the green roof are radiation, convection , latent heat and conduction through the soil.

2. Mass transfer

- The principle mode of mass transfer is the transfer of water into vapor through the evapotranspiration process, which can be described as latent heat transfer. The Bowen Ratio Energy Balance principle is used as the basic principle.

5.2. Boundary conditions

The boundary condition for this study is illustrated in Fig 5.1. This study neglected the conduction heat, as it is assumed that the thickness of the PV module is thin. This assumption is valid (Skolapky ,2009; Trinuruk, 2009). Therefore the boundary condition is defined by the sky temperature, the green roof temperature, the ambient temperature above the PV module and the ambient temperature between the PV module and the ground surface. The flow of energy in the control volume is shown by the arrows.

$$-k\frac{\partial T_{pv}(0,t)}{\partial x} = h_{cpv}(T_{pv} - T_{\infty}) + \sigma\varepsilon_{pvfront}(T_{pv}^{4} - T_{sky}^{4}) \qquad h_{cpv}(T_{\infty} - T_{pv}) + \sigma\varepsilon(T_{sky}^{4} - T_{pv}^{4}) = -k\frac{\partial T_{pv}(0,t)}{\partial x}$$

$$h_{cpv}(T_{\infty} - T_{pv}) + \sigma\varepsilon_{leaf}(T_{gr}^{4} - T_{pv}^{4}) = -k\frac{\partial T_{pv}(0,t)}{\partial x} \qquad -k\frac{\partial T_{pv}(0,t)}{\partial x} = h_{cpv}(T_{pv} - T_{\infty}) + \sigma\varepsilon_{pvback}(T_{pv}^{4} - T_{gr}^{4})$$

Figure 5.1. Boundary condition

The predictive numerical model is developed from the investigation of physical parameters in the system under the following prerequisites:

- Local thermal equilibrium:
  ➢ The PV module temperature is assumed to be homogenous across its area. A local equilibrium is assumed between the PV module and the green roof. The soil condition of the green roof is assumed to be rich of water content by providing a regular irrigation from an automatic irrigation system, so that the evapotranspiration process can take place without interruption.

- Solar radiation is assumed to be the dominant factor in the energy balance of the evapotranspiration process (Sailor, 2008). While, the incoming energy from convection is neglected, since that energy only contributes less (0.9%) (Feng et al., 2010).

- The green roof is considered as diffuse gray body which radiates and reflects diffuse solar radiation.

- The plant's metabolism such as photosynthesis and respiration are negligible. Feng et al (2010) reported that only 9.5 % of total incoming solar radiation was converted by net photosynthesis in which the use for respiration is also included. Respiration can be regarded as the backward reaction of photosynthesis for the calculation of its thermal effect.

- Precipitation is not considered; only dry weather with clear, intermediate and overcast sky was investigated.

5.3. The proposed equation for determining the PV module temperature influenced by the evapotranspiration for tropical climate

5.3.1. Physical investigation

The physical model of the energy exchanges involving the PV module system, the plants system and the environment are illustrated as follows:
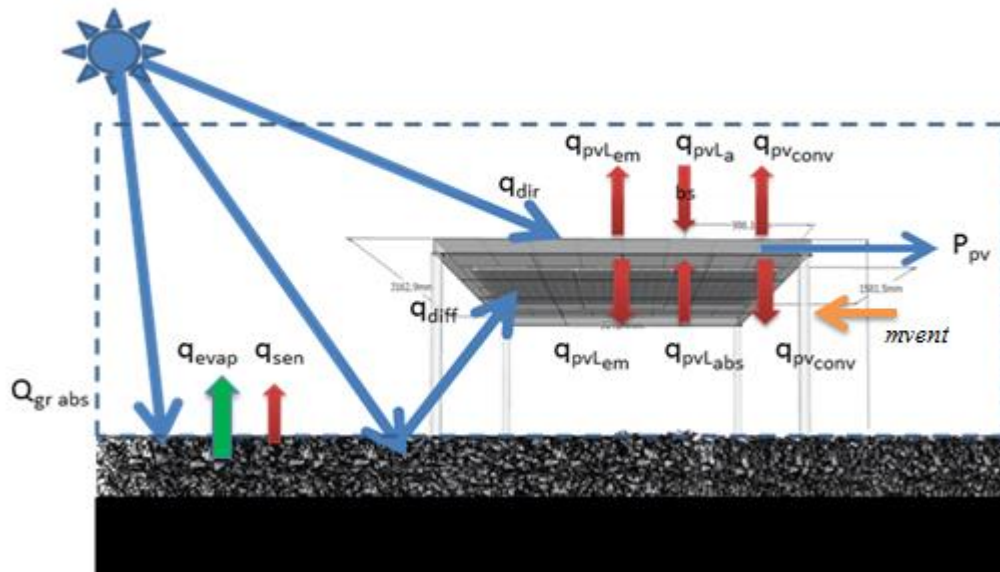
Figure 5.2. Schematic of energy exchanges between a green roof and a PV module within the boundaries of this study

where :

q_{dir} : heat flux from direct sunlight absorbed by the front surface of PV module.

q_{diff} : heat flux from reflected sunlight absorbed by the back surface of the PV

      module.

q_{pvLem} : heat flux from long wave radiation emitted from the front and back surface

      of the PV module.

q_{pvLabs} : heat flux from long wave radiation absorbed by the front and back surface

      of the PV module.

q_{pvconv} : convective heat flux above and under the PV module.

P_{pv} : electric power generation by the PV module.

$Q_{gr\,abs}$: heat flux from solar radiation absorbed by green roof.

q_{evap} : latent heat flux of the evapotranspiration process

q_{sen} : sensible heat flux from the green roof

mvent   : convection from the PV module to the air gap

From the concept above, Equation 5.1 to 5.3 describes the energy exchange mechanism in the integrated PV and green roof based on steady-state case:

$$Q_{pvstorage} = Q_{pv} + Q_{greenroof} + mvent \ [\text{Wm}^{-2}] \tag{5.1}$$

$$Q_{pvcell} + \frac{P_{pv}}{A_{pv}} = Q_{pvabsorb} - (Q_{pvemmit} + Q_{pvconv}) + Q_{grsens} - Q_{grevap} - mvent \ [\text{Wm-2}] \tag{5.2}$$

$$m_{pv}\frac{C_{pv}}{A}T_{pvcell} + \frac{P_{pv}}{A_{pv}} = q_{pvdirr} + q_{pvdif} + 2q_{Lpvabsorb} - 2q_{Lpvemmit} - 2q_{pvconv} + q_{grsens} - q_{grevap} - mvent$$
[Wm-2]   (5.3)

where,

$Q_{pvstorage}$ = heat storage in the PV module

Q_{pvcell} = net sum of the incoming and outgoing heat flows at the PV module

$Q_{greenroof}$ = net sum of all heat flows the green roof, incoming heat flows, sensible

          heat and latent heat.

m_{pv} = mass of the PV module (kg)

C_{pv} = specific heat of the PV module (Jkg^{-1}K^{-1})

A =   PV area (m^2)

T_{pvcell} = temperature of PV cell (°C)

P_{pv} = PV electrical generation (Watt)

$Q_{pvabsorb}$ = heat absorbed by PV module (Wm^{-2})

$Q_{pvemmit}$ = heat emitted by PV module (Wm^{-2})

Q_{pvconv} = heat flow by natural convection over PV module (Wm^{-2})

Q_{grsens} = sensible heat over green roof (Wm^{-2})

5.3.2. Final equation

The complete prediction model of PV module temperature influenced by the evapotranspiraiton process is as follows:

$$m_{pv}\frac{C_{pv}}{A}dT_{pv} = I\alpha dt + I\rho_{leaf}dt + \sigma\varepsilon_{sky}(T_{sky}^4 - T_{pv}^4)dt + \sigma\varepsilon_{leaf}(T_{gr}^4 - T_{pv}^4)dt + \sigma\varepsilon_{pvfront}(T_{pv}^4 - T_{sky}^4)dt + \sigma\varepsilon_{pvback}(T_{pv}^4 - T_{gr}^4)dt +$$

$$h_{cpv}(T_{pv} - T_{apvtop})dt + h_{cpv}(T_{pv} - T_{apv\_gr})dt + h_{cgr}(T_{gr} - T_{apv-gr})dt - fV_w\rho c_p(T_{in} - T_{out}) - \lambda Edt - \frac{P_{out}}{A}dt$$

(5.4)

PV energy storage

The energy stored in the PV module is defined by the PV module heat capacity, the PV module temperature and the electricity generation of the PV module. It is calculated by the following equation:

$$Qpv_{storage} = m_{pv}\frac{C_{pv}}{A}T_{pvcell} + \frac{P_{pv}}{A_{pv}}[\text{Wm-2}]$$

(5.5)

where, m_{pv} is the mass of the PV module, C_{pv} is the PV module heat capacity and A is the PV module area. The electricity generation uses Eq. 2.2 and 2.3.

The energy absorbed by the PV module

The energy absorbed by the PV module ($Q_{pvabsorb}$) is the sum of all the incoming short wave radiation, the direct and the reflected solar radiation, and the longwave radiations from the sky and the green roof. It is calculated using the following equation:

$$Q_{pvabsorb} = I\alpha_{pv} + I\rho_{leaf} + \sigma\varepsilon_{sky}(T_{sky}^4 - T_{pv}^4) + \sigma\varepsilon_{leaf}(T_{gr}^4 - T_{pv}^4) \, [\text{Wm-2}] \qquad (5.6)$$

where:

I = solar radiation (Wm^{-2})

α_{pv} = PV module absorption coefficient

ρ_{leaf} = leaf reflectivity coefficient

T_{sky} = sky temperature (K)

The absorption coefficient of PV module (α_{pv}) is defined as 0.9 and the leaf reflectivity (ρ_{leaf}) is 0.5. The emissivity of the sky for clear and cloudy sky is 0.95 and 1 respectively (Hanlin and Stein, 2012). The emissivity of the leaf is 0.94 (Bramson, 1968). The sky (T_{sky}) temperature for clear sky is derived from Swinbank's (Tang et al, 2004):

$$T_{sky} = 0.0552(T_a)^{1.5} \, [\text{K}] \qquad (5.7)$$

while T_{sky} for a cloudy sky is equal to the air temperature (Jones, 2001)

The energy emitted by the PV module

The emitted energy from a PV module ($Q_{pvemmit}$) is the long wave radiation from the PV module to the sky and to the green roof. It is calculated using the following equation:

$$Q_{pvemmit} = \sigma \varepsilon_{pvfront}(T_{pv}{}^4 - T_{sky}{}^4) + \sigma \varepsilon_{pvback}(T_{pv}{}^4 - T_{gr}{}^4) \text{ [Wm-2]} \qquad (5.8)$$

The PV module in the experiment set up is covered by a transparent tempered glass and a white Polyethylene terephthalate (PET). To simplify the equation, the absorptance as well as the emittance values of the PET is assumed to be 0.9 and 0.8 respectively. σ is the Stefan-Boltzman constant.

The convective heat transfer

The convective heat transfer above and below the PV module is calculated using Equation:

$$Q_{pvconv} = h_{cpv}(T_{pv} - T_{apvtop}) + h_{cpv}(T_{pv} - T_{apv\_gr}) \text{ [Wm}^{-2}\text{]} \qquad (5.9)$$

The convective heat coefficient for convective energy exchange above and below the surface of the PV module is determined by the Nusselt number, which is explained in the following equation:

$$Nu = 0.664 \, \text{Re}^{1/2} \text{Pr}^{1/3} \text{ [dimensionless]} \qquad (5.10)$$

where, Re is the Reynolds number and Pr is the Prandtl number. To define the convective heat coefficient, it is necessary to check the pattern of the wind over the PV module by calculating the Reynolds number. The expression is as follows:

$$\text{Re} = \frac{\rho V_x}{\mu} \text{ [dimensionless]} \qquad (5.11)$$

where, ρ is the density of the fluid, V_x is the kinematic viscosity and μ is the dynamic viscosity of the fluid. In external condition the laminar flow is defined when the Re number is less than 5×10^5.

The Prandtl number is calculated to compares two molecular transport mechanisms. This number is the function of temperature and is influenced by the physical properties of the fluid (Krauter, 2006). The equation is as follows:

$$\text{Pr} = \frac{\mu c_p}{k} \text{ [dimensionless]} \qquad (5.12)$$

where, μ is the dynamic viscosity of the fluid, c_p is the specific heat capacity, and k is the thermal conductivity of air.

Hence, the heat convective coefficient is calculated by the following equation:

$$h_{cpv} = \frac{Nu k_{fluid}}{D_h} \text{ [Wm}^{-2}\text{K}^{-1}] \qquad (5.13)$$

where, Nu is Nusselt number, k_{fluid} is the fluid's thermal conductivity, where the value is 0.0257 $\text{Wm}^{-1}\text{K}^{-1}$. D_h is the hydraulic diameter (here is the distance between the canopy and the PV module temperature (300 mm).

The heat from green roof

The incoming heat from green roof ($Q_{greenroof}$) into the PV module is determined by the sensible heat (Q_{grsens}) and the latent heat flux (Q_{grevap}). The sensible heat flux from green roof is calculated by the following equation:

$$Q_{grsens} = h_{cgr}(T_{gr} - T_{apv-gr}) \, [\text{Wm-2}] \qquad (5.14)$$

The heat convective coefficient uses Eq 5.13.

Convection from the PV module to the air gap

The convection heat from natural ventilation in the air gap is defined as the mass transfer heat of the PV module to the air gap (*mvent*). The equation model is adopted from Friling et al (2009):

$$m_{vent} = fV_w \rho c_p (T_{in} - T_{out}) \, [\text{kgm}^{-2}\text{s}^{-1}] \qquad (5.15)$$

where,

f is the effectiveness of the openings which depends on the geometry and the orientation and with regards to the wind. The value of this fraction is adopted from the EnergyPlus documentation and the value is in the range of between 0.25 and 0.6 and the smallest fraction is used for this equation. V_w is the air velocity. ρ is the air density and the value for Singapore climate condition, where the air temperature and the relative humidity is around 30 °C and 80%, is 0.910 kgm^{-3}. It is obtained from Kaye and Laby (1973) (Table 5.1). c_p is the specific heat of air and (T_{in}-T_{out}) is the

difference between inlet and outlet. These temperatures are measured 15 cm from the canopy of the plants.

Table 5.1 Density of Air at different absolute Pressures, Temperature, and Relative humidities (from Kaye and Laby, 1973)

Density of Air, ρ_a (kg/m^3)			
Absolute Air Pressure, $\bar{u}$ (kPa)	Temperature, t (^{0}C)		
	10	20	30
80.000	0.982	0.946	0.910
85.000	1.043	1.005	0.968
90.000	1.105	1.065	1.025
95.000	1.167	1.124	1.083
100.000	1.228	1.184	1.140
101.000	1.240	1.196	1.152
105.000	1.290	1.243	1.198

Source: Fredlund and Rahardjo, 1993
Latent heat flux from the evapotranspiration process

The latent heat flux as the product of the evapotranspiration process (Q_{grevap}) is determined by: multiplying the latent heat vaporization (λ) and evapotranspiration rate. The evapotranspiration rate is derived from the model described in Eq. 4.11. Details are discussed in Chapter 4. All variables used in the ET rate model as well as their sources are provided in Appendix 4 and 5.

5.4. Calculation method.

The proposed equation (Eq. 5.4) of the dynamic temperature change is nonlinear which has to be reflected in the numerical solution rather than the analytical solution, especially for each irradiance and temperature value. The calculation therefore will use the Euler method for integration of a differential equation. The Euler method of calculation of T_m (PV module temperature) at time step (t+1), given T_m at time step

(t) and the rate of change from eq. 5.4 can be illustrated as follows (Jones and Anderwood, 1999):

$$T_m(t+1) = T_m(t) + step \frac{dT_m}{dt} \; [°C]$$ (5.16)

The Euler method is an initial value method, so that the first time step value of T_m is required. In this study the initial T_m is set equal to the ambient temperature. This assumption is reasonable, since the calculation of the PV module temperature starts at 07:00 am, when the solar radiation intensity is around zero.

5.5. Validation procedure

The procedure for validating the prediction model used Root Mean Standard Deviation (RMSD). The equation is explained as follows:

$$RMSD = [\frac{1}{n} \sum (P_i - O_i)^2]^{1/2}$$ (5.17)

where, n is the number of observation, P_i is the value of the measured PV module temperature and O_i is the predicted value of the PV module temperature.

5.6. Field Experiment

The instrumented integrated PV module and green roof was located on the roof top of the School of Design and Environment at National University of Singapore. The

details of the experiment set up are provided in Chapter 6.2 and 7.2. In general, the experiment set up consists of two PV modules which were mounted on two different sub layers, concrete roof and green roof. The total area of the green roof is 6.25 m^2. The arrangement of the set-up is derived from the energy balance principle (Fig. 7.1) and used a single PV module for each roof top material.

The use of a single PV module to validate thermal and optimal modeling of PV module has also been applied by Krauter (2006). His experiment set-up is illustrated in Fig. 5.3. The temperature sensors were attached at the backside of the PV module. Furthermore, according to his study, there was a large difference occurred when the wind speed exceed far from 2 ms^{-1}.
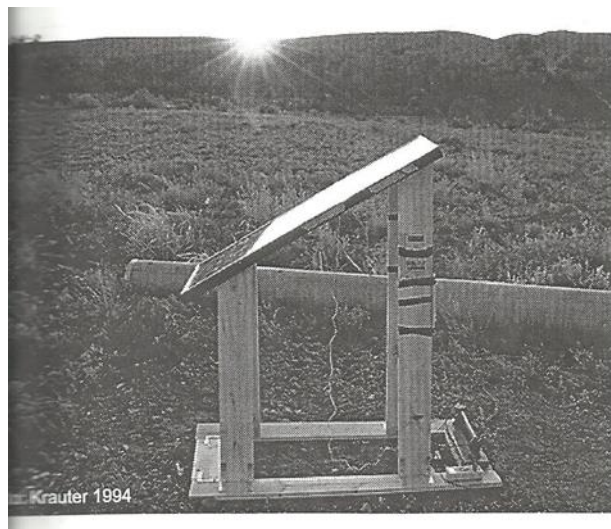
Figure 5.3. Experiment set-up conducted by Krauter (2006)

5.7.   Results and discussion

Clear Day

Figure 5.4 shows one typical example of the calculated and measured PV module temperature comparison under clear sky condition. The selected day is 16th June

2012. Table 5.2 summarises the prevailing weather conditions on that day. It can be observed from Fig 5.4 that the curve of measured and calculated PV module temperature over green roof are in good agreement. The root mean square deviation (RMSD) of the calculated PV module temperature is 2.13 °C. Large deviations occur in the morning and in the afternoon with around 2 °C, while on the mid-day the difference is smaller.

Table 5.2 Weather conditions on 16th June 2012

Total hourly Solar radiation (Whm-2)	Average wind speed (ms-1)	Average air temperature (°C)	Average relative humidity (%)
5.639	2.1	30.1	72.2
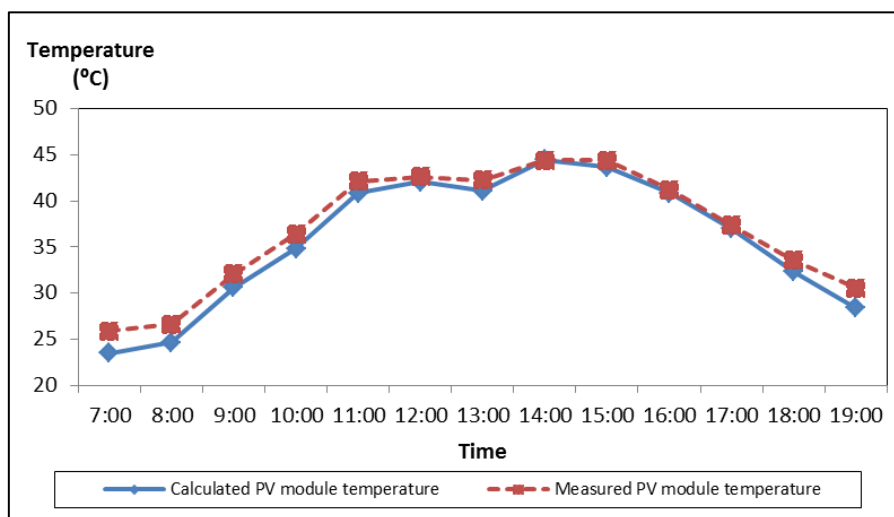
Figure 5.4. Comparison between measured and calculated PV module temperatures over the green roof under clear sky condition on 16th June 2012

Furthermore, based on the regression analysis (Fig. 5.5) the coefficient of determination (R^2) of the calculated PV module temperature over the green roof under clear sky condition is 0.98. Three days of measured and calculated PV module temperature over green roof are used in the regression analysis. Figure 5.6 shows the comparison of the diurnal measured and calculated PV module temperature over green roof of three days measurements and calculations.
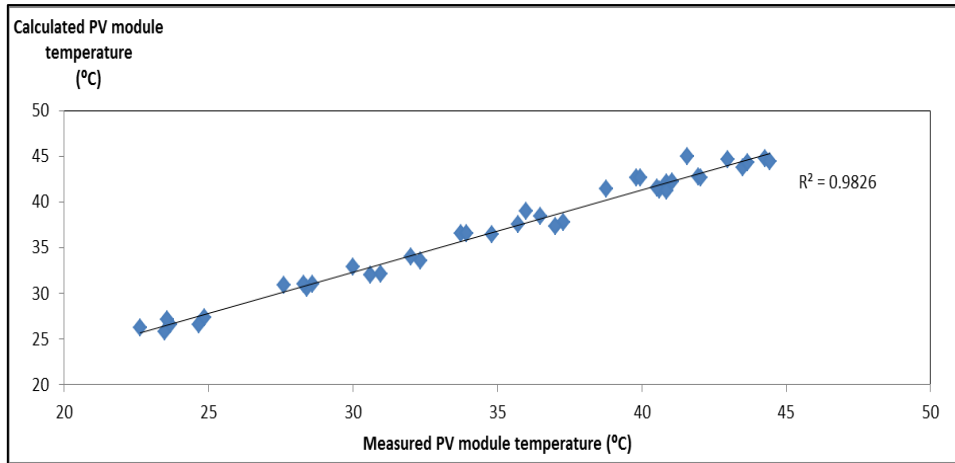
Figure 5.5. Regression analysis between calculated and measured PV module temperatures over the green roof under clear sky conditions

Figure 5.6. Three days calculated PV module temperature on clear days

Intermediate Days

The selected intermediate day for the comparison between the calculated and measured PV module temperature over green roof is 19th June 2012. The weather conditions are summarized in Table 5.3

Table 5.3 Weather conditions on 19th June 2012

Total hourly Solar radiation (Whm-2)	Average wind speed (ms-1)	Average air temperature (°C)	Average relative humidity (%)
4,717	1.5	29.6	77.9

The comparison between measured and calculated PV module temperature over green roof under intermediate sky condition (Fig. 5.7) shows a relatively larger deviation as compared to that under clear sky conditions. The prediction model of the PV module temperature has an RMSD of 2.25 °C. It is observed that on mid-day the calculated temperature is higher than the measured temperature, on the other hand, an opposite trend is occurs in the morning and in the afternoon (Fig.5.7).

However, from Fig. 5.9, it can be observed that there is a relatively unstable trend on the calculated PV module temperature, which is particularly occur in the mid-day and the regression results show less than 0.9 (Fig. 5.8). It indicates that the equation model is less accurate for the intermediate sky condition.
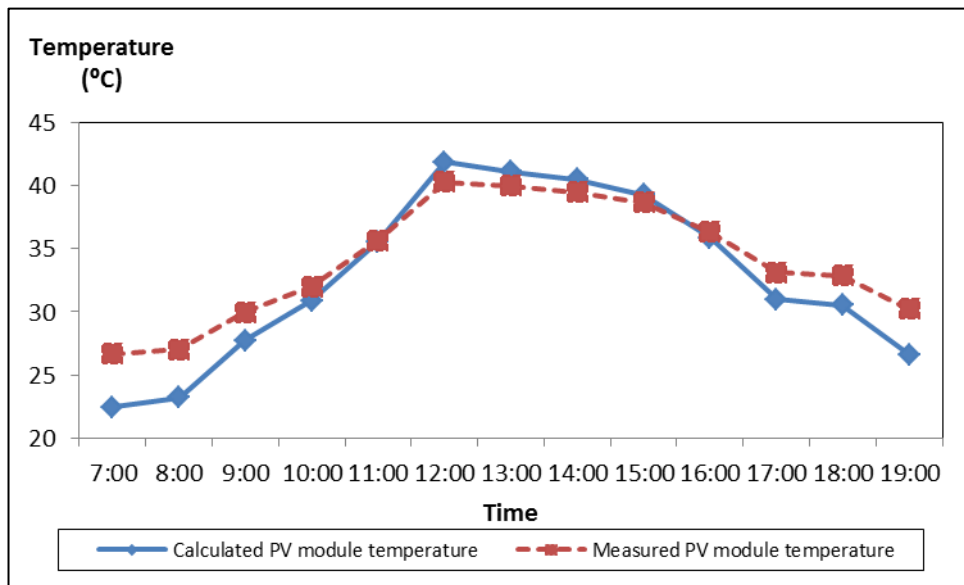
Figure 5.7. Comparison between measured and calculated PV module temperatures over the green roof under intermediate sky condition

104
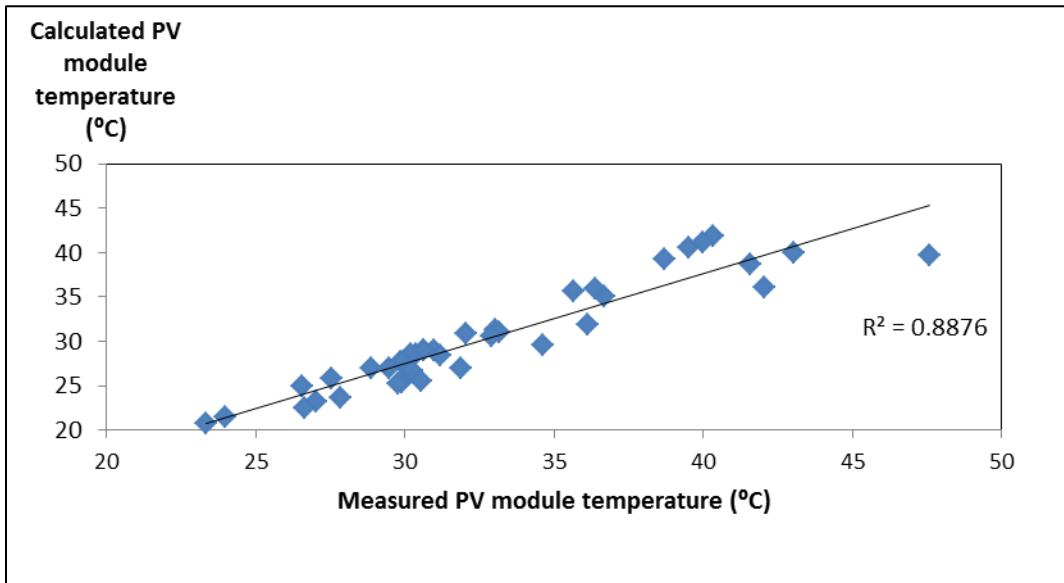
Figure 5.8. Regression analysis between calculated and measured PV module temperatures over the green roof under intermediate sky condition
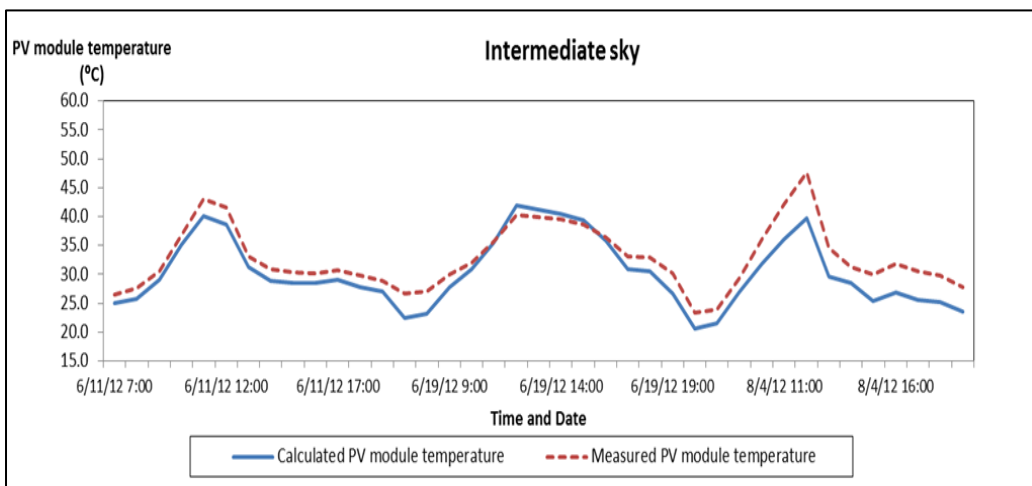
Figure 5.9. Three days calculated PV module temperature on intermediate days

Overcast days

On overcast days, the calculated PV module temperature showed a minor temperature variation as compared to the measured PV module temperature for the entire whole day, with the shape of the curve of the calculated PV module temperature closely following the actual PV module temperature (Fig. 5.10). Furthermore, the R^2 value

is 0.93 with the RMSD of 1.192 °C. The value of the RMSD is obtained from the three days measurements (Fig. 5.12).

Table 5.4 summarizes the weather conditions on that day. It is observed that the relative humidity was high and may cause a high vapor pressure and result in a more complex environment condition as compared to which on clear day. However, the equation model could calculate the PV module temperature relatively well which can be observed in Fig 5.10.

Table 5.4 Weather conditions on 8th June 2012

Total hourly Solar radiation (Whm-2)	Average wind speed (ms-1)	Average air temperature (°C)	Average relative humidity (%)
2,048	1.3	28.4	84.9
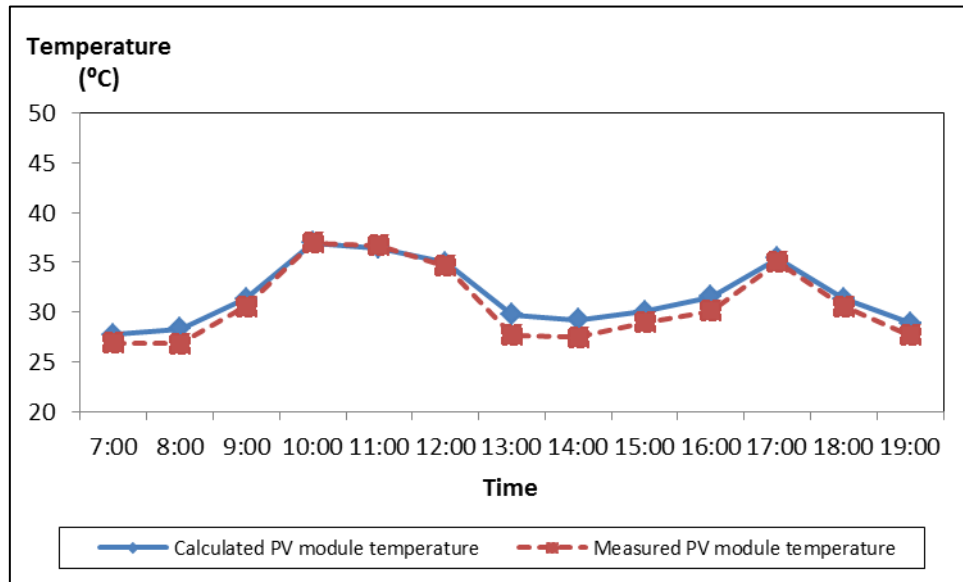
Figure 5.10. Comparison between measured and calculated PV module temperatures over the green roof under overcast sky condition
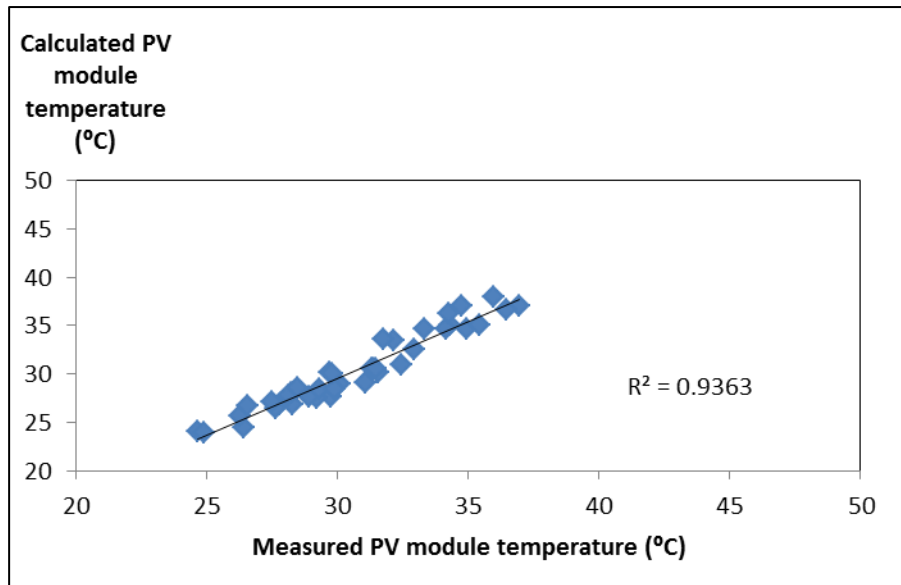
Figure 5.11. Regression analysis between calculated and measured PV module temperatures over the green roof under overcast sky condition
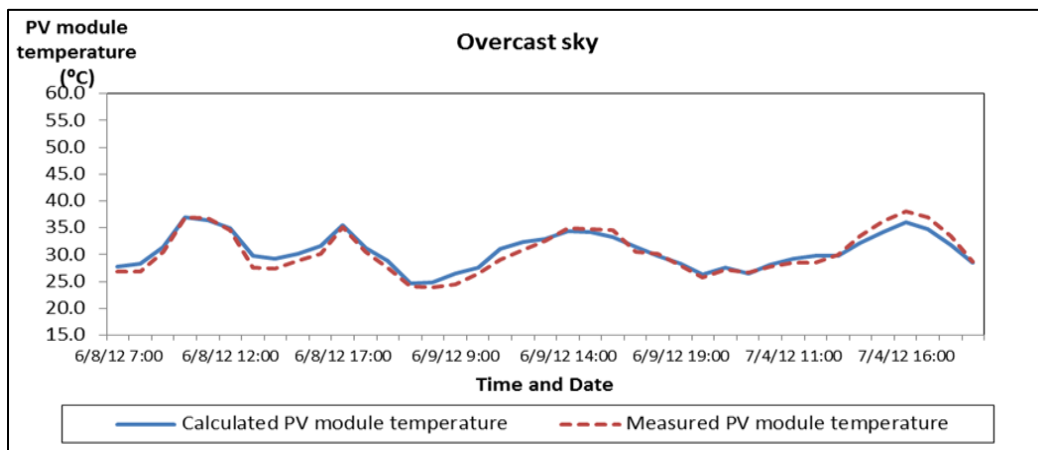
Figure 5.12 Three days calculated PV module temperature on overcast days

From Fig. 5.4-5.12, the calculated PV module temperature over green roof could show a relatively good agreement with the measured PV module temperature (The R^2 is above 0.8). The overall RMSD of the calculated PV module temperature over green roof for all sky is between 1.19 °C and 2.25 °C, in which the RMSD of the PV module under intermediate sky condition was the highest.

From all the comparison analyses above, a significant notification can be identified that a larger temperature difference occurs generally over intermediate sky condition. Noticeable evidence can be observed from the value of its coefficient of determinant which is less than 0.9. The fluctuated solar radiation value and the wind speed may cause larger temperature variation between the measured and the calculated PV module temperature.

5.7.1. The effect of the PV module temperature predictions over the green roof on the expected PV module power output

The measured power output in this study was obtained by Eq 2.2 and 2.3 in which the operating PV module temperature is provided by the measurement. In terms of the calculated power output, the temperature is provided by the predicted PV module temperature calculated by the proposed equation (Eq 5.4).

Fig. 5.13 shows that in the morning, from 08:00 h to 12:00 h, and the afternoon, from 16:00 h to 19:00 h, the measured power output was similar with the calculated value, even though the measured PV module temperature is slightly higher than the calculated PV module temperature. On the opposite, there is a slightly difference in the power output between the measured and the calculated PV module performance when the PV module temperature exceed far from 30 $^{\circ}$C which occurred in mid-day. This evidence implies that the PV power performance is influenced by the PV module temperature when it increases above 30 $^{\circ}$C. Hence, the RMSD of the calculated PV power output is 0.03 Watt.

The same trend of PV module performance also appeared on the intermediate day. It can be observed in Fig. 5.14 that the PV module temperature influences the PV module power output when the module temperature is above 30 $^{\circ}$C. As a result, the

RMSD of the calculated PV module power output under this type sky condition is 0.05 Watt.
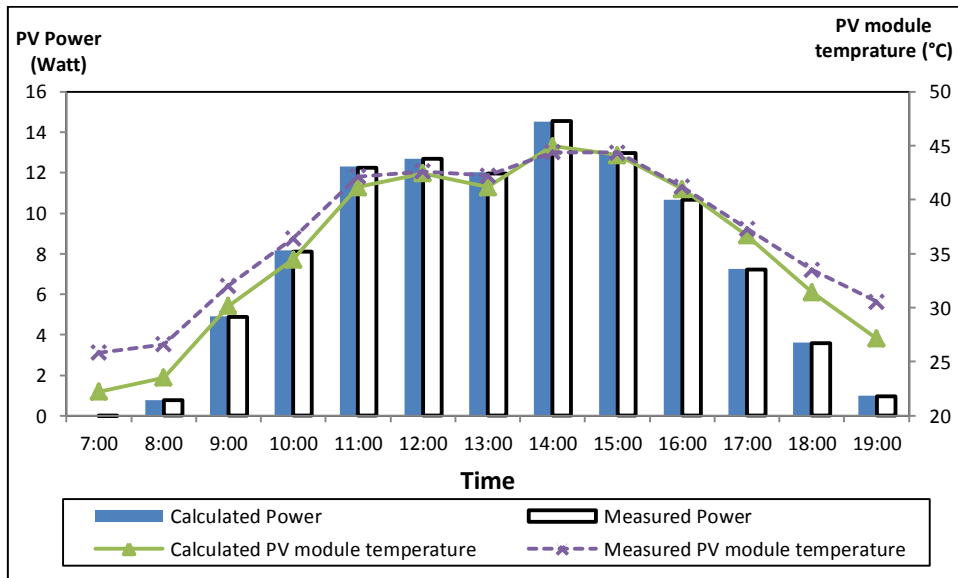
Figure 5.13 Calculated and measured PV module power output and module temperature over the green roof on a clear day
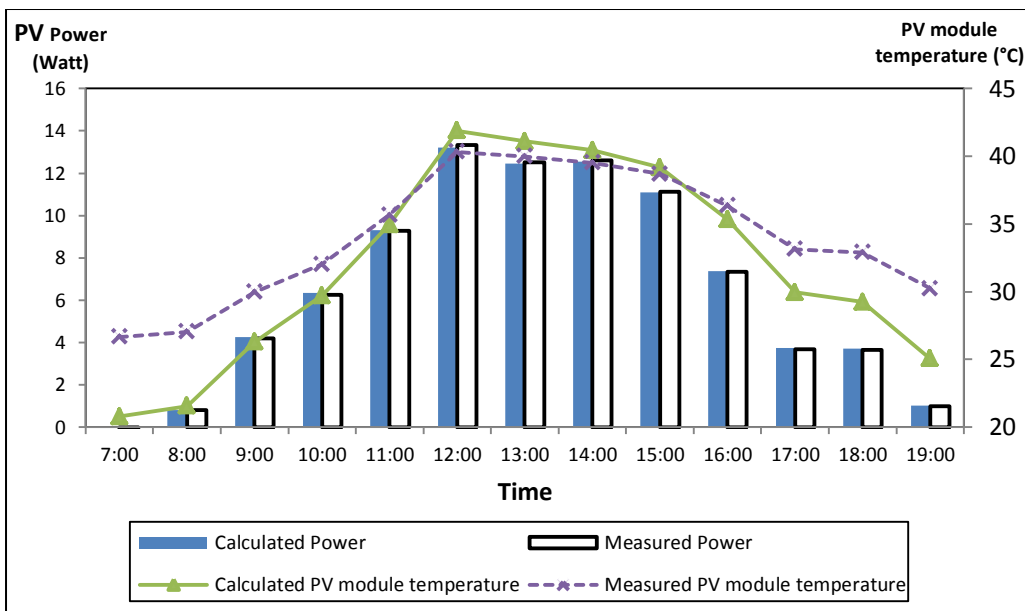
Figure 5.14. Calculated and measured PV module power output and module temperature over the green roof on an intermediate day
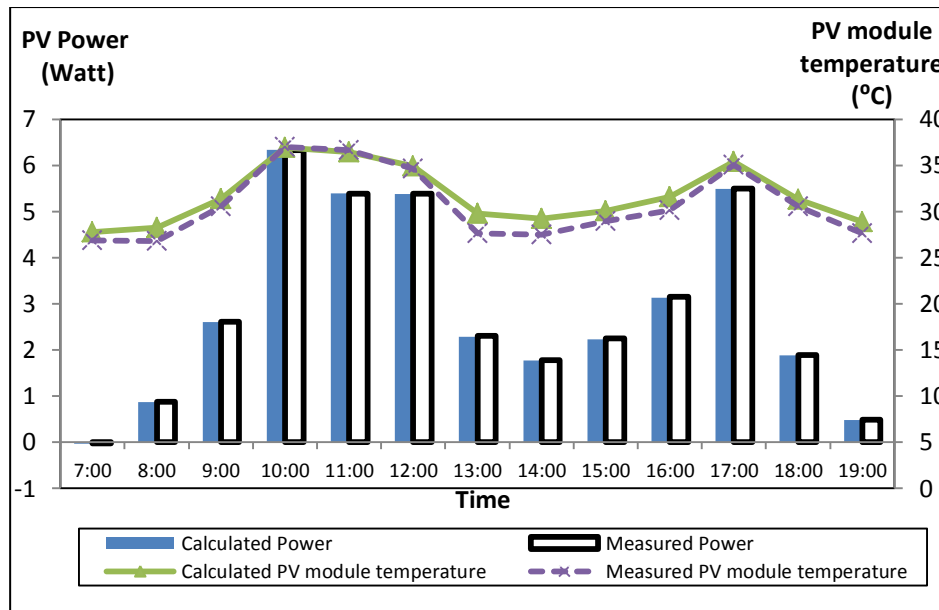
Figure 5.15. Calculated and measured PV module power output and module temperature over the green roof on an overcast day

On the overcast day, the RMSD of the calculated PV power performance is 0.04 Watt, with the temperature difference between the calculated and the measured PV module temperature of around 1 °C for almost the whole day. This evidence is in line with the previous trend that the PV performance variation is not significant, if the PV module temperature difference occurred below 30 °C.

Based on the results above, the expected calculated PV power output shows relatively small deviations. The RMSD is between 0.03 Watt and 0.05 Watt.

5.8. Predicted PV module temperature over concrete roof

In addition, the predicted dynamic change of PV module over concrete roof is also derived here. The numerical model is derived from the proposed equation (5.4), but the portion of the latent heat flux is eliminated. Hence, the equation is outlined in Eq. 5.18.

$$m_{pv}\frac{C_{pv}}{A}dT_{pv} = I\alpha dt + I\rho_{cr}dt + \sigma\varepsilon_{sky}(T_{sky}^{4} - T_{pv}^{4})dt + \sigma\varepsilon_{cr}(T_{cr}^{4} - T_{pv}^{4})dt + \sigma\varepsilon_{pvfront}(T_{pv}^{4} - T_{sky}^{4})dt + \sigma\varepsilon_{pvback}(T_{pv}^{4} - T_{cr}^{4})dt +$$

$$h_{cpv}(T_{pv} - T_{apvtop})dt + h_{cpv}(T_{pv} - T_{apv\_cr})dt + h_{cr}(T_{gr} - T_{apv-cr})dt - fV_{w}\rho c_{p}(T_{in} - T_{out}) - \frac{P_{out}}{A}dt$$

(5.18)

This analysis uses the same approach as in Chapter 5.6.

5.8.1. Results and discussion

Figure 5.15 to 5.23 show the comparisons between the measured and the calculated PV module temperatures over the concrete roof under three sky conditions.

Clear days
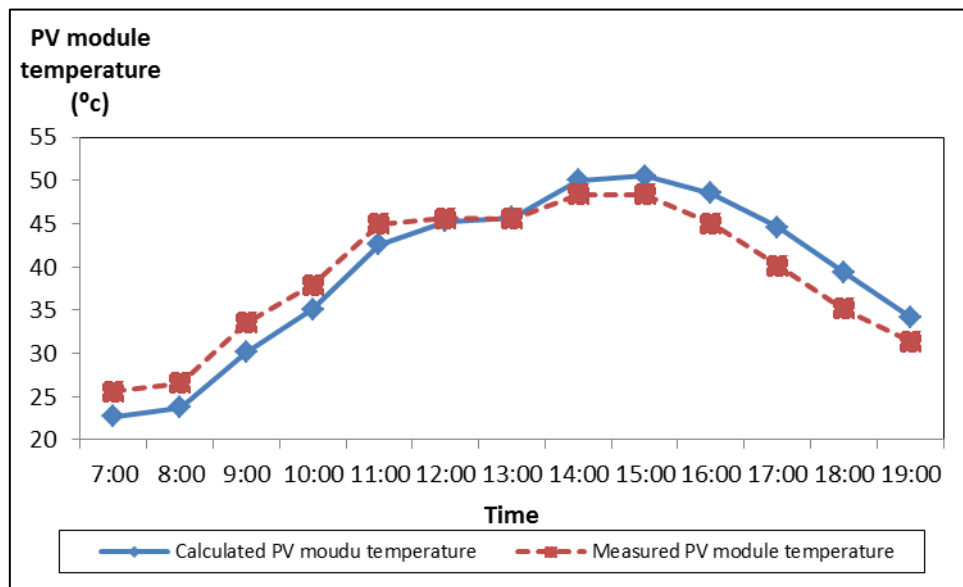
Figure 5.16. Comparison between measured and calculated PV module temperature over the concrete roof under clear sky conditions

Figure 5.16 shows that on a clear day the diurnal temperature of both measured and calculated is relatively in good agreement. A large deviation occurs in the morning between 07:00h and 10:00h, and in the afternoon between 14:00h and 19:00h. The

root mean deviation square (RMSD) for the calculated PV module temperature is 2.70 °C. This small variation is also apparent in the regression analysis (Fig.5.17). The R^2 is above 0.92 and it demonstrates a good correlation between the measured and the calculated PV module temperature. The regression analysis is computed based on data from three days of measurements (Fig. 5.18).
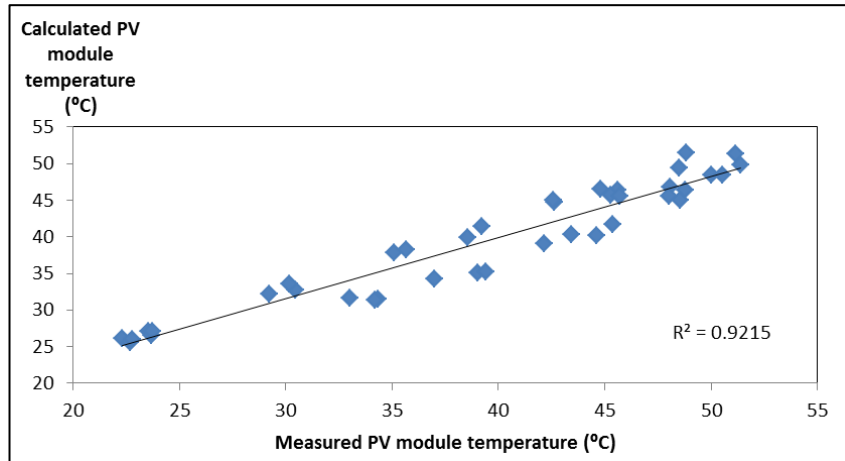
Figure 5.17. Regression analysis between calculated and measured PV module temperatures over the concrete roof under clear sky condition
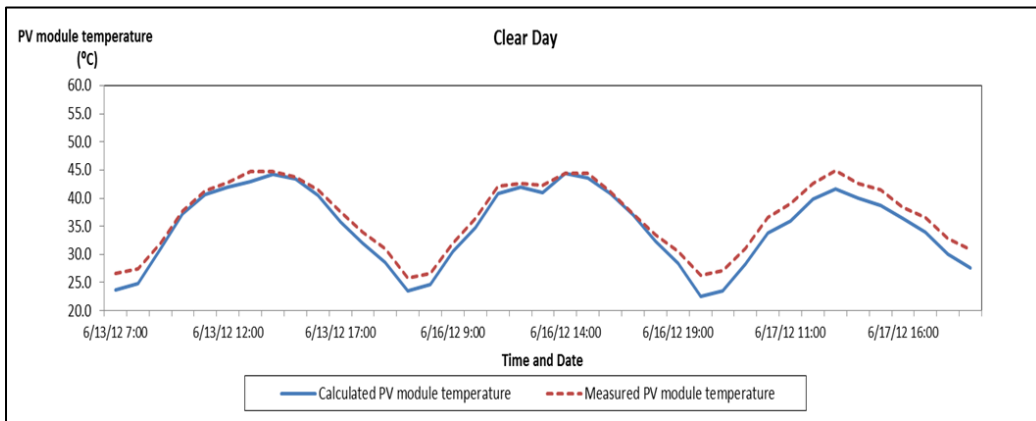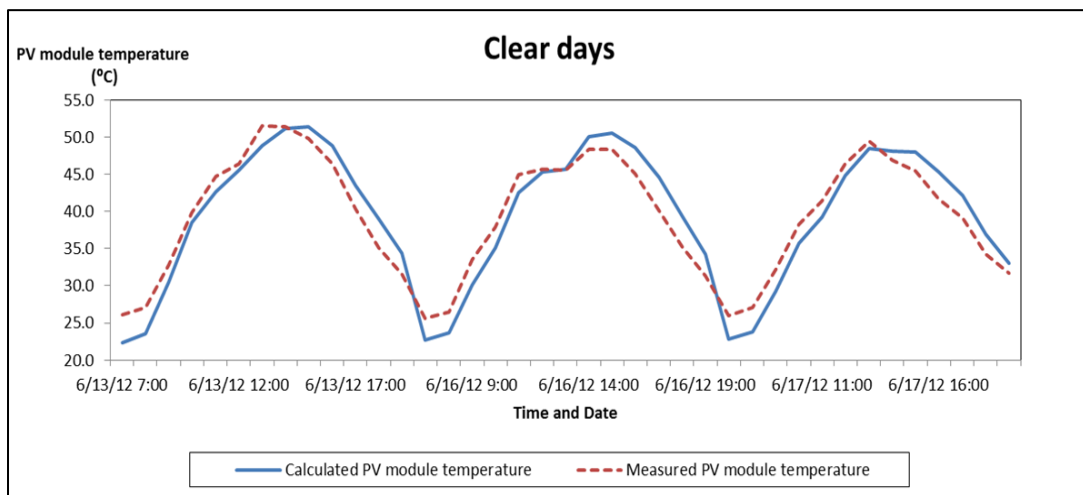

Figure 5.18. Three calculated PV module temperature over concrete roof on clear days

Intermediate days

Figure 5.19 shows an example of the calculated PV module temperature compared to the measured PV module temperature under a typical intermediate sky conditions. It

can be observed that a relatively large difference occurred in the afternoon. The difference between the two graphs can be as large as 2.5 °C and the total the RMSD of the calculated PV module temperature is 2.26 °C and it is derived from three days measurement. From the three days measurement, it can be observed that the diurnal calculated PV module temperature is in a good agreement with the measured PV module temperature (Fig. 2.20).
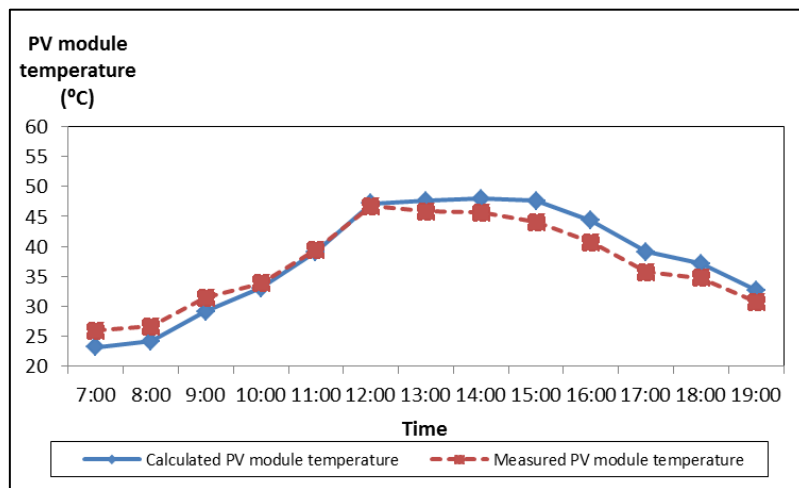
Figure 5.19. Comparison between measured and calculated PV module temperature over the concrete roof under intermediate sky conditions
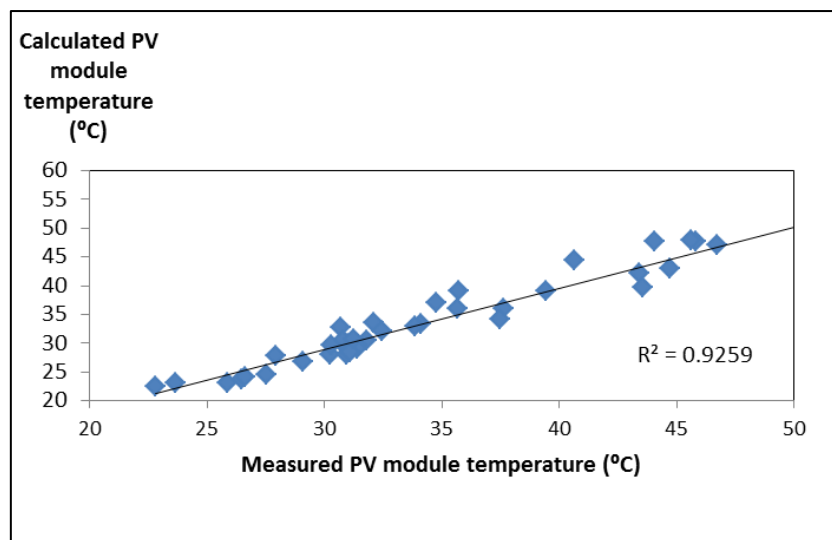
Figure 5.20. Regression analysis between calculated and measured PV module temperatures over the concrete roof under intermediate sky condition

113
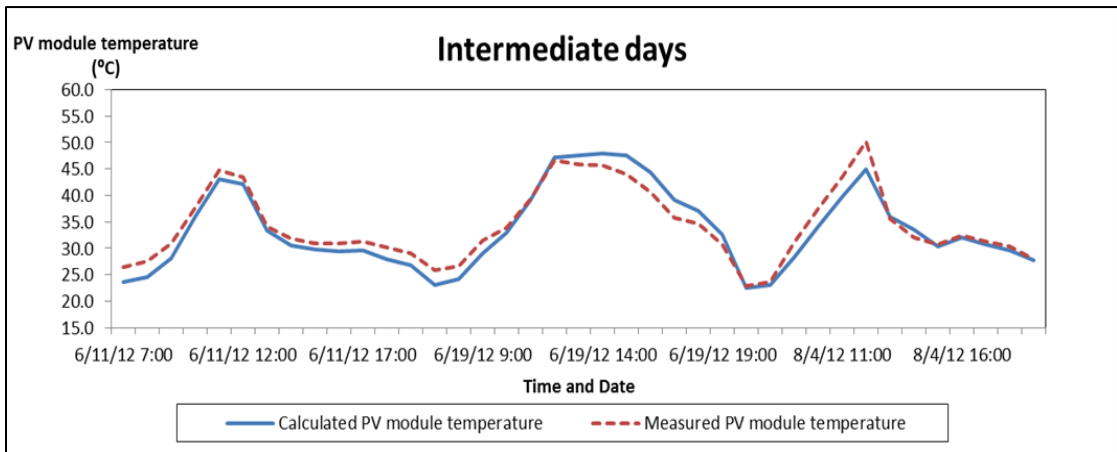
Figure 5.21 Three calculated PV module temperature over concrete roof on intermediate days

In terms of the correlation between the measured and the calculated PV module temperature, Fig. 5.20 shows that the correlation is high ($R^2=0.92$).

Overcast days
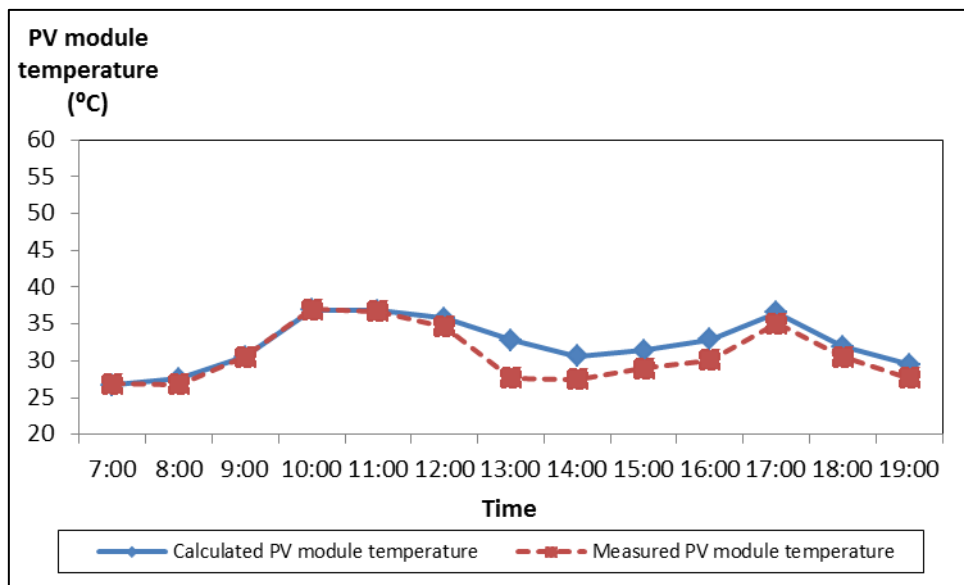
Figure 5.22. Comparison between measured and calculated PV module temperature over the concrete roof under overcast sky conditions
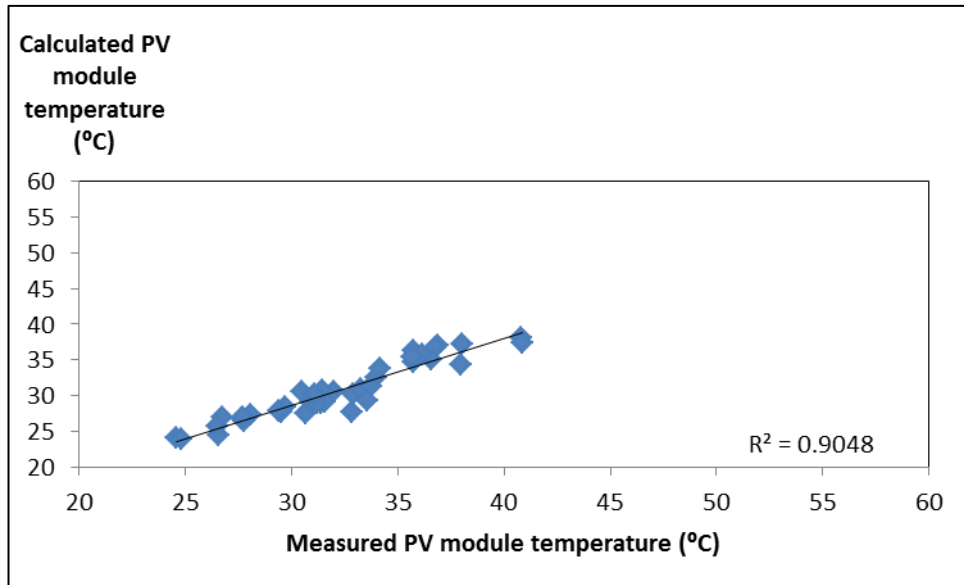
Figure 5.23. Regression analysis between calculated and measured PV module temperatures over the concrete roof under overcast sky condition

On overcast days, a relatively small temperature difference between the calculated and the measured PV module temperature is apparent for almost the whole day (Fig. 5.22), with the RMSD of 2.02 °C. This relatively small temperature difference impacts also on the coefficient of determinant (R^2) which is 0.90 for three days measurement and calculation (Fig. 5.23 and Fig. 5.24).
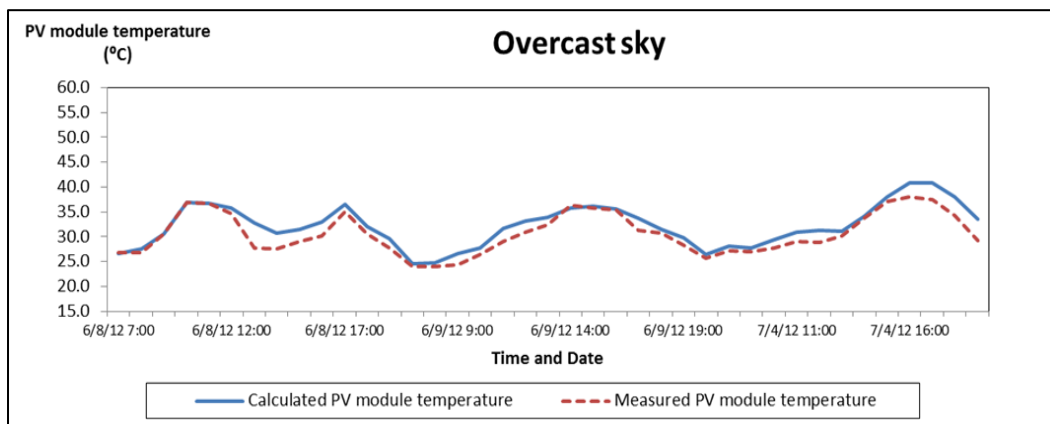
Figure 5.24. Three calculated PV module temperature over concrete roof on overcast days

115

5.8.2. The effect of the PV module temperature predictions over a concrete roof on the expected PV module power output

The analysis uses the same approach of PV power output calculation which also be done in Chapter 5.6.1. The predicted PV module temperature is derived from Eq. 5.18.

Figure 5.25 shows that there is no significant difference on the amount of the PV power output. A large temperature difference between the calculated and the measured PV module temperature, which occured in the morning when the overall PV module temperature were still within 30 °C, do not result in large variation of the PV power output when the. This is in accordance with the findings on the PV power output prediction of the PV modules over the green roof. Hence, the RMSD for the predicted PV power for PV module over concrete roof under clear sky condition is 0.1 W.
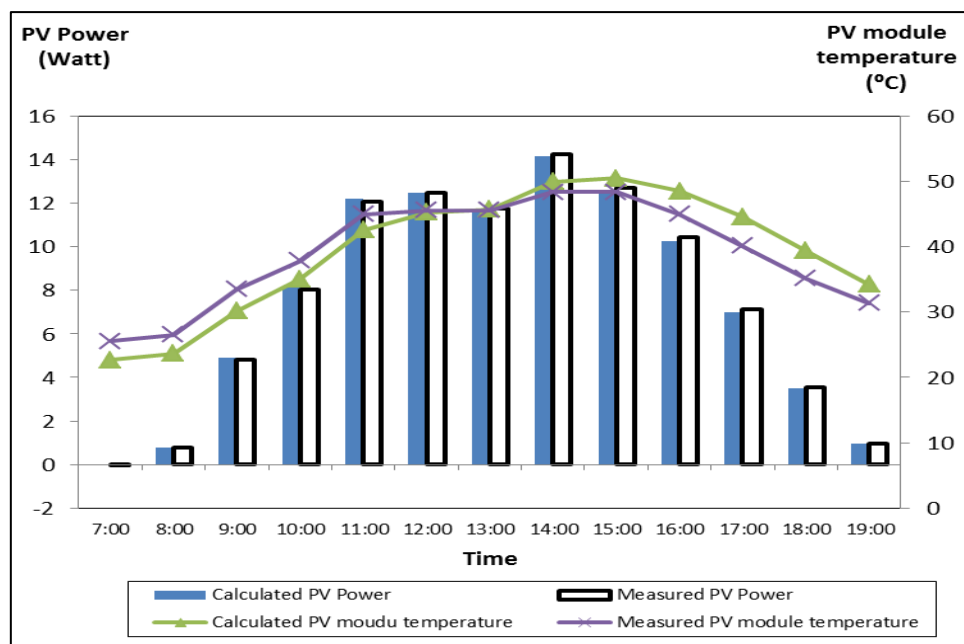
Figure 5.25. Calculated and measured PV module power output and module temperature over the concrete roof on a clear day

116

On an intermediate day, since there is a relatively larger difference between the calculated and the measured PV module temperature in the afternoon, therefore, the measured PV power output shows a relatively higher than the calculated PV power output (Fig. 5.26). Hence, the RMSD for the calculated PV power in this typical day is 0.08 Watt.
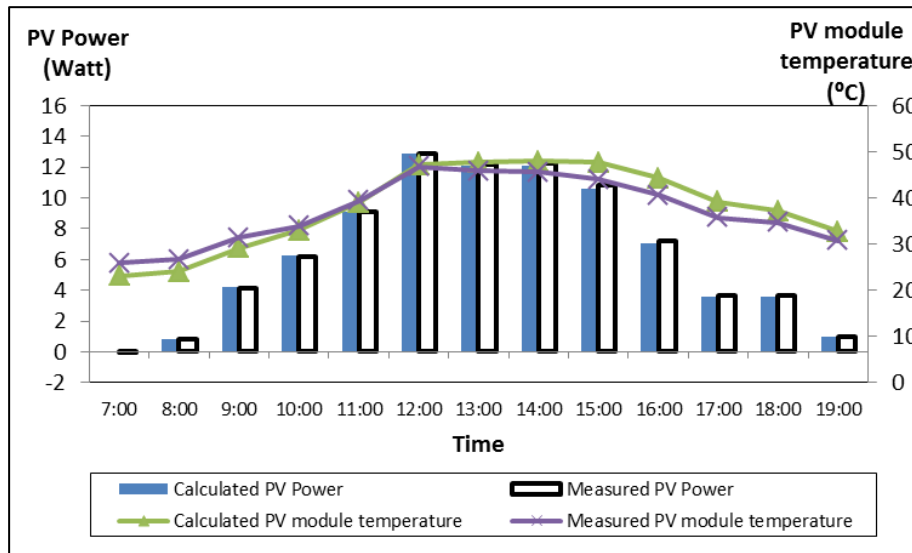
Figure 5.26. Calculated and measured PV module power output and module temperature over the concrete roof on an intermediate day
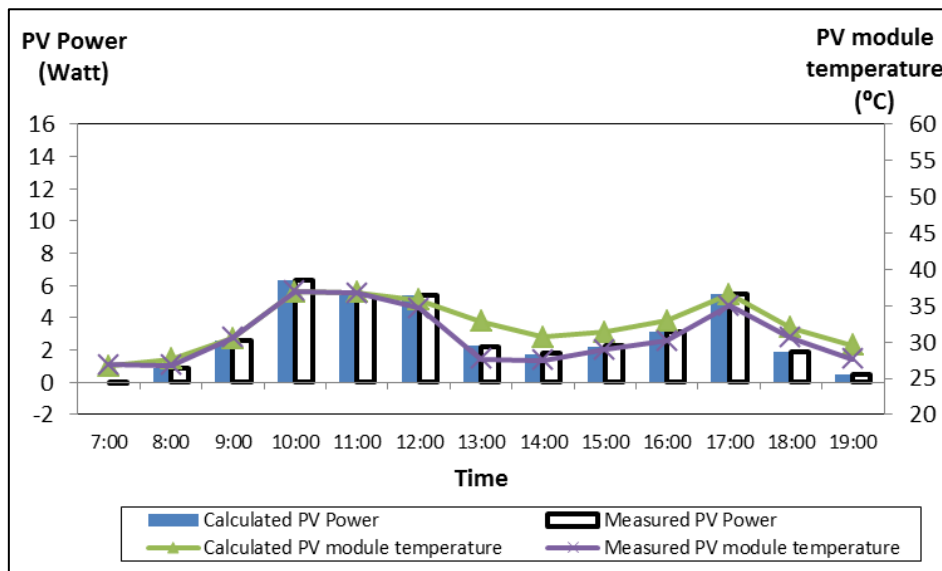
Figure 5.27. Calculated and measured PV module power output and module temperature over the concrete roof on a overcast day

On an overcast day the PV power output which is derived from the calculated PV module temperature, shows similar compared to the PV power output which was derived from the measured PV module temperature (Fig. 5.27). Hence, the RMSD for the calculated PV power is only 0.02 Watt where this value is smaller than the RMSD on intermediate day. It is in accordance with the findings from the prediction of the PV power output over the green roof on an overcast day (Fig. 5.18). This evidence underline the fact that temperature differences arises at below 30 °C have a small impact on the PV power output.

5.9. Conclusion.

A numerical model for predicting the PV module temperature over a green roof influenced by evapotranspiration process has been outlined based on the principle of Energy Balance and resulted in a modified numerical model (Eq. 5.4). In addition, a numerical model for the PV module over a concrete roof is also formulated by eliminating the term for the evapotranspiration rate (Eq. 5.19). A comparison study of the calculated and the measured PV module temperatures has been conducted to validate the proposed numerical model. Furthermore, this chapter also presents the analysis of the expected PV power output derived from the calculated PV module temperature. Based on the comparison study between the calculated and the measured PV module temperatures, there are some substantial evidences:

1. Calculated PV module temperature over green roof:
- The modified equation could represent suitably the measured PV module temperature over the green roof, particularly on a clear day and overcast day with the RMSD of 2.13°C and 1.19 °C respectively . The coefficient of determinant is observed above 0.9. While, on an intermediate day, an unstable trend of calculated PV module temperature occurred particularly in

the mid-day. In consequence, the RMSD is slightly higher (3.26 $^{\text{o}}$C). Eventually, it also impact on the results of the coefficient of determinant (R^2 =0.88).

- It is observed that there is an increase in the RMSD when the weather condition is unstable like on intermediate day.

- Hence, this evidence indicates that the proposed numerical model may not capture the temperature of a PV module under intermediate condition.

- The expected PV module power output, calculated from the calculated PV module temperature, could represent the measured PV performance. The RMSD for all type of sky conditions are marginal.

2. Calculated PV module temperature over a concrete roof:

- In general, the results of the comparison study show that the calculated PV module temperature over concrete roof is in accordance with the measured PV module temperature.

- The predicted numerical model suitably corresponds to the measured PV module temperature.

- RMSD and the R^2 of the calculated PV module temperature are generally below 3 °C and above 0.9 respectively.

CHAPTER 6 THE EVALUATION OF THE EVAPOTRANSPIRATION

This chapter presents the evaluation of the evapotranspiration rate obtained from the field experiments. It was conducted to investigate the amount of water change into vapor over particular vegetation, namely *Complaya trilobata*. These particular plants were planted in the tested green roof system under the tropical climate conditions of Singapore. Furthermore, this experiment is also to determine the amount of latent heat flux transferred from the plants into the environment.

6.1. Methodology

The measurement methodology applies the Bowen Ratio Energy Balance (BREB) approach. The sensor allocations for measuring the gradient temperature and water vapor pressure follow the ratio between the length of the fetch and the highest elevation point of the sensor. The ratio should not be less than the minimum requirement of 10:1. The Advection index (AI) is also calculated for each measurement series to check the level of the advective heat influence over the green roof. If the AI, calculated by Eq. 6.1, is higher than 1, it means that the evapotranspiration rate is significantly affected by the advective heat. The results with high AI will consequently not be considered for the ET analysis, as it breaks the assumption of a closed system where the sum of all energy is zero.

6.1.1. Bowen Ratio Energy Balance

The latent heat flux is obtained from the calculation of the energy budget of the surface covered with an active growing crop. The required data, however, cannot be

measured directly; therefore, the method of Bowen ratio is applied. Further details of the Bowen ratio energy balance equation can be found in Chapter 4.2.1.
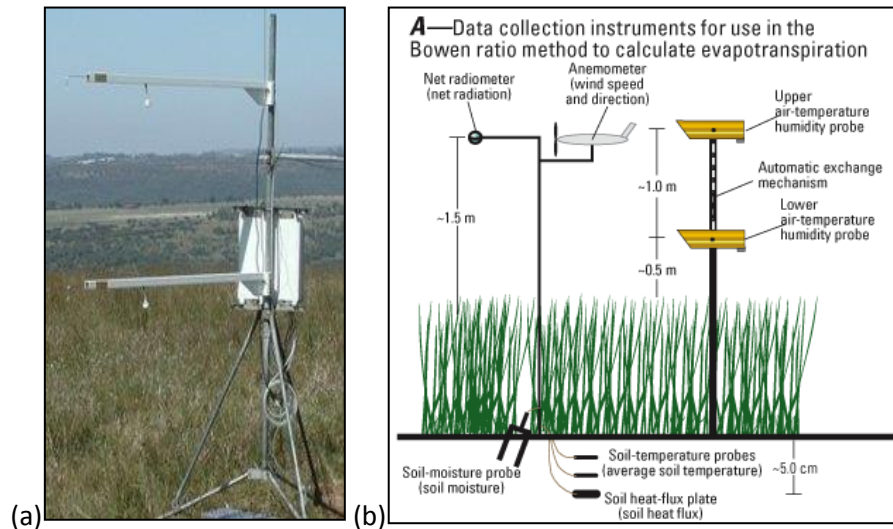
Figure 6.1 (a) Example of a Bowen ratio measurement equipment; (b) Schematic diagram of Bowen ration energy balance from a particular experimental set up. The height of temperature and humidity probe is determined by the area of the green roof.
Source: (a) http://www.mdpi.com; (b) http://pubs.usgs.gov

The approach of this method is generally applied to measure the gradients of air temperature and vapor pressure in the near surface layer above the evaporating surface. Figure 6.1 illustrates the example of the set-up of the Bowen ratio energy balance field experiment. The temperature and vapor pressure gradient are generally measured around 0.3 m above the dense canopy but should be installed higher up in case of tall and sparse crops and in order to avoid disturbance of the temperatures and vapor profiles due to micro-scale turbulences from within the plants and differences between locations from where heat and evaporation process originate. The temperature and relative humidity measurement should consider the ratio between the fetch and the height of the equipment to gain an average representatives surface condition. It also applies for the upwind measurement. The soil heat flux density is generally read at 0.05-0.15 m below the surface. It has to be ensured that the soil flux

density is obtained below the zone of soil water vaporization, also to reduce the effect of the vertical heat conduction near the flux plate (Allen et al., 2011).

The advantages of BR calculation method are as follows: (1) it is a preferred estimation method as it requires no data about the aerodynamic characteristics of a particular surface, (2) it can estimate the heat fluxes on a constrained time scale and (3) it allows for continuous and unattended measurements. Additionally, Tanner (1960) stated that the Bowen Ratio provide advantages for calculating the latent heat flux, because (1) BR is less sensitive to errors in the measurement of the gradient temperature and water vapor pressure; (2) Wind profile data is not required for the Bowen ratio calculation; (3) The ratio between fetch and the sensors location is not critical. All those advantages can be leveraged for an area of plants with rich of water as well as in humid environment.

Todd et al (2000) highlighted that for the BR measurement method several assumptions are required which however do not significantly compromise its accuracy. The transport is assumed to be one-dimensional and with no horizontal gradients. Sensors which measure gradients are assumed to be located within the equilibrium sub layer where fluxes are assumed to be constant with height. The surface is assumed to be homogeneous with respect to sources and sinks of heat, water vapor and momentum.

6.1.2. Ratio between fetch and sensors

Homogeneous conditions of the surface are important to avoid a large error in the calculation. In order to achieve the equilibrium condition, Panofsky and Townsed

(1964) has stated that the ratio of the fetch to the highest position of BR measurement for temperature and humidity gradient could be from 10:1 to 200:1. Subsequently, Heilmann and Brittin (1989) confirmed that the Bowen ratio method can be used successfully at fetch-to-height ratio as low as 20:1, much less than the often quoted value of 100:1. This recent study also supported the calculation of Yeh and Butsaert (1971) which reported that the BR method is not sensitive to imperfect fetch conditions as long as the Bowen ratio is small. The term of fetch is determined by the distance of the field edge to the location of the BR equipment, and it is illustrated in Fig 6.2. In the figure there are three different locations which is determined by the ratio between the fetch and the highest measurement point. The fetch are arranged at 5 m, 15 m, 30 m and 70 m from the South East direction. The equilibrium sub layer is shown in Fig 6.2. (b). The thermocouples are installed above the equilibrium sub layer, only for the one at the fetch of 30 m and 70 m which are measured at 2 August. From Heilmann and Brittin (1989) study, the results of the Bowen ratio measurement, which were not within the equilibrium sub layer, is similar.
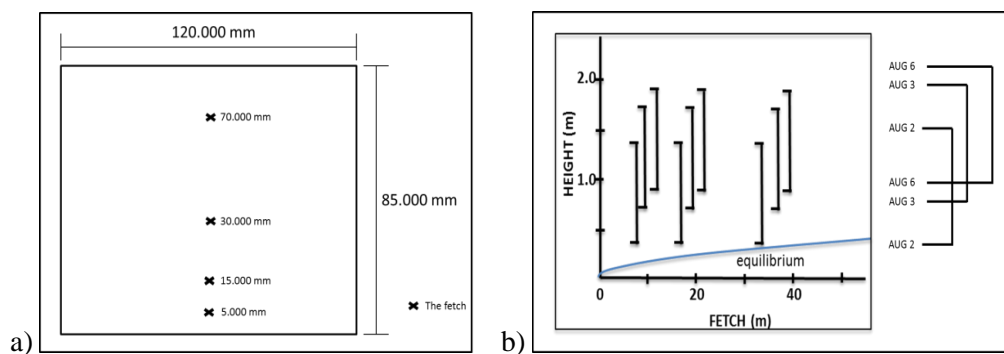
Figure 6.2. (a) The experimental area. (b) The equilibrium sublayer over the fetch
Source: Heilmann and Brittin (1989)

6.1.3. Energy advection calculation and correction

When the area of the green roof is relatively small compared to surrounding roof surface material such as concrete, it is possible that advection transports energy horizontally in the downwind direction. The Advection Index (*AI*) provided by Todd et al (2000), is therefore used to identify the advection resulting from the combined effect of temperature, vapor pressure deficit, available energy and wind speed. The index is the ratio of latent heat flux λET and the difference between net radiation (R_n) and soil heat flux (G):

$$AI = \frac{\lambda ET}{R_n - G} \text{ [dimensionless]} \tag{6.1}$$

The advection can be significant if the index exceed 1 (*AI* >1).

Todd et al (2000) also indicated that the greatest bias of the BR method occurred on days that were hot, dry and windy. In this condition the value of BR (β) can levels of up to -1. To avoid any distortion, the observations under these conditions should be consider as invalid data and discarded from the data analysis.

6.2. Experiment set up

The green roof was built from 50 cm x 50 cm planter boxes with the depth of 13 cm, consisting of hi-green lite composite substrate and a treated non-organic soil-less volcanic ejecta substrate (see Fig. 6.3). *Complaya trilobata* or Weedelia, a type of shrub that can grow well under semi-shaded conditions, was selected for evapotranspiration rate evaluation. The leaf area index of the plants is around 3.5 in order to provide sufficient evapotranspiration rate and cooling effect. The total weight

of the planter box including the soils and the plants under full water storage is around 25 kg.

Water is supplied by perforated pipes with the diameter of 1 cm and is distributed at 6 am and 6 pm for 1 hour by a timer-controlled valve. The total water mass distribution for 1 day irrigation is around 5 kg. The pipes are installed on the top of the soil. The automatic irrigation is used to deliver sufficient water for the plants in order to facilitate an unrestricted evapotranspiration process. The area of the green roof is constructed larger than the PV module to provide homogeneous conditions around the PV module. This arrangement is designed also to enable infrared radiation exchange between gray surfaces (Duffie, 2006). Otherwise, if there are two parallel plates and the ratio between the first and the second is close to zero, no radiation leaving the small object is reflected back from the large enclosure, which means that the large enclosure absorbs all radiation from the small object and acts like a black body.
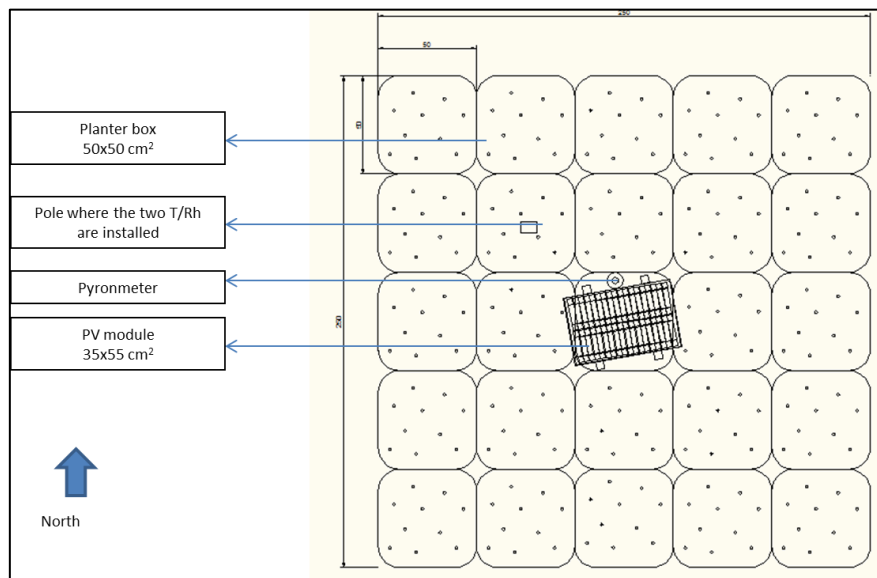
Figure 6.3. Lay out of the experimental green roof with the PV module in the center

The experiment was carried out on the unshaded roof top of the School of Design and Environment at the campus of the National University of Singapore (NUS) (Fig. 6.4). The selected roof top is a concrete roof top with the latitude and longitude of 1.2971°N and 103.7706°E respectively.

Figure 6.4. The experiment location at campus of the National University of Singapore

6.2.1. Method of data collection

The method of data collection can be described as follows:

1. The solar radiation values were measured by a CM 6B Pyranometer in 5-min intervals for 24 hours a day and were collected by datalogger.

2. A weather station with anemometer, rain gauge and data logger was used to measure the microclimate condition, such as wind speed, air temperature, humidity and rainfall data. The data also logged in 5-minute intervals for 24 hours day. The weather station was mounted 2 m above the roof surface and was located near the green roof.

3. The differences in temperature (ΔT) and humidity (ΔRh) were measured at two different heights and it is assumed that the diffusivity for heat and water vapor are equal (Dugas et al., 1991). There are two such concurrent measurement points at 6 cm and 12 cm height using a HOBO H8 Pro

temperature/relative humidity data logger. The data were recorded also in 5-minutes intervals, 24 hours a day.

4. The surface temperature of the green roof is defined at the space between the top canopy of plants and the soil and it was measured by thermocouples.

The list of equipment and their respective accuracy is summarized in Table 6.1.

1. T/Rh Hobo with data logger
2. Pyranometer
3. Thermocouple
4. Planter box
5. PV module
6. Thermocouple in between leaf's canopy and soil.
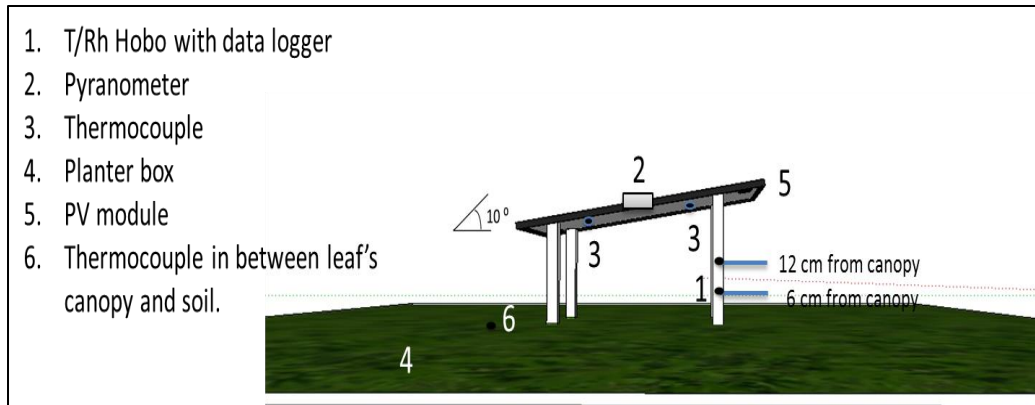
Figure 6.5. The schematic of sensors allocation at PV over green roof

a) PV module over concrete roof
b) PV module over green roof
c) Weather station with raing gauge and datalogger
d) Yokogawa datalogger
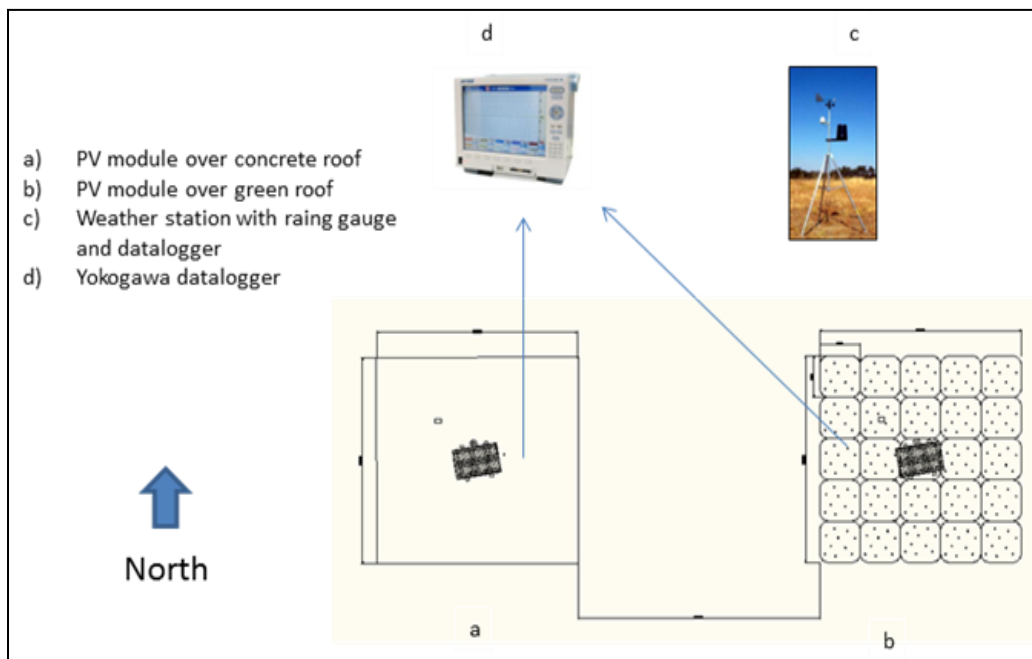
Figure 6.6. The schematic of data logging

6.2.2. Instrumentation

The technical details of the instrumentation used in the experiment is listed in Table

6.1

Table 6.1. List of equipment with the parameters and accuracy

Parameter	Instruments	Accuracy
Local weather	HOBO weather station with rain gauge	NA
Irradiance	Pyranometer CM 6B, Kipp&Zonen	$\pm 5\%$
Surface temperature	Type T-thermocouple wire	$\pm 0.2\%$
	Yokogawa datalogger	NA
Ambient temperature and humidity	HOBO H8 Pro temperature/relative humidity data loggers	± 0.5
Voltage	Yokogawa datalogger	NA

6.3. Results and Discussion

6.3.1. Clear sky condition

A typical day was selected for this analysis (13 June 2012). The weather conditions

are summarized in Table 6.2. The diurnal evapotranspiration rate under clear sky

condition is illustrated in Fig 6.7 with respect to the solar radiation level.

Table 6.2. Weather conditions on 13 June 2012

Total hourly Solar radiation (Whm-2)	Average wind speed (ms-1)	Average air temperature (°C)	Average relative humidity (%)
6,075	1.7	30.2	74.2

In general, it is observed that the highest evapotranspiration rate was around 1.2×10^{-4} $kgm^{-2}s^{-1}$ and the average evapotranspiration rate during this type of day was 8.3×10^{-5} $kgm^{-2}s^{-1}$. Fig. 6.8 shows that the water vapor deficit under clear sky condition is high. The deficit can reach to almost 4500 Pa. This high deficit could be caused by reducing the moist condition over the green roof under high solar radiation intensity.
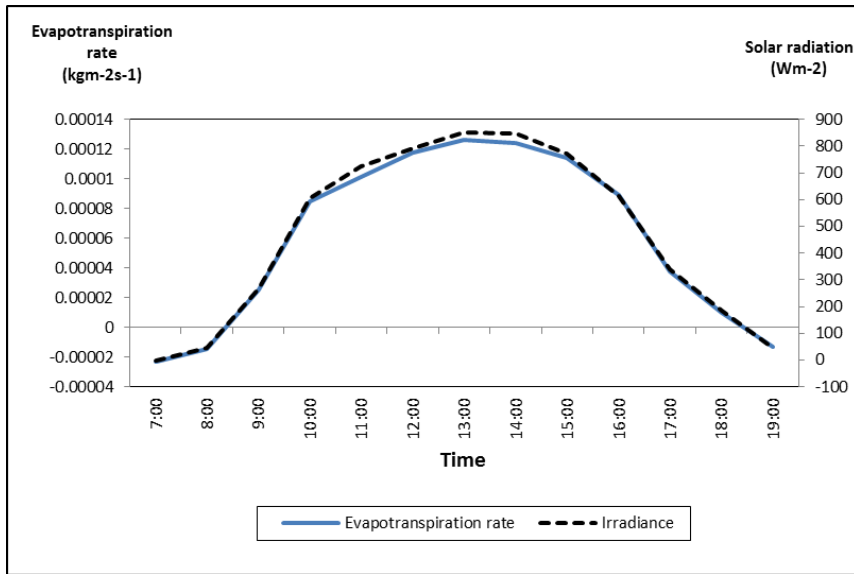
Figure 6.7 The diurnal evapotranspiration rate and under irradiance level under clear sky conditions
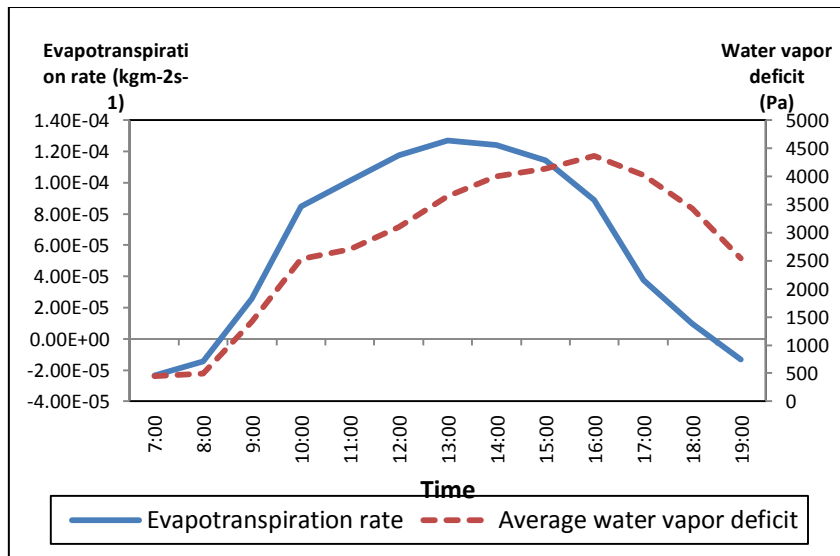
Figure 6.8 The diurnal evapotranspiration rate and water vapor deficit under clear sky conditions

Table 6.3 shows the latent heat flux with respect to the advection index. The values are calculated by the Bowen ratio energy balance (BREB) equation using the Bowen Ratio (β) and then multiplied by the latent heat of vapourisation of water (Eq. 4.2). It can be seen from the table that the latent heat fluxes are below the net radiation, which eventually resulted in a low Advection Index (AI). The index was between 0.96 and 0.95 with the Bowen Ratio between -0.0039 and 0.0062. These Advection Index ratios demonstrate that the source energy of the evapotranspiration rate still predominantly causes from the solar radiation. Nevertheless, the advection heat from the surrounding does appears but only in a little magnitude.

Table 6.3 Latent heat flux and Advection Index under clear sky condition

Time	Bowen ratio β	Latent heat flux (Wm^{-2})	Net radiant (Wm^{-2})	Advection Index
7:00	0.0028	-57.05	-59.59	0.96
8:00	0.0062	-35.35	-37.05	0.95
9:00	0.0045	62.64	65.54	0.96
10:00	0.0040	206.14	215.59	0.96
11:00	0.0045	246.10	257.51	0.96
12:00	0.0040	285.38	298.46	0.96
13:00	0.0049	304.56	318.81	0.96
14:00	0.0051	301.14	315.30	0.96
15:00	0.0062	278.03	291.41	0.95
16:00	-0.0008	215.94	224.76	0.96
17:00	-0.0039	91.59	95.04	0.96
18:00	0.0016	23.56	24.58	0.96
19:00	0.0047	-31.90	-33.38	0.96

6.3.2. Intermediate sky condition

Table 6.4 shows the weather conditions for a typical intermediate day (12 June 2012) with lower average solar radiation, but similar average wind speeds resulted in lower levels of average air temperature but higher level of relative humidity in the air. Those conditions lead to a reduction of the average water vapor deficit by around 25% (Fig. 6.10). These conditions resulted in the reduction of the average evapotranspiration rate by 5.0×10^{-5} $kgm^{-2}s^{-1}$ or 40% compared to that on clear day.

Table 6.4 Weather conditions on 12 June 2012

Total hourly Solar radiation (Whm-2)	Average wind speed (ms-1)	Average air temperature (°C)	Average relative humidity (%)
4,133	1.6	29.0	81.0
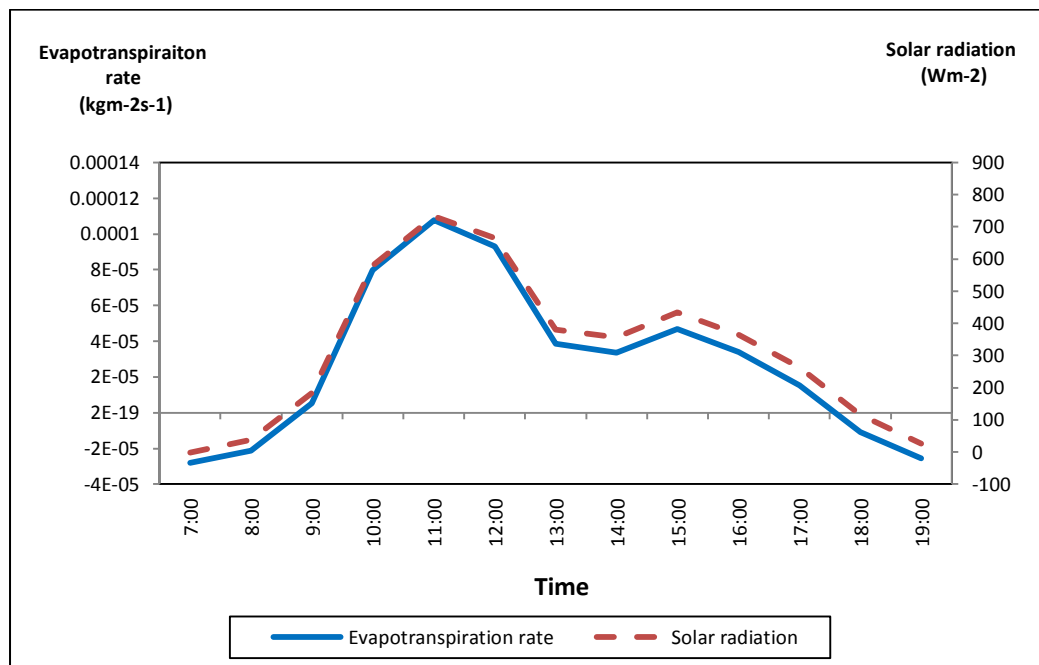
Figure 6.7 The diurnal evapotranspiration rate and under irradiance level under intermediate sky conditions
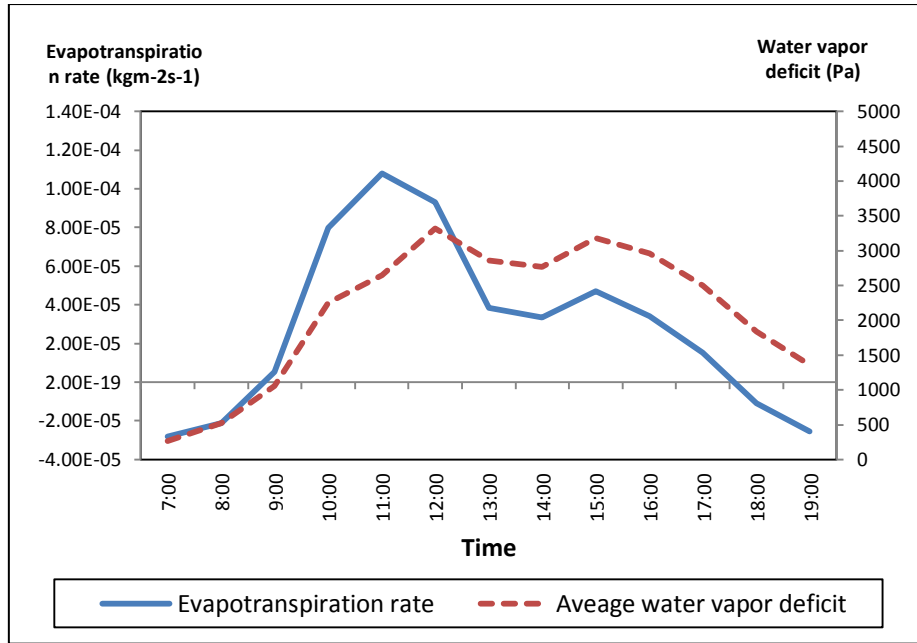
Figure 6.8 The diurnal evapotranspiration rate and water vapor deficit under intermediate sky conditions

Table 6.5 Latent heat flux and Advection Index under intermediate sky condition

Time	Bowen ratio β	Latent heat flux (Wm^{-2})	Net radiant (Wm^{-2})	Advection Index
7:00	0.012206	-68.78	-72.52	0.95
8:00	0.008328	-51.57	-54.17	0.95
9:00	0.003432	12.91	13.49	0.96
10:00	0.003476	194.20	202.99	0.96
11:00	0.002998	261.99	273.72	0.96
12:00	0.003069	225.85	235.98	0.96
13:00	0.002941	93.46	97.64	0.96
14:00	0.002002	81.34	84.90	0.96
15:00	0.001892	113.95	118.93	0.96
16:00	0.001355	82.67	86.23	0.96
17:00	0.00047	37.29	38.87	0.96
18:00	0.002691	-26.50	-27.68	0.96
19:00	0.005006	-62.54	-65.47	0.96

From Fig 6.9, it can be observed that the diurnal evapotranspiration rate is fluctuating in parallel with the available energy provided by the solar radiation. The highest ratio of the Advection Index is 0.96 at the Bowen Ratio of 0.00047 while the lowest ratio of the Advection Index is 0.95 at the Bowen Ratio of 0.012 (Table 6.5). The average advection index is less than 1 with the average Bowen ratio of 0.0034. Hence, it shows that the influence of advection heat from the surrounding is relatively small.

6.3.3.   Overcast sky conditions

Table 6.6 shows that during overcast sky conditions (here: 19th June 2012), the total hourly solar radiation is very low resulting in a low air temperatures (26 °C). However, the average relative humidity is comparably high at around 88%.   The average wind speed is about the same as in clear and intermediate sky conditions. These weather conditions result in a large variation of evapotranspiration rate as compared to the clear day readings.

Table 6.6 Weather conditions on 19 June 2012

Total hourly Solar radiation (Whm-2)	Average wind speed (ms-1)	Average air temperature (°C)	Average relative humidity (%)
1,940	1.5	26.0	88.0

As expected the evapotranspiratio rate under overcast sky conditions is relatively low, with the average rate of only 2.7×10^{-5} kgm^{-2}s^{-1}, equivalent to a 68% reduction from the average of evapotranspiration rate under clear sky conditions.   The evapotranspiration rate under overcast conditions also shows higher variability.

The ratio of the Advection Index shown in Table 6.7 is generally between 0.94 and 0.99. The Bowen Ratio during this period of the day is between -0.044 and 0.026. The highest ratio of the Advection Index occurs at the Bowen Ratio of -0.044, while the lowest ratio of the Advection Index occurs at the Bowen Ratio of 0.026. These results show that, in general, the advection heat from the surrounding is still relatively low, indeed the main source of energy is still provided by solar radiation.
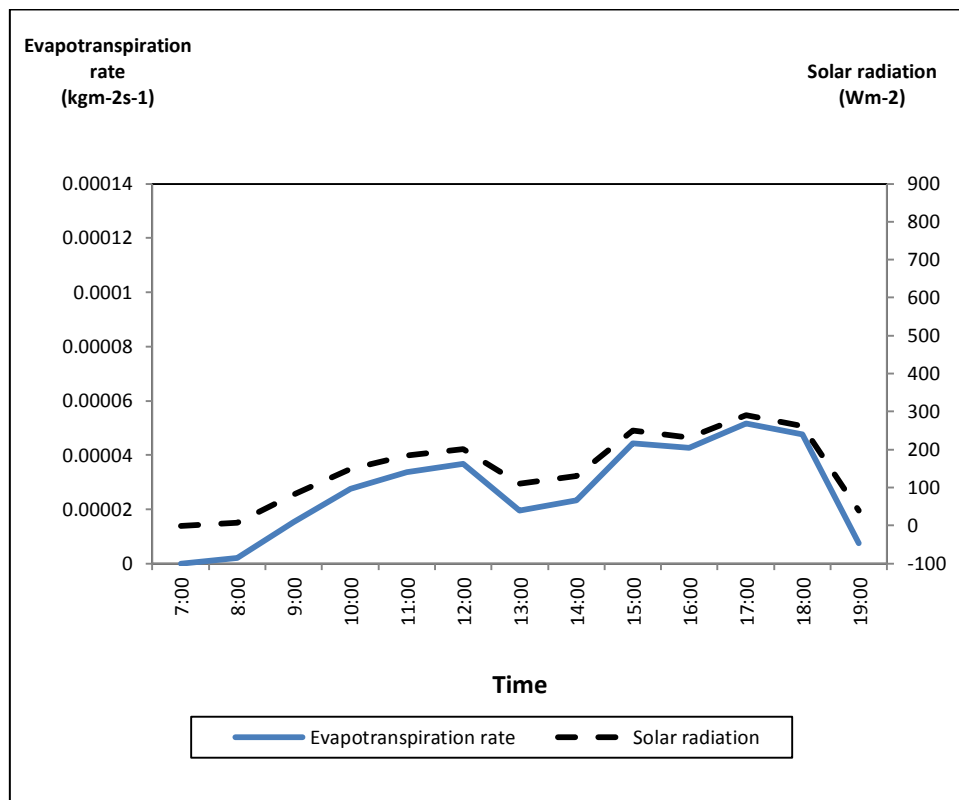
Figure 6.11 The diurnal evapotranspiration rate under clear overcast condition with respect to the irradiance level.

Figure 6.12 shows that in overcast sky conditions the average water vapor deficit is relatively low, only between 0 Pa and 1800 Pa. This result indicates that in these sky conditions, the atmospheric layer contains a lot of water vapor. Furthermore, low wind speed further causes the stagnancy of water vapor movement. However, in the afternoon there is an upward trend of solar radiation intensity and water vapor deficit. This trend leads to a higher evapotranspiration rate.
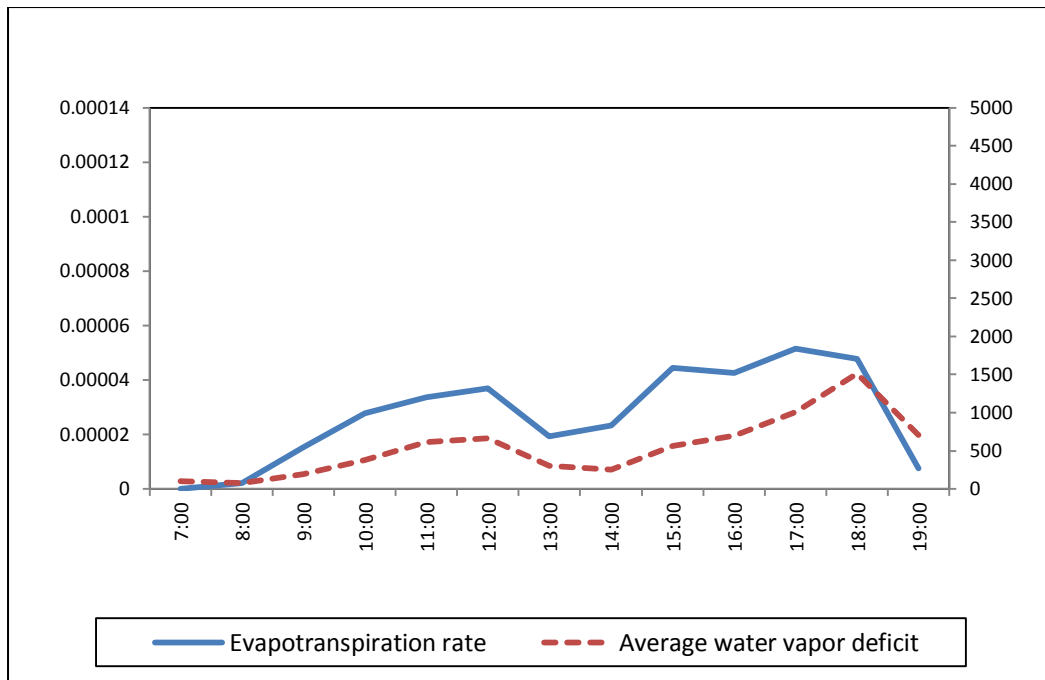
Figure 6.12 The diurnal evapotranspiration rate under overcast sky condition with respect to the water vapor deficit

Table 6.7 Heat flux and Advection Index under overcast sky condition

Time	Bowen ratio β	Latent heat flux (Wm^{-2})	Net radiant (Wm^{-2})	Advection Index
7:00	-0.00129	1.26	1.32	0.96
8:00	-0.00115	5.17	5.38	0.96
9:00	0.001352	37.51	39.13	0.96
10:00	0.002154	67.55	70.51	0.96
11:00	0.001791	82.07	85.64	0.96
12:00	0.002233	90.03	93.99	0.96
13:00	0.026245	47.42	50.70	0.94
14:00	0.000669	57.05	59.47	0.96
15:00	0.001587	108.38	113.07	0.96
16:00	-0.04468	104.17	105.66	0.99
17:00	0.007818	125.97	132.24	0.95
18:00	0.0102	115.94	122.01	0.95
19:00	-0.01051	18.22	18.78	0.97

6.3.4. Discussion

In principle, evapotranspiration process is a process where water contained in soil and plants changes phase into vapor using energy from the outside environment. As mentioned previously in Chapter 2.3.2 that the energy comes from solar radiation, wind and water vapor gradient. Water vapor gradient corresponds to the water vapor deficit. To understand which energy source plays the most important role in evapotranspiration process, a regression analysis was conducted.
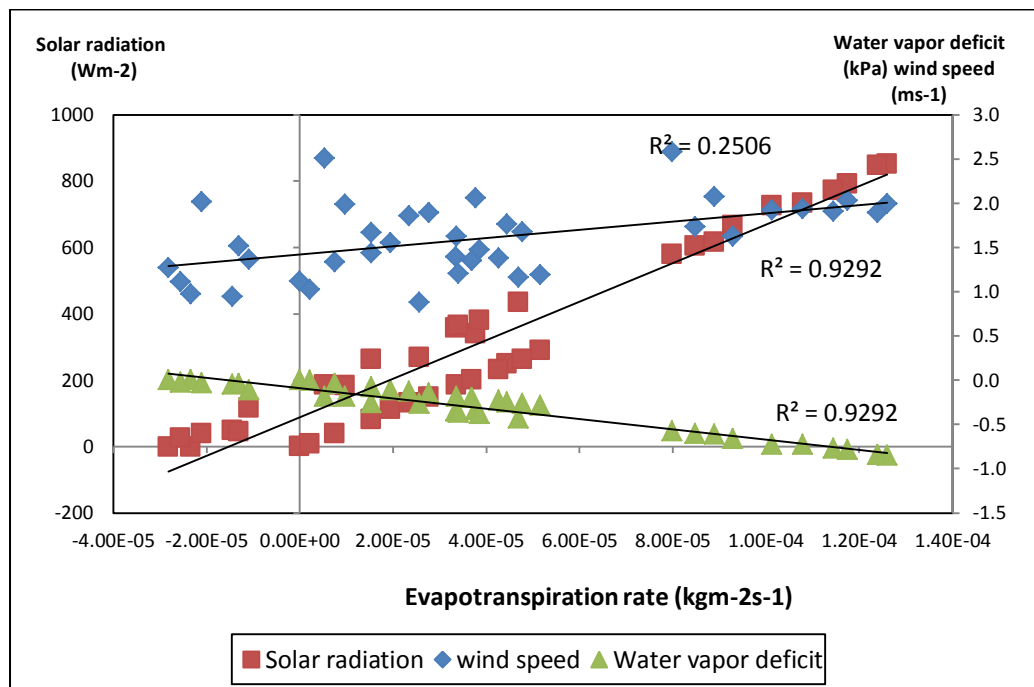
Figure 6.13 Regression analysis on the influence of the three source energy on evapotranspiration rate

Figure 6.13 shows that solar radiation and water vapor deficit have a substantial influence on the evapotranspiration rate. On the other hand, an opposite trend occurs on wind speed. The coefficient determination (R^2) of wind speed is very low (0.25) and this could indicate that wind speed has no influence to the evapotranspiration

process in the experimental set up. This evidence may indicate that wind speed below 2 ms^{-1} provide insufficient energy to increase the evapotranspiration rate. These results further indicate that the Bowen Ratio measurement method is acceptable for measuring small green roofs in urban areas of tropical climates.

6.4.   Conclusion

The experiment results have demonstrated that :

-   Solar radiation plays the most important role in determining the evapotranspiration rate. The evapotranspiration rate under clear sky condition is double compared to that under overcast sky condition.

-   High amounts of solar radiation are in good correlation with the reduction of the water vapor in the atmospheric layer.

-   The level of wind speed proved not to be sufficient to remove water vapor from the green roof.

CHAPTER 7 THERMAL AND PERFORMANCE EVALUATION OF THE PV MODULE INTEGRATED WITH THE GREEN ROOF

This chapter presents the evaluation of the thermal conditions and the performance of the PV module integrated with the green roof from field experiments that were conducted from June 2012 to January 2013. The results are classified into two parts. The first part is the impact of evapotranspiration process on thermal conditions around the PV module, which also includes its impact on the surface temperature of the PV module. The second part is the study of the impact of the evapotranspiration process on PV system performance particularly the performance ratio of the PV modules.

The analyses are performed separately for three different sky conditions: clear, intermediate and overcast. Furthermore, a box and whisker analysis is also conducted to study the overall PV module temperature and the performance ratio distribution.

7.1. Methodology

The methodology used to investigate the ability of the evapotranspiration process on improving both the thermal condition and the performance of the PV module is a comparative study. The experiment employs two PV modules which were installed over a green roof and over a concrete roof. The one over the concrete roof was used as the reference.

The energy balance principle is used as the fundamental theory to construct the field experiment. Figure 5.1 had introduced the energy balance mechanism in a defined boundary layer of an integrated PV module and green roof system. The definition of

the boundary layer of the integrated PV module and green roof system is the layer between the substrate of the green roof and the PV module and between the PV module and the sky. That hypothetical energy balance mechanism is then translated into the experiment set up. Figure 7.1 is provided to retain Fig. 5.1.
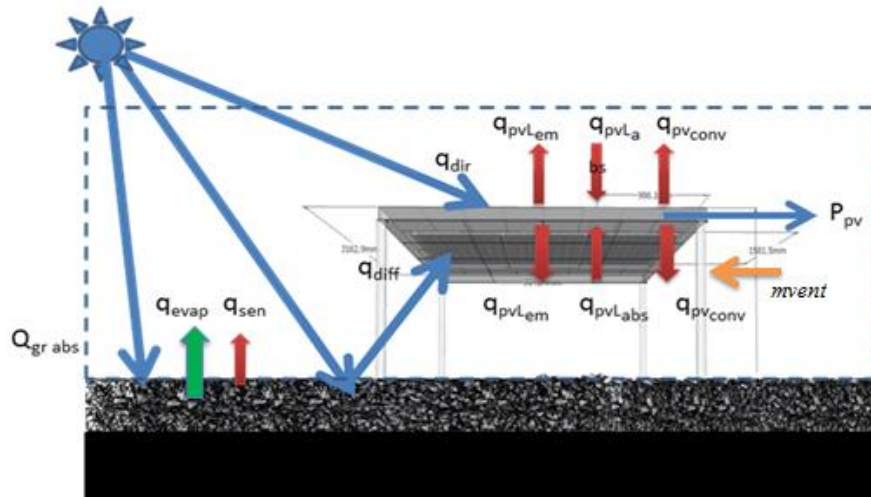
Figure 7.1. Schematic of energy exchanges between a green roof and a PV module within the boundaries of this study

Furthermore, the ratio between fetch and height was used to define the distance between PV module and green roof. The details about this ratio are explained in Chapter 6.1.2.

7.2. Experimental set up

To capture all the heat fluxes shown in Fig.7.1 the experimental set up was constructed as follows:

- The area of the green roof was built larger than the area of the PV module to provide a sufficient homogeneous condition over green roof and to avoid the

reflected solar radiation of the concrete roof to the PV module. Details of the experimental set up can be seen in Figure 6.3 and 6.5.

- The distance between the green roof and the PV module was set 30 centimeters away from the top canopy of the plants. This arrangement was set to provide sufficient ventilation and to maximize the effect of evapotranspiration process. As stated in Chapter 4.1.2 that a homogeneous condition over a particular layer can be achieved through a ratio between the fetch and the appointed elevation of 10: 1 (the minimum requirement). In this experiment, the appointed elevation for the PV module position is 30 centimeters above the top canopy of the plants and is based on the following estimation :

  - 12 centimeters above the green roof is the approximation layer of homogeneity condition over green roof resulted from the ratio of the fetch and T/Rh sensor of 10:1.

  - The remaining distance for the cavity (18 cm) was to facilitate the air movement to transfer heat (long wave radiation) from both side of PV module and green roof.

- Thermocouples at the back surface PV module temperature were used to examine the effect of the green roof on its temperature. This set up is an accepted method to approximate the solar cell temperature, which is also suggested by Skoplaki and Palyvos(2009) and Trinuruk et al (2009). Furthermore, PV modules were exposed to the sun and exhibit no significant temperature delta between the PV module over the concrete roof (Appendix 1). Therefore, only the back surface temperature of each PV module was measured for further investigation of the effect of green roof on the PV module temperature.

The measurement points for PV surface temperature, ambient temperature and roof surface temperature are illustrated in Figure 7.2:
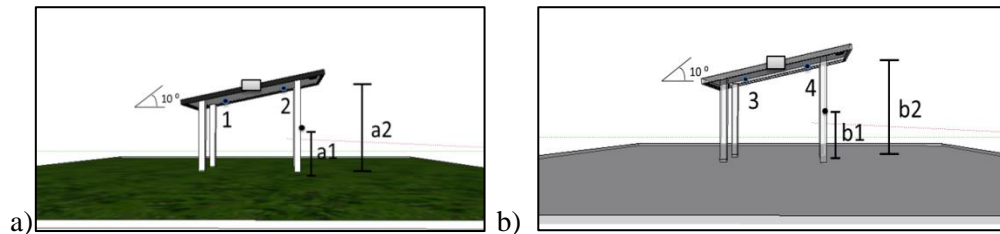
Figure 7.2 The measurement positions for the PV surface temperature analysis; a): PV over green roof and b): PV over concrete roof)

The various surface temperature measurement points are detailed in the following:

- **Point 1** : surface temperature measured on the lower side of the back surface of the PV module over the green roof

- **Point 2** : surface temperature measured on the upper side of the back surface of the PV module over the green roof

- **Point 3** : surface temperature measured on the lower side of the back surface of the PV module over the concrete roof

- **Point 4** : surface temperature measured on the upper side of the back surface of the PV module over the concrete roof

- **a1**: the distance between the top canopy of green roof to the second sensors of T/Rh (temperature and relative humidity): 12 cm.

- **a2**: the distance between the top canopy of green roof to the lowest side of PV module: 30 cm.

- **b1**: the distance between the top surface of concrete roof to the ambient temperature sensors: 15 cm.

- **b2**: the distance between the top surface of concrete roof to the lowest side of PV module : 30 cm.

The details of the complete set up for both PV modules, the data logging arrangement and the list of equipment with their accuracy can be seen in Fig. 6.5 and Table 6.1.

7.3.   Method of data collection

The PV module temperatures were measured by the thermocouple and were logged every 5 minutes by a data logger. As for the voltage measurement, the volt reading can be directly read by the data logger by connecting it to the voltage cable. The reading procedure was also every 5 minutes.

7.4.   Results and discussion

7.4.1.   PV module temperature evaluation

Table 7.1 Weather conditions for each typical sky condition during the outdoor experiments

Date and sky condition	Weather characteristics	Value
17th June Clear	Total hourly solar radiation (Wm^{-2})	5,606
	Average wind speed(ms-1)	2.41
	Average air Temperature(°C)	30
	Average relative Humidity(%)	74
4th August Intermediate	Total hourly solar radiation (Wm^{-2})	3,241
	Average wind speed (ms-1)	1.3
	Average air Temperature (°C)	28
	Average relative Humidity (%)	84
9th June Overcast	Total hourly solar radiation (Wm^{-2})	2,060
	Average wind speed (ms-1)	1.3
	Average air Temperature (°C)	27
	Average relative Humidity (%)	83

The selected days for the analysis are 17 June 2012, 4 August 2012 and 9 June 2012 respectively. The weather condition on those three days are summarized in Table 7.1.

An evaluation of the impact of the green roof on the improvement of the surface and the ambient temperature is presented first before the evaluation of the impact of the green roof on the PV module temperature.

7.4.1.1.   Impact of the green roof on the roof surface temperature

Figure 7.3-7.5 show a comparison between the surface temperature of the concrete roof and the surface temperature of the green roof under three different sky condition. It can be observed that on clear day, the surface temperature of the concrete roof is much higher than the surface temperature of the green roof. The temperature difference can be as large as 20 $^{\circ}$C in mid day. The highest surface temperature measured was 50 $^{\circ}$C for the concrete roof, and 32 $^{\circ}$C for the green roof.

Another significant notification is that the surface temperature of the green roof was relatively stable at around 33 $^{\circ}$C, especially in the afternoon. This fact may prove that the plants have used the heat of the solar radiation for their biological activities, such as evapotranspiration, respiration and photosynthesis so that the surface temperature remains stable.
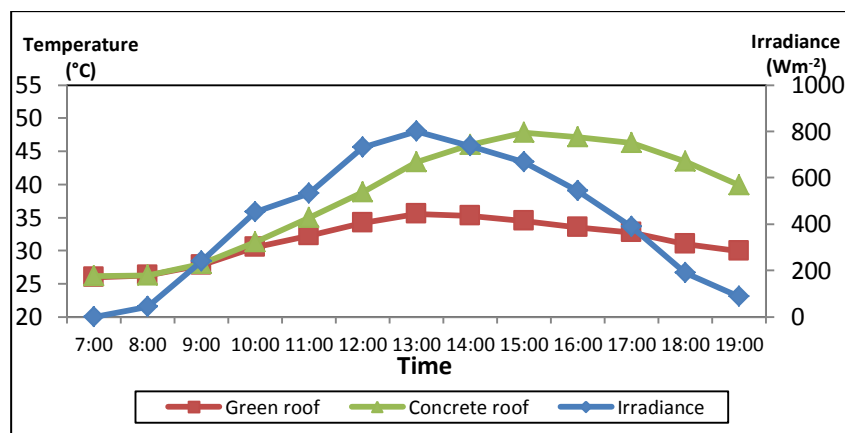
Figure 7.3. Concrete and green roof surface temperatures on a clear a day (here: 17 June 2012).

143
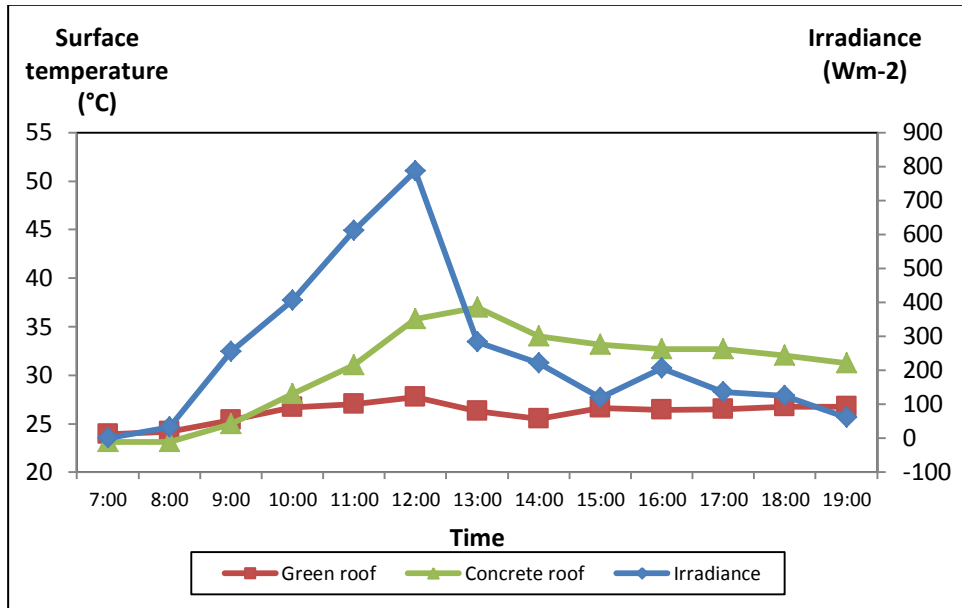
Figure 7.4. Concrete and green roof surface temperatures on an intermediate day (here: 4 August 2012).

The temperature difference between the concrete roof and the plants canopy is reduced in the typical intermediate day. It can be observed in Fig. 7.4 that the difference is only 10 °C as compared to up to 20 °C on a typical clear day. Furthermore, a remarkable notification is seen that the maximum temperature of each material is unlike. This may demonstrate a substantial amount of solar radiation is necessary to heat up the concrete roof since the heat capacity of the concrete roof is higher than that of the green roof. The highest temperature of the concrete roof surface was around 37 °C at around 14:00 h, then it reduced to around 31 °C, while, the surface temperature of the green roof reached its peak at around 27 °C at around 12:00 h, which then is reduced to around 19 °C after 14:00 h. It clearly shows that the surface temperature has no significant variation, except on the mid day when the solar radiation reach its peak.
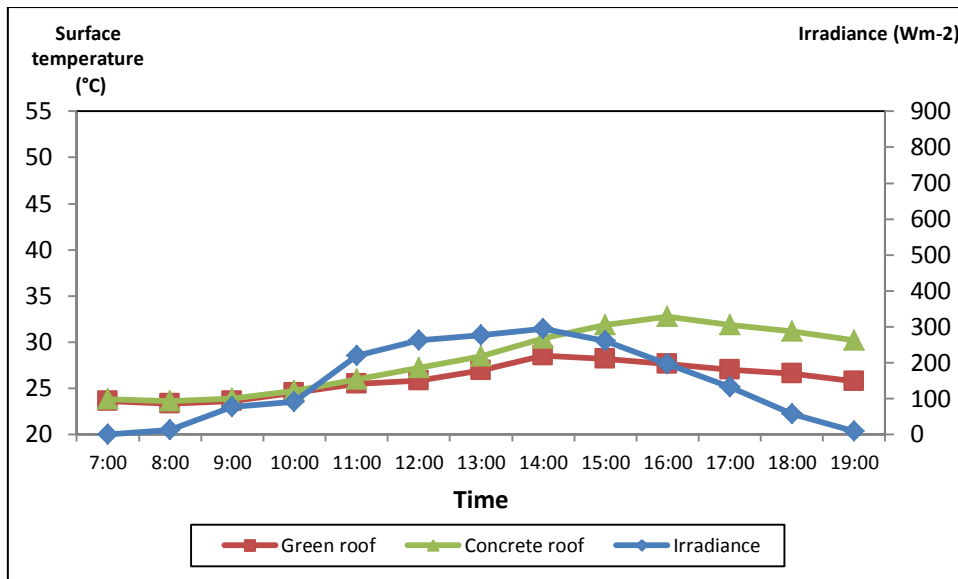
Figure 7.5. Concrete and green roof surface temperature on an overcast day (here: 9 June 2012).

On a cloudy day, the maximum temperature difference between the green roof surface and the concrete roof surface is only 4 ⁰C (see Fig. 7.5). The highest surface temperature of the concrete roof and the green roof are 34 ⁰C and 30 ⁰C respectively. This evidence shows that the surface temperature of concrete roof under overcast sky conditions (the total hourly solar radiation is < 2500 Wm-2), is much lower than under clear sky condition, (the total hourly solar radiation is > 5000 Wm-2). In general the variation of the surface temperature of the green roof is relatively small, less than 5 ⁰C.

Furthermore, the value of the albedo of each material also influences the surface temperature. The albedo of concrete and plants can found in Table 1.1. Due to its low albedo, concrete absorbs large amounts of solar radiation. In consequence, the surface temperature can increase sharply particularly on a clear day when solar radiation intensity reaches 600-1000 Wm^{-2}. The high surface temperatures then will generate high radiant heat transfer back to the surrounding, resulting in high ambient

temperatures over the concrete roof. The value of the ambient temperature over each surface is explained in the following sub-chapter.

7.4.1.2. Impact of the green roof on the ambient temperature

As expected, the ambient temperature over the green roof is lower than the ambient temperature over the concrete roof under all sky conditions (see Fig. 7.6-7.8). The figures show a similar trend. In the mid-morning the ambient temperature over the concrete roof is lower than the ambient temperature over the green roof, while the opposite trend occurs in the afternoon.

The average temperature reduction measured during the clear day was around 2 ^{o}C, while, the average temperature reduction during intermediate and overcast sky condition was around 1.5 ^{o}C and 1 ^{o}C respectively.
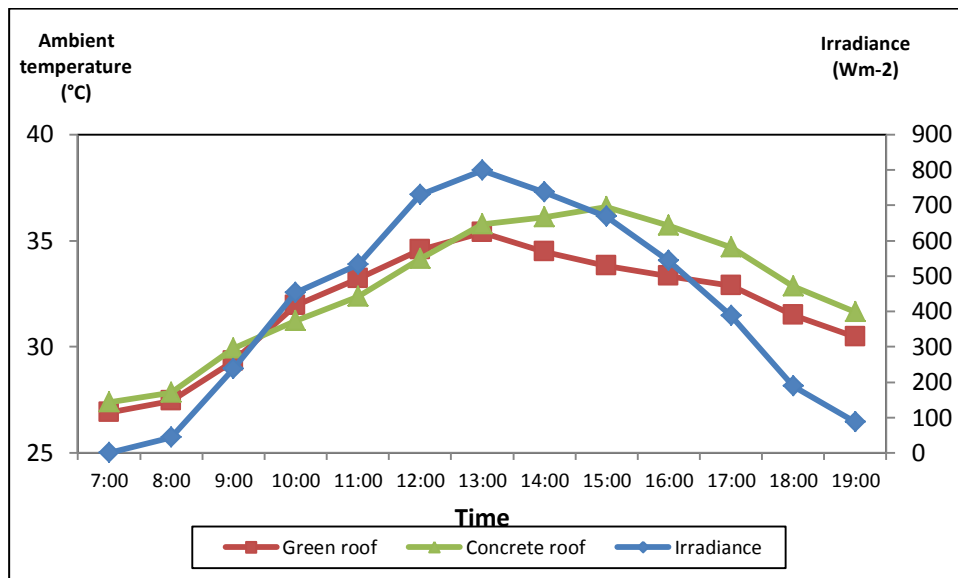
Figure 7.6 Ambient temperatures over different roofs on a clear day (here: 17 June 2012)
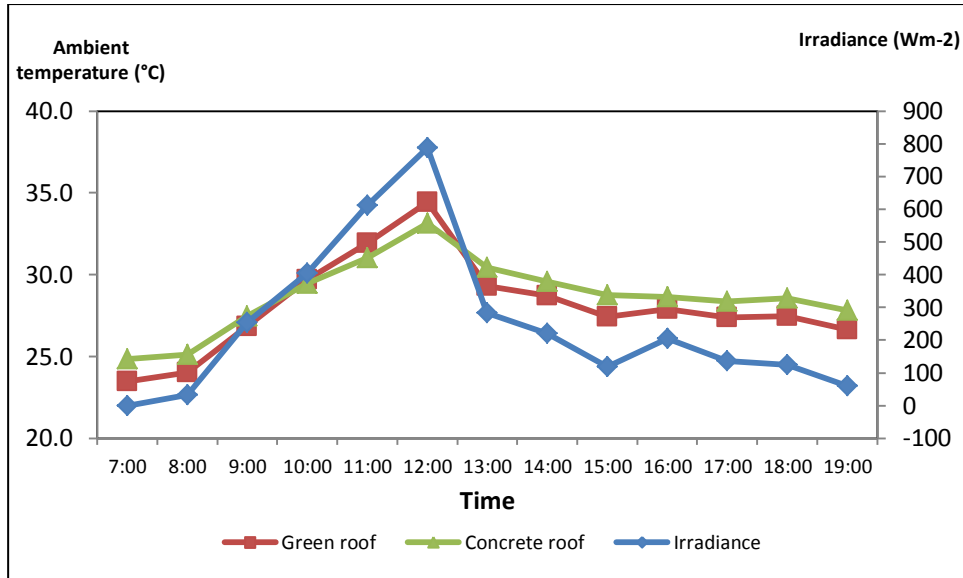
Figure 7.7 Ambient temperatures over different roofs on an intermediate day (here: 4 August 2012)
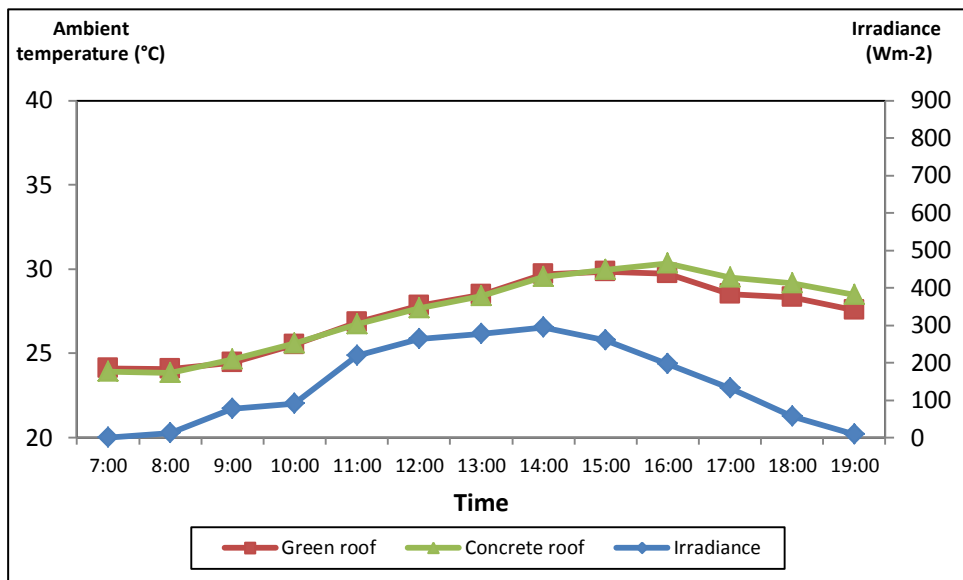
Figure 7.8 Ambient temperatures over different roofs on an overcast day (here: 9 June 2012)

Effect of the surface and the ambient temperature on the radiation and the convective heat fluxes

Radiation and convective heat transfer from a heated surface influences the ambient temperature. Fig 7.9 and Fig 7.10 illustrate the effect of these heat transfers on the

ambient temperature over the two different surfaces: green roof and concrete roof. The value of radiant heat flux (Q_{rad}) is obtained by the equation 7.1:

$$Q_{rad} = \sigma\varepsilon(T_{surf}^{4} - T_{sky}^{4}) \, [\text{Wm}^{-2}] \qquad (7.1)$$

Where σ is the Stefan Boltzmann constant and is equal to $5.667\text{x}10^{-8}$ $\text{Wm}^{-2}\text{K}^{-4}$, T_{sky} is sky temperature, ε is the emissivity of the roof top material and T_{surf} is the surface temperature. The emissivity of the plants is typically between 0.64 and 0.98 (Bramson, 1968). For this study 0.93 was selected as the input for radiant heat flux calculation. As for the concrete material, the emissivity is 0.94. The convective heat flux, the calculation is determined by a heat convection coefficient (h_c) which is obtained from Eq 5.13 in sub chapter 5.3.1.

As can be seen in Fig 7.9, the radiant heat flux from the concrete roof is much higher than the flux from the green roof, especially in the afternoon, caused by the large difference in surface temperatures between the green roof and the concrete roof (Fig.7.3). The average daytime reduction of the heat flux is around 50% with peak value up to 100%. While, for the comparison of convection heat flux over each surface, Fig. 7.10 shows that the pattern of the convective heat flux and the radiant heat flux (Fig. 7.9) is similar. The convective heat flux over the concrete roof reaches its maximum at 140 Wm^{-2} at around 17:00h. However, by applying a green roof, the highest heat flux on the surrounding environment was only 11 Wm^{-2}, occurred at around 14:00 h. The average daytime heat convection reduction is 106 Wm^{-2} or 103%.
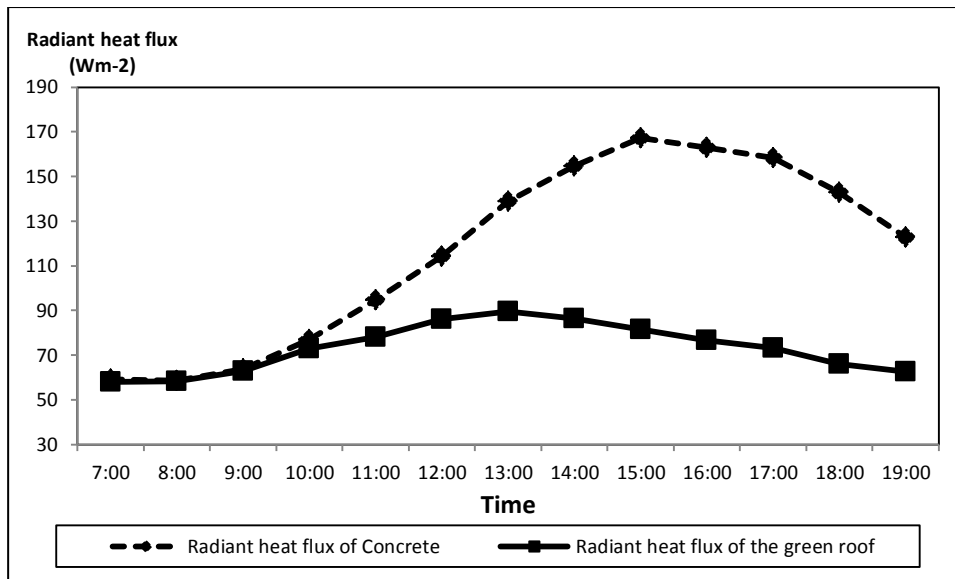
Figure 7.9 Radiant heat fluxes over the green roof and the concrete roof on a clear day
(here: 17 June 2012)
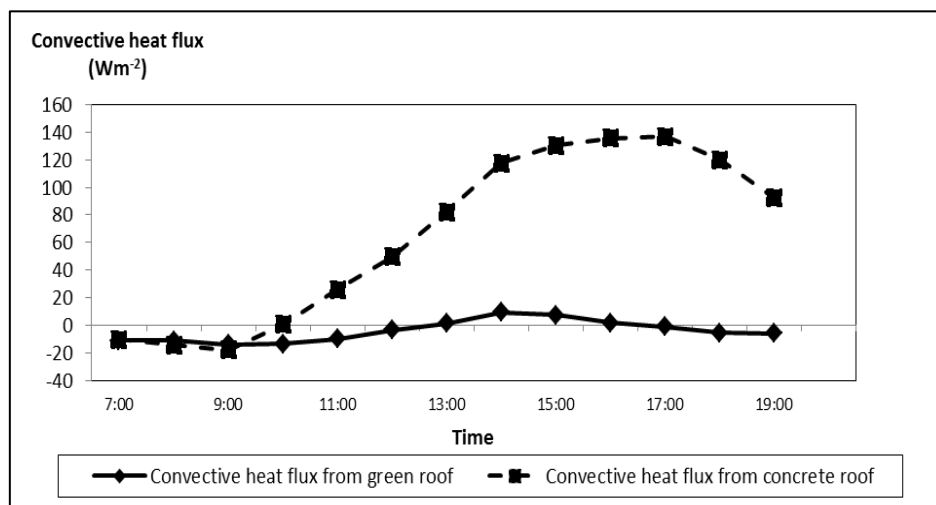
Figure 7.10 Convective heat fluxes over the green roof and the concrete roof on clear day

The two figures above (Fig.7.9 and Fig. 7.10) shows that the surface temperature as well as the ambient temperature play important roles in determining the ambient condition or the surrounding environment.

7.4.1.3. Impact of the green roof on the PV module temperature

As stated earlier, the back surface temperature of the PV module is used to determine the effect of green roof on PV module temperature. Figure 7.11 illustrates the temperature reduction of the back surface of the PV modules over the two different roof top materials. The temperatures shown in the figure are the average values of thermocouples readings set within the back surface of the PV modules.

It can be observed that a significant reduction occurs at the back surface of the PV module over the green roof on a clear day. The reduction can be as high as 6 °C at mid-day, while the average daytime reduction is between 2 °C and 3 °C. On intermediate and overcast days, the average reduction was around 2 °C and 0.8 °C respectively. Temperature reduction on intermediate day varies with the fluctuation of the irradiance.
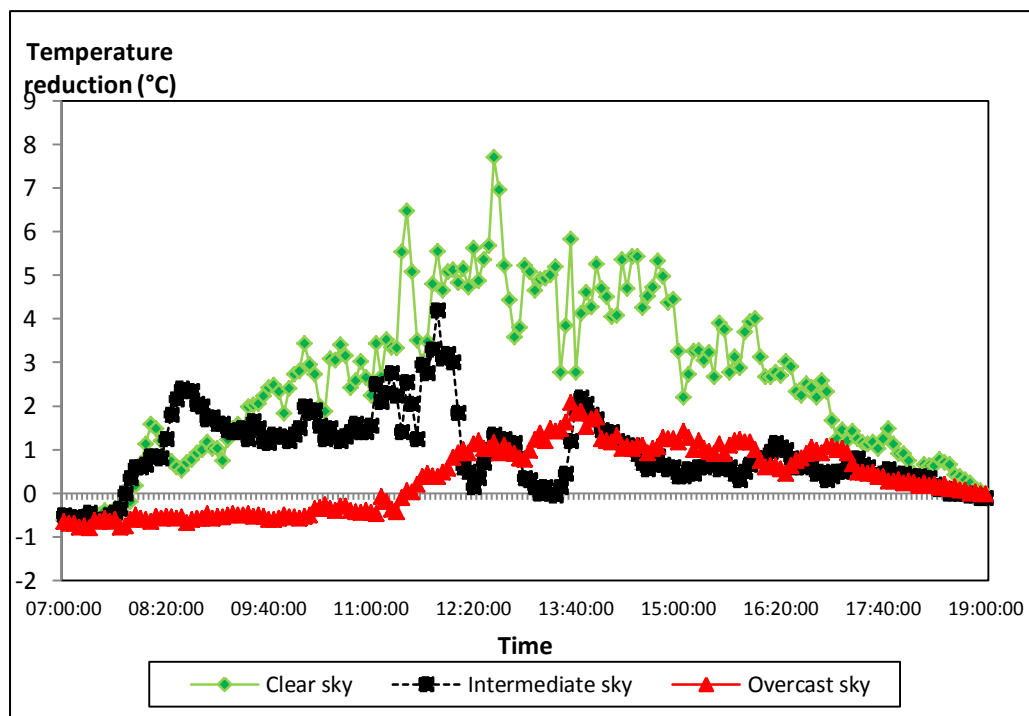
Figure 7.11 PV surface temperature reductions on clear, intermediate and cloudy days

150
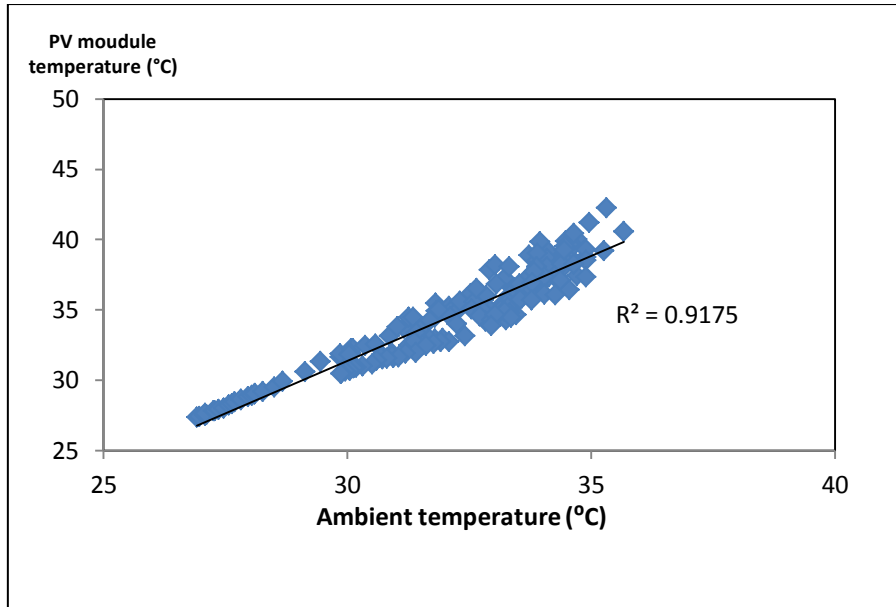
Figure 7.12 Regression analysis of the inter-dependency of the ambient and the surface temperatures of the PV module over the green roof
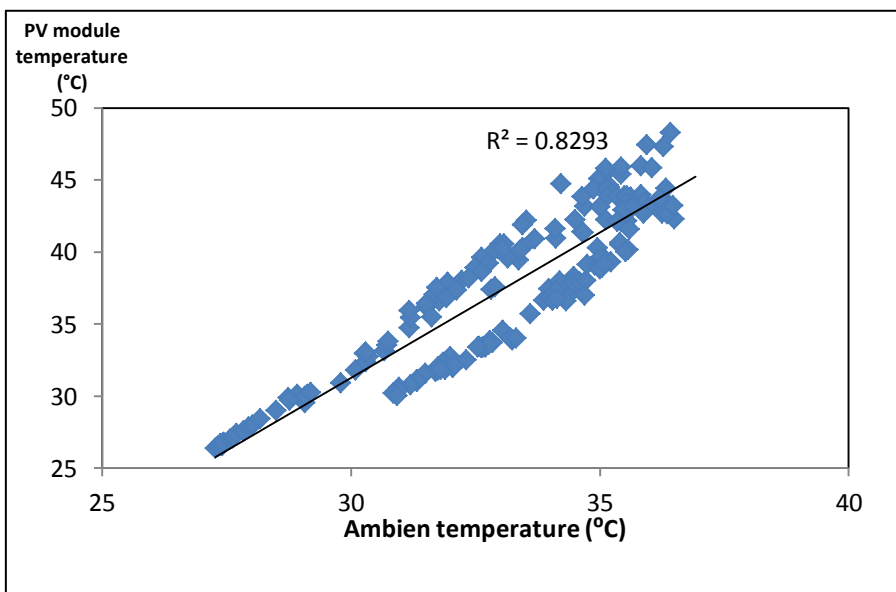
Figure 7.13 Regression analysis of the inter-dependency of the ambient and the surface temperatures of the PV module over the concrete roof

Figure 7.12 and 7.13 show how the surrounding conditions around the PV module affect its temperature, demonstrated for a typical clear day. It can be seen that the ambient temperature has a substantial influence on the PV module temperatures. The coefficient determinant (R^2) for the ambient temperature over the green roof is 0.92

while the R^2 for the ambient temperature over concrete roof is 0.83. It could be explained by referring to Fig. 7.9 and 7.10 that the diurnal curve of the radiant and convective heat flux over the concrete roof has more variant in the afternoon as compared to which over green roof. Therefore, solar radiation plays a higher role on the increase of PV module temperature in the morning. Hence, the highest PV module temperature over the green roof and concrete roof is around 45 °C and 52 °C respectively.

Box and Whisker Analysis

The following figures (Fig 7.14 – 7.16) show the results from the box and whisker analysis. The analysis employed 5 months experimental data which include data from the three sky conditions: clear, intermediate and overcast. The box demonstrates 50% data computed in the analysis and it presents the mean value of the data, the whisker demonstrate the remaining values of the data distribution.

It is observed from Fig 7.14 that there is a slightly different median line between the two boxes. The box representing the temperature data from the PV module over the concrete roof shows that 25% of 50% surface temperature data is between 31 °C and 38 °C. While the rest 25% of those data is range between 38 °C and 45 °C. While, on the box represents those from the PV module over green roof shows the range between Quartile 1 and Quartile 2 is 7 °C, while the range between Quartile 2 to Quartile 3 is 6 °C. These results shows that the data distribution of the PV module temperature over the green roof is slightly smaller compared to those over the concrete roof. Furthermore, the whisker plot of the PV module temperatures over the green roof also shows a smaller distribution between the green roof and the concrete roof (by 3.3 °C).
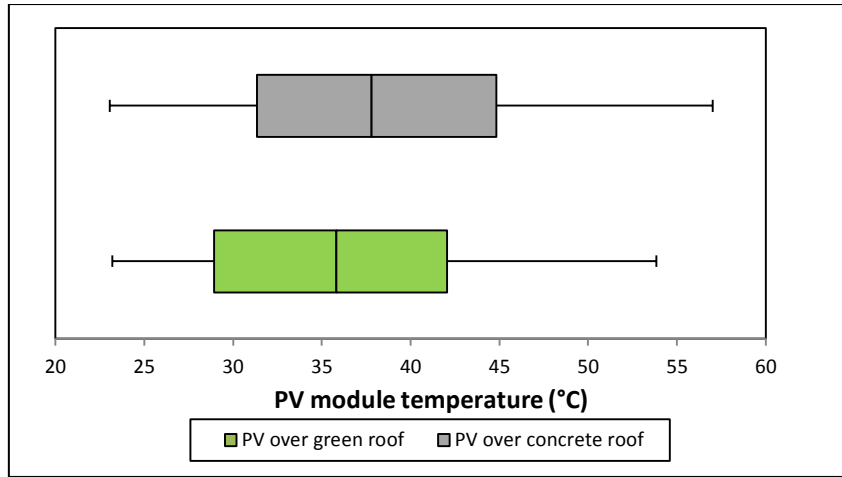
Figure 7.14 Box and whisker analysis of the PV module temperatures under clear sky conditions

Better data distribution of the PV module temperature over green roof can also be seen on intermediate day (see two boxes as well as the whiskers in Fig 7.15). The box represents the temperature distribution of PV module over concrete roof is larger than the one over green roof with the difference of 2 °C, as well as the whisker plots at the right hand side, while, the whiskers at the left hand side show no significant difference.
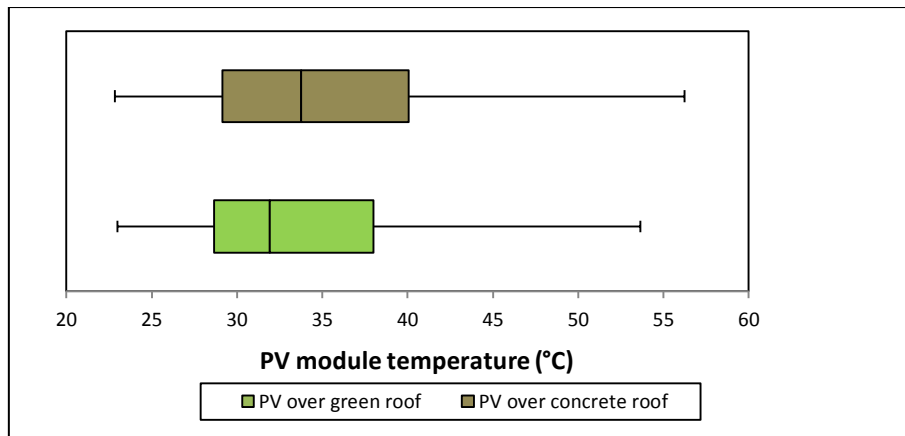
Figure 7.15 Box and whisker analysis of the PV module temperatures under intermediate sky conditions
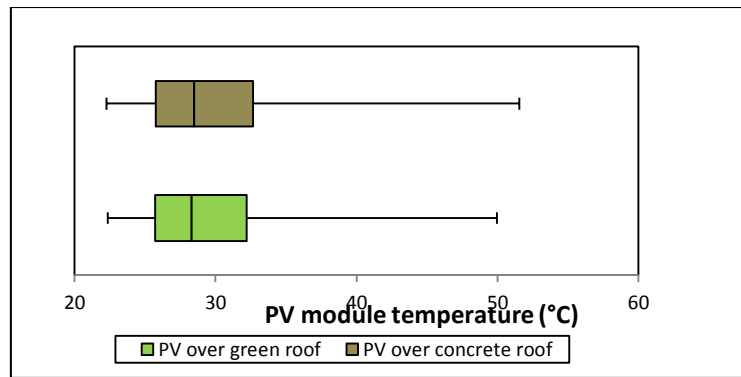
Figure 7.16 Box and whisker analysis of the PV module temperatures under overcast sky conditions

On cloudy days, the two boxes demonstrate a similar distribution, only the right side of the whiskers shows 1 degree Celsius larger as compared to that of the PV module temperature over green roof.   This distribution pattern explains that there is relatively small difference between the PV module temperature over the green roof and the PV module temperature over the concrete roof.   The data distribution of both PV modules is summarized in Table 7.2

Table 7.2 Box and whisker data used for the (Fig. 7.14-7.16) plots

PV module over green roof			PV module over concrete roof		
		DIFF			DIFF
min	23.2	23.2	min	23.1	23.1
Q1	29.0	5.8	Q1	31.3	8.3
Q2	35.8	6.9	Q2	37.8	6.5
Q3	42.1	6.2	Q3	44.8	7.0
max	53.9	11.8	max	57.0	12.2
Min	23.0	23.0	Min	22.9	22.9
Q1	28.6	5.6	Q1	29.2	6.3
Q2	31.9	3.3	Q2	33.8	4.6
Q3	38.0	6.1	Q3	40.1	6.3
max	53.7	15.7	max	56.3	16.2
Min	22.4	22.4	Min	22.3	22.3
Q1	25.7	3.4	Q1	25.8	3.5
Q2	28.3	2.6	Q2	28.5	2.7
Q3	32.2	3.9	Q3	32.7	4.2
max	50.0	17.8	max	51.6	18.9

Based on those results, it can be highlighted that the temperature variation of PV module over green roof is smaller compared to that over concrete roof. Smaller data distribution may shows that thermal condition of PV module over green roof is improved.

7.4.1.4. PV module temperature using Thermography
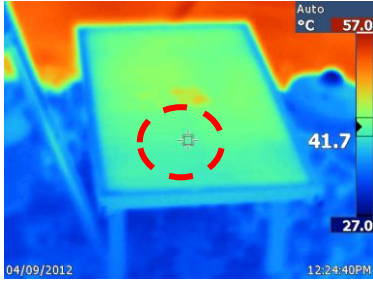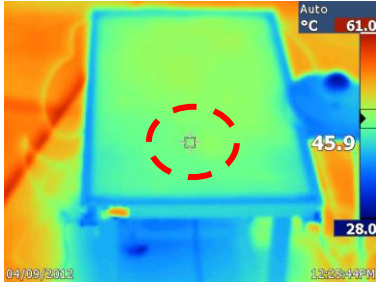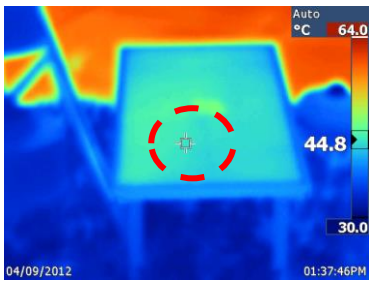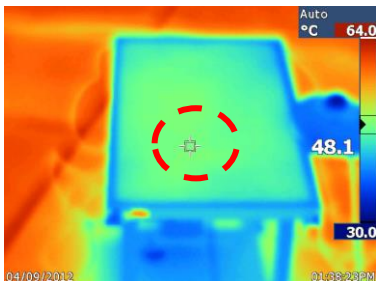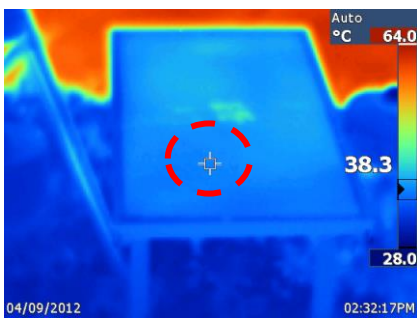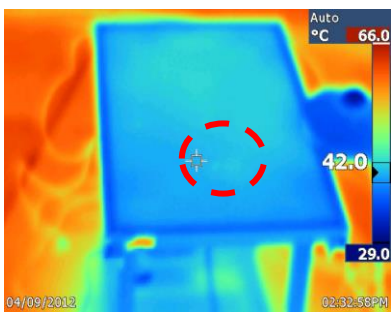
Additionally, an infrared camera was also utilized in this field study to determine the PV module temperatures. Figure 7.17 shows the surface temperatures of the PV modules over the concrete roof and the green roof on 4 September 2014 at three consecutive times (12:30 h, 13:30 h and 14:30 h). It can be seen that the surface temperature of the PV module can be reduced by 3.3 – 4.2 °C by using a green roof.

The weather condition on the day of the measurement is summarized in Table 7.3.

Table 7.3 Weather condition on 4th September 2012

Total hourly solar irradiation (Whm^{-2})	Sky condition	Average wind speed (ms^{-1})	Average relative humidity (%)
5768	Clear sky	2.1	76

The blue color that appears on the green roof represents low temperature while the red color on the concrete roof represents high temperature. This color images show that the surface temperature over the concrete roof is much higher than the surface temperature over the green roof. It illustrate that high temperature on a surface provides a disadvantage effect on a PV module.

Time	PV module temperature over green roof	PV module temperature over concrete roof
04/09/2012 12:30 PM	41.7° C	45.9° C
04/09/2012 01:30 PM	44.8° C	48.1° C
04/09/2012 02:30 PM	38.3° C	42.0° C

Figure 7.17 Thermal images of the PV modules over the concrete and the green roof

7.4.2. PV module performance analysis

7.4.2.1. The open circuit voltage (V_{oc})

Figure 7.18 and 7.19 shows that the open circuit voltage (V_{oc}) of the PV module the over green roof is slightly higher than the V_{oc} of the one over the concrete roof. The differences of the V_{oc} are 0.16 V, 0.14 V and 0.07 V for clear, intermediate and overcast day respectively. The difference increases with the increase of the solar radiation. This is also in accordance with the fact that the PV module temperature differences also increase with higher solar radiation, showing the impact positive of the green roof on clear days.
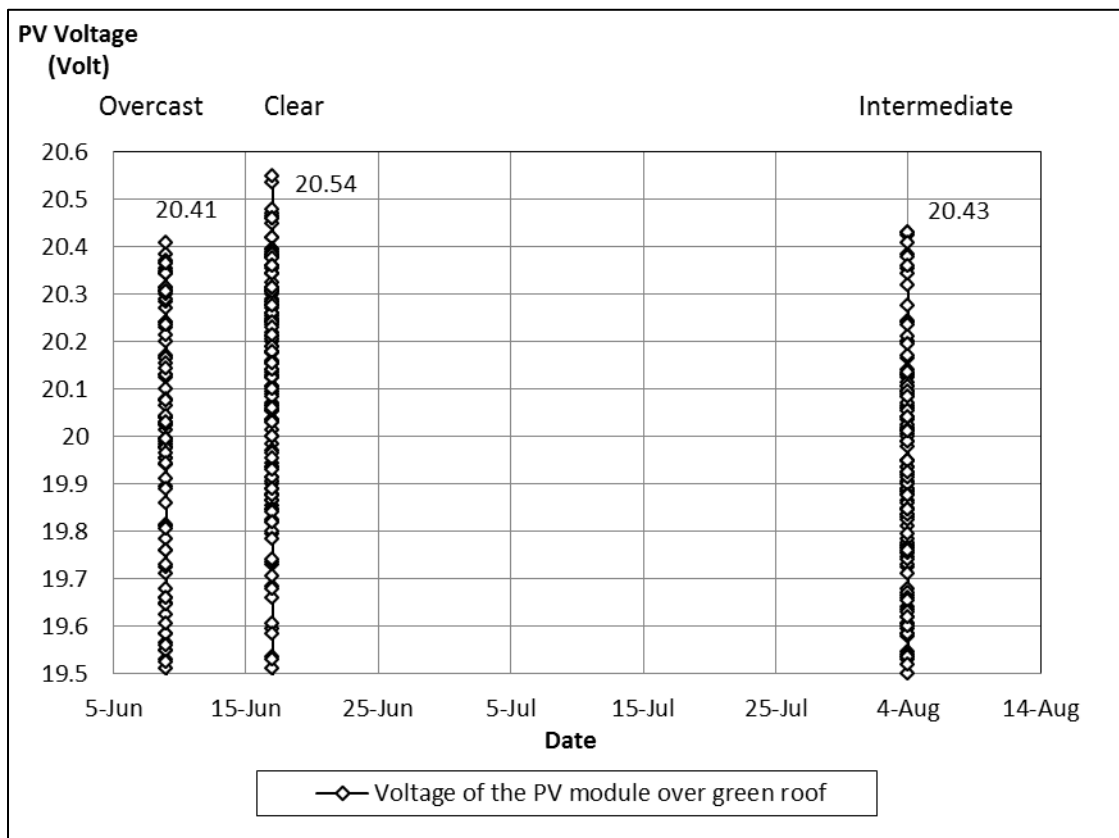
Figure 7.18 Open circuit voltage of the PV module over the green roof on different days

157
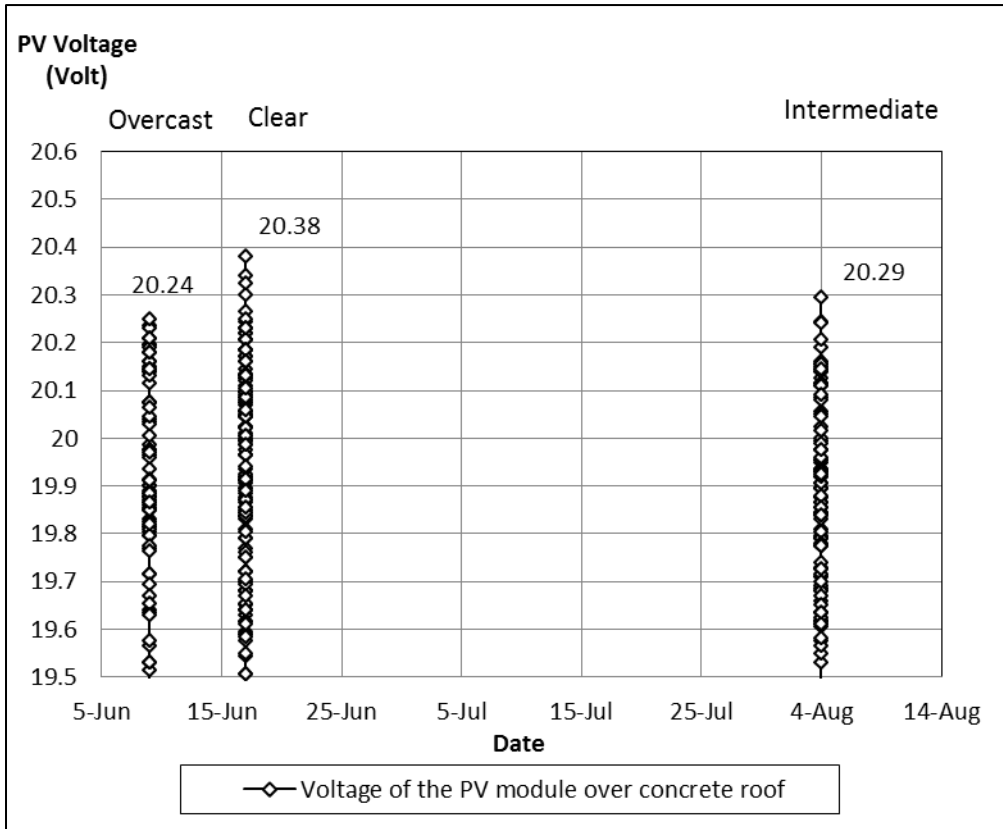
Figure 7.19 Open circuit voltage of the PV module over the concrete roof on different days

7.4.2.2. The performance ratio

The criterion to gauge the conversion of sunlight into electricity is the so-called Performance Ratio. The standard equation from the IEC standard is adopted for reference.

Energy yield is equal to the energy output (DC) divided by the power from the manufacture. It is explained in the following equation:

$$Y_e = \frac{E_{output}(kWh)}{E_{ref}(kWp)} \text{ [Joule]} \tag{7.1.}$$

The performance ratio is the ratio of energy yield (Y_e) over the reference yield (Y_{ref}). This study focuses only on the losses due to the module temperature. The equation is as follows:

$$Performance_{ratio} = \frac{Y_e}{Y_{ref}} \qquad [\%] \tag{7.2}$$

where, the reference yield is the ratio of daily in plane irradiance (I_{daily}) over the STC reference in-plane irradiance (I_{ref}).

$$Y_{ref} = \frac{I_{daily}}{I_{ref}} \quad [Joule] \tag{7.3}$$

In terms of efficiency, the equation used in this study follows the Energy Balance principle where the efficiency is determined by the variation of the operating temperature (T_c), the temperature coefficient of PV module (β_{ref}), the reference temperature (T_{ref}) and the reference efficiency (η_{ref}). The equation is as follows:

$$\eta_{operating} = \eta_{ref} - \eta_{ref}\beta_{ref}(T_c - T_{ref}) \qquad [dimensionless] \tag{7.4}$$

Hence, the operating performance of PV module (P) is determined by Irradiance (E), operating efficiency ($\eta_{operating}$) and area of the PV module (A).

$$P = E \times A \times \eta_{operating} \quad [W] \tag{7.5}$$

The initial measurement of the PV modules

The initial measurement of the voltage of the two PV modules was conducted on 16th April 2014. The sky condition was around 750 Wm^{-2} with the average wind speed of around 2 ms^{-1}. The results of the initial measurement are tabulated in Table 7.4.

Table 7.4 The initial measurement of the two PV modules

	PV module 1			PV module 2		
Time	08:00	09:00	10:00	08:00	09:00	10:00
Voltage (Volt)	18.125	19.375	20.137	18.142	19.374	20.124

From the initial measurement, it was found that there was a difference in voltage. In average the difference was between 0.008 Volt, which then this number was used to normalize the performance ratio calculation.

In the experiment, PV module 1 was used for the set of PV module over green roof, while PV module 2 was used for the set of PV module over concrete roof.

Performance ratio in clear sky condition

It can be observed from Fig 7.20 that the performance ratio of the PV module over the green roof has a relatively higher than the performance ratio of PV module over concrete roof. In average, the difference is 2% with the minimum performance ratio of the PV module over the green roof is equal to the quartile 1 of the PV module over

the concrete roof performance ratio, and the value of Q3 of the PV module over the green roof is equal to the maximum value of the PV module over the concrete roof.
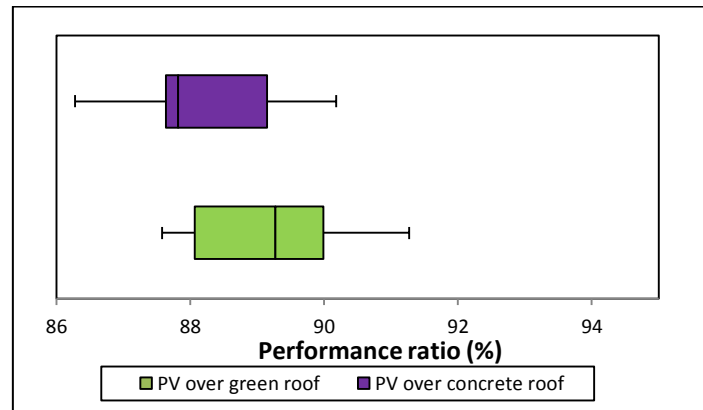
Figure 7.20 Performance ratio of the PV modules over different roof tops on a clear day

Performance ratio on an intermediate sky condition

In intermediate sky conditions, the performance ratios of both PV modules show a slightly larger variation. In general, the performance ratio of the PV module over the green roof higher than that over the concrete roof by 2% (Fig. 7.21).
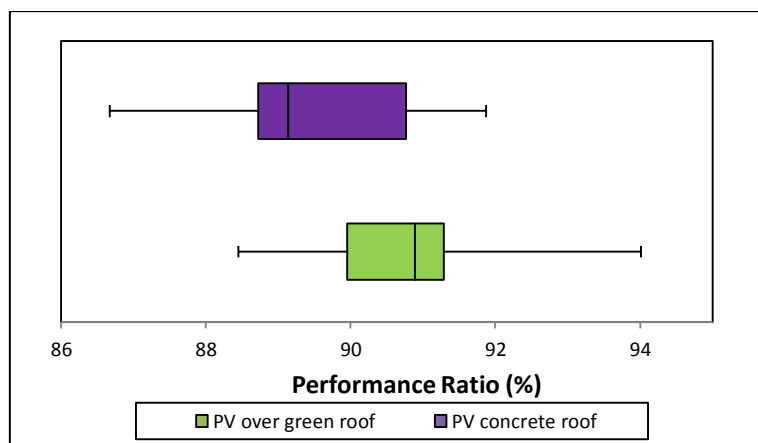
Figure 7.21 Performance ratio of the PV modules over different roof tops on a intermediate day

161

Performance ratio in overcast sky condition

Under overcast sky conditions, the performance ratios demonstrate an opposite trend compared to that under intermediate sky condition. In general, the ratios are similar; however, the median value of PV module over green roof shows slightly higher by 1 %.
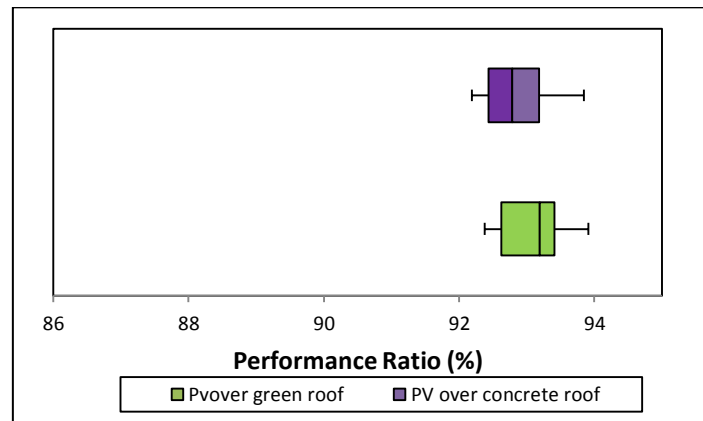
Figure 7.21 Performance ratio of the PV modules over different roof tops on an overcast day

The results above confirmed that that green roof has an impact on the performance of the PV module by improving its performance ratio. In general, the performance ratio can be improved by 2%.

7.5. Conclusion

The measurement of the PV module temperatures data have been analysed and they demonstrate some important evidences:

1. The green roof can reduce the PV module temperature significantly particularly on clear days when the total hourly solar radiation is above 5000 Wm^{-2}. The average reduction in the mid-day can be as high as 6 °C. While

on intermediate days, the reduction is only significant when the solar radiation intensity is above 600 Wm^{-2}. On overcast days, the effect of green roof is small, with less than 1 °C reduction average.

2. Those temperature reductions mentioned in point 1 are in relation to the reduction of the ambient temperature over the roof tops. It is confirmed by the value of the coefficient of determination (R^2), where 0.9 for the one over green roof and 0.8 for the one over concrete roof. The evidences show that lower ambient temperature lead to a lower PV module temperature.

3. The effect of green roof on the PV module performance can be also seen in the PV module performance ratio. From the box and whisker analysis, the performance ratio of the PV module over the green roof improves by 2% particularly on clear and intermediate day. While on overcast day, the difference on the performance ratio is less than 1%.

CHAPTER 8 THE OVERALL EFFECT OF THE EVAPOTRANSPIRATION OF GREEN ROOF TOP ON PV MODULE TEMPERATURE

8.1.   Introduction

This chapter presents the overall influence of the evapotranspiration on the PV module temperature and performance. Additionally, the effect of the integrated PV module and green roof to the environment is also demonstrate here, in order to illustrate further advantage of this two integrated systems to the environment.

8.2.   PV module temperature influenced by the evapotranspiration

Table 8.1 shows the classification of the PV module temperature reduction as a function of the amount of solar radiation. Both PV module temperature and the temperature reduction values obtained from 3-months averages. It can be observed, that the average temperature reduction increase with the increase of the amount of solar radiation. Highest average temperature reduction is around 10% at solar radiation of more than 500 Wm^{-2} and more, with the minimum impact still at around 3% for solar radiations as low as 100 Wm^{-2}. These results may imply that the green roof effectively reduces the PV module temperature at any irradiance level, but with stronger effect the higher the irradiance.

The benefit of green roof for PV module temperature improvement is relatively significant for over a year, since the total hours for solar radiation of between 600 Wm^{-2} and >900 Wm^{-2} is taking 22% of the total daytime hour, where the reduction of PV module temperature is between 8.3% and 9.9%.

Table 8.1 Classification of PV module temperature reduction based on the amount of solar radiation

Solar radiation	Average temperature of PV module over green roof	Average temperature of PV module over concrete roof	Temperature reduction	Temperature reduction	Frequency in 1 year	Percentage
(Wm^{-2})	(°C)	(°C)	(°C)	(%)	(hours)	(%)
0-100	27.3	28.1	0.8	2.8	869	20
101-200	30.4	31.7	1.3	4.1	734	17
201-300	32.2	33.8	1.6	4.7	605	14
301-400	34.6	36.6	2.0	5.5	490	11
401-500	36.1	38.4	2.3	6.0	374	9
501-600	38.2	40.8	2.6	6.4	299	7
601-700	40.7	44.4	3.7	8.3	262	6
701-800	42.4	46.6	4.2	9.0	273	6
801-900	46.5	51.6	5.1	9.9	241	5
>900	50.3	55.8	5.5	9.9	233	5

Note: The percentage of the hourly solar radiation of each classification is calculated from the hourly frequency of its occurrence in one year divided by total daytime hour. Total daytime hours are 4380 hours. The irradiance data is provided by a single year measurement (2012) conducted by Solar Energy Research Institute of Singapore (SERIS) and it is adjusted with the data from Metonorm 7.0, where the annual total irradiance is 1623 kWh/m2.

The reduction of the PV module temperature, subsequently also reduces the negative temperature impact on the PV module performance, which in turn lead to a higher energy yield. As shown in Table 8.2 the increase of the PV performance is in accordance with the reduction of its temperature. The improvement of the energy yield can reach to 6 kWh/kWp when the solar radiation is above 900 Wm^{-2}. This evidence shows that the green roof effectively improves the specific yield of a PV module when the intensity of solar radiation is high as compared to a PV module over a concrete roof.

Table 8.2 Classification of PV module performance improvement based on the amount of solar radiation.

Solar radiation (Wm^{-2})	Average PV module specific yield over the green roof (kWh/kWp)	Average PV module specific yield over the concrete roof (kWh/kWp)	PV module energy improvement for 1 year (kWh/kWp)	Percentage (%)
0-100	52	52	0	0.35
101-200	108	108	1	0.66
201-300	147	146	1	0.76
301-400	165	164	2	1.02
401-500	155	154	1	0.94
501-600	156	154	2	1.28
601-700	160	157	3	1.84
701-800	191	187	4	2.07
801-900	186	181	5	2.62
>900	208	203	6	2.87
		Total	24	Average:1.8%

Note: PV module specification: 250 Wp, Area = 1.6368m^2, efficiency = 15.4%

The following sub chapter presents the details of the evapotranspiration rate, which is the underlying roof cause for the PV module temperature reduction over the green roof.

8.3.   The evapotranspiration rate

Table 8.3 shows the classification of evapotranspiration rate as a function of the amount of solar radiation. The classification is an average evapotranspiration rate obtained from three months measurements. All the values presented in the list have an Advection Index (AI) below 1.

Table 8.3 Classification of evapotranspiration rate based on the amount of solar radiation

Solar radiation (Wm^{-2})	Evapotranspiration rate (kgm^{-2}s^{-1})	Latent heat flux (Wm^{-2})	Share of latent heat flux relative to solar radiation %
0-100	-1.54E-05	-38	-
101-200	8.07E-06	20	13
201-300	2.58E-05	63	22
301-400	3.60E-05	88	25
401-500	5.04E-05	123	27
501-600	6.95E-05	170	31
601-700	8.67E-05	212	33
701-800	1.09E-04	267	35
801-900	1.26E-04	307	36
>900	1.50E-04	366	39

It can be observed, that the evapotranspiration rate as well as the latent heat flux are below zero when solar radiation ranges from 0 Wm^{-2} to 100 Wm^{-2}. The highest evapotranspiration rate and latent heat flux are 1.5×10^{-4} kgm^{-2}s^{-1} and 366 Wm^{-2} respectively when the solar radiation is above 900 Wm^{-2}. The increase of the evapotranspiration rate with respect to the increase of solar radiation intensity is around 1.8×10^{-5} kgm^{-2}s^{-1} per 100 Wm^{-2}.

In terms of the energy conversion of solar radiation into latent heat, the selected type of plants (*Complaya trilobata*) is able to convert energy from solar radiation into latent heat, with an increasing conversion rate increases at higher irradiances, latent heat share goes up from 13% to 39%. The evapotranspiration process is beneficial to improve the conditions around the green roof at any irradiance level above 100 Wm^{-2}, but more intensively through at higher solar radiation values.

Table 8.4 The frequency and percentage of ET rate for one year

Solar radiation (Wm^{-2})	Evapotranspiration rate (kgm-2s-1)	Frequency (hours)	Percentage (%)
0-100	-1.54E-05	869	20
101-200	8.07E-06	734	17
201-300	2.58E-05	605	14
301-400	3.60E-05	490	11
401-500	5.04E-05	374	9
501-600	6.95E-05	299	7
601-700	8.67E-05	262	6
701-800	1.09E-04	273	6
801-900	1.26E-04	241	5
>900	1.50E-04	233	5

In terms of Singapore climate, this study also investigated how the various evapotranspiration rate corresponds to the frequency distribution of the solar radiation in a full year (Table 8.4). It can be observed that the rate of recurrence of evapotranspiration at high solar radiation (600 Wm^{-2} - >900Wm^{-2}) is 22% for one year in which the heat from solar radiation could be changed into latent heat by an average of 36% (Table 8.5).

8.4. Evapotranspiration rate and its relation to the reduction of PV module temperature

Table 8.5 shows the combined inter-dependency of the temperature reduction, the evapotranspiration and the share of the latent heat flux there-in. In the case of >900 Wm-2, for example, the temperature reduction by 5,5 ^{o}C arises from an evapotranspiration rate of 1.5x10-4 kgm^{-2}s^{-1}, which requires 366 Wm-2 of latent heat flux. That latent heat comes to 39% from the solar radiation, a share which then will not add to the heat-up of the environment and the PV module anymore. In general, to reduce 1 °C of the PV module temperature requires approximately 82 Wm^{-2} of latent

heat flux. This value may, however, only be applicable only for Singapore climate, where the experiment have been carried out.

Table 8.5 Comparison of the PV module reduction with the evapotranspiration rate and the Latent heat flux

Solar radiation (Wm-2)	Temperature reduction (°C)	Evapotranspiration rate (kgm-2s-1)	Latent heat flux (Wm-2)	Share of latent heat flux relative to solar radiation %
0-100	0.8	-1.54E-05	-38	-
101-200	1.3	8.07E-06	20	13
201-300	1.6	2.58E-05	63	22
301-400	2.0	3.60E-05	88	25
401-500	2.3	5.04E-05	123	27
501-600	2.6	6.95E-05	170	31
601-700	3.7	8.67E-05	212	33
701-800	4.2	1.09E-04	267	35
801-900	5.1	1.26E-04	307	36
>900	5.5	1.50E-04	366	39
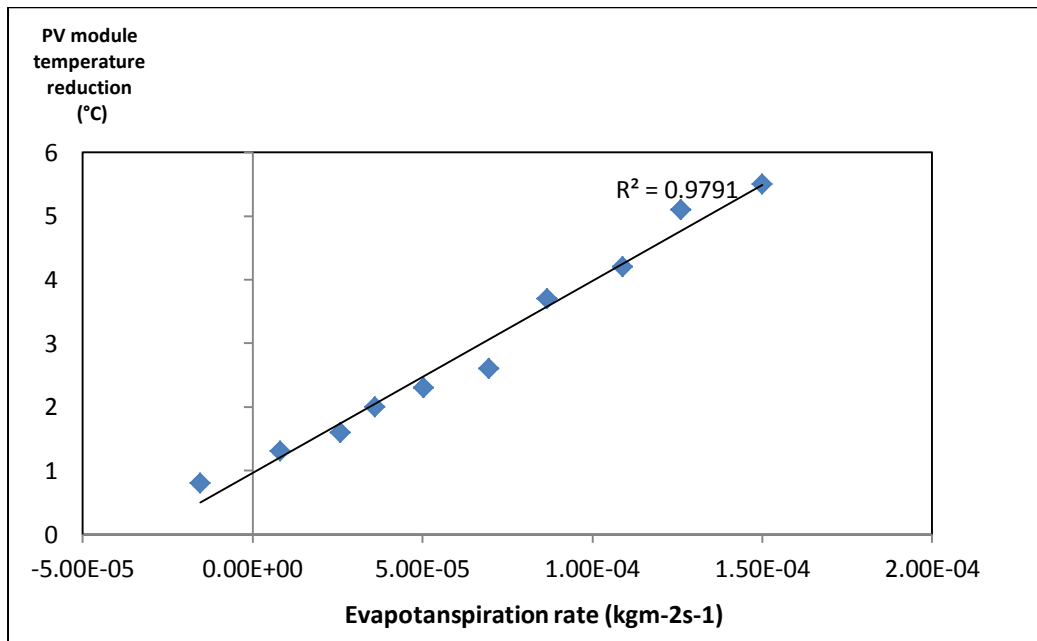
Figure 8.1 Regression analysis of the influence of evapotranspiration rate on PV module temperature reduction

Figure 8.1 demonstrates that the influence of evapotranspiration over the green roof on the PV module temperature reduction is significant. The coefficient of determination is 0.97. The regression analysis is computed based on data in Table 8.5.

8.5. The impact of the reduction of PV module temperature to the environment

8.5.1. Impact on the surroundings

The effect of the surface temperatures of the PV modules on the surrounding thermal condition was assessed through convective and radiant heat transfer analysis. The selected data were retrieved from a typical clear day of the experiments in Singapore where the solar radiation intensity is between 800-900 Wm^{-2}.

- **Radiant Heat Analysis**
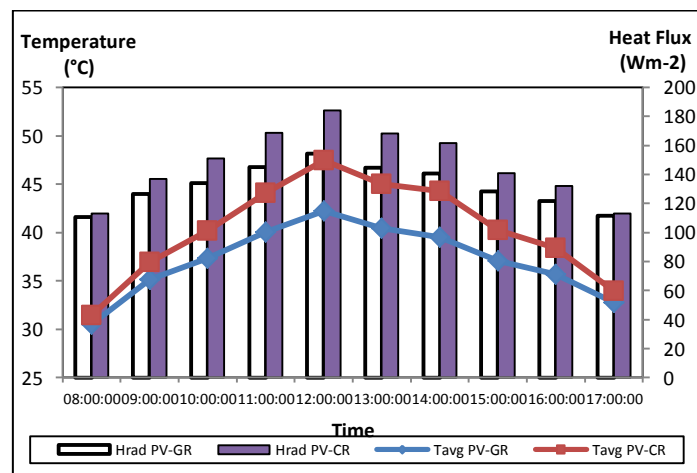
Figure 8.2 Radiant heat transfer from the PV modules installed over different roof materials to the sky
Hrad PV-GR: Average radiant heat of the PV module over green roof
Hrad PV-CR: Average radiant heat of the PV module over concrete roof
Tavg PV-GR:Surface temperature of the PV module over green roof
Tavg PV-CR: Surface temperature of the PV module over concrete roof

The emissivity of roof top material and the surface temperature are essential in the radiant heat analysis. Figure 8.2 shows the comparison of the radiant heat from the two PV modules over different roof types to the sky. It can be seen that the heat flux was reduced by 16% for the PV module installed over the green roof at mid-day, with an average daytime reduction of the heat flux by around 9%.

- **Convective Heat Analysis**

Convective heat is influenced by the wind speed and the ambient temperature. Wind speed act as the medium to remove heat. Therefore, the convective heat transfer is assumed to be dominated by wind velocity. The heat convection coefficient over a surface can be assumed as a linear function of wind speed (Jones and Underwood, 2001). The convective heat coefficient is determined by Eq. 5.13.
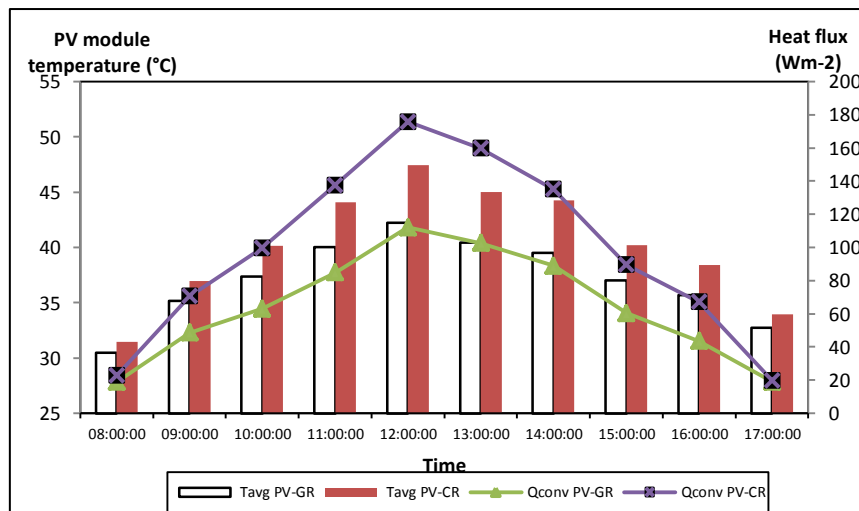
Figure 8.3 Convective heat transfer from the PV modules installed over different roof materials to the surroundings
Tavg PV-GR:Surface temperature of the PV module over green roof
Tavg PV-CR: Surface temperature of the PV module over concrete roof
Qconv PV-GR: Convective heat of the PV module over green roof
Qconv PV-CR: Convective of the PV module over concrete roof

Figure 8.3 shows that the convective heat flux from the PV module over the green roof to the surroundings is lower than that of a PV module over the concrete roof. By

171

applying a green roof as the sub-layer of a PV module on roof tops, the highest reduction can reach up to 63 Wm^{-2} or 38% at 11:00 h, with an average daytime reduction of the heat convection by 33.6 Wm^{-2} or 34%.

8.5.2. Impact on the ground surface

- **Radiant Heat Analysis**
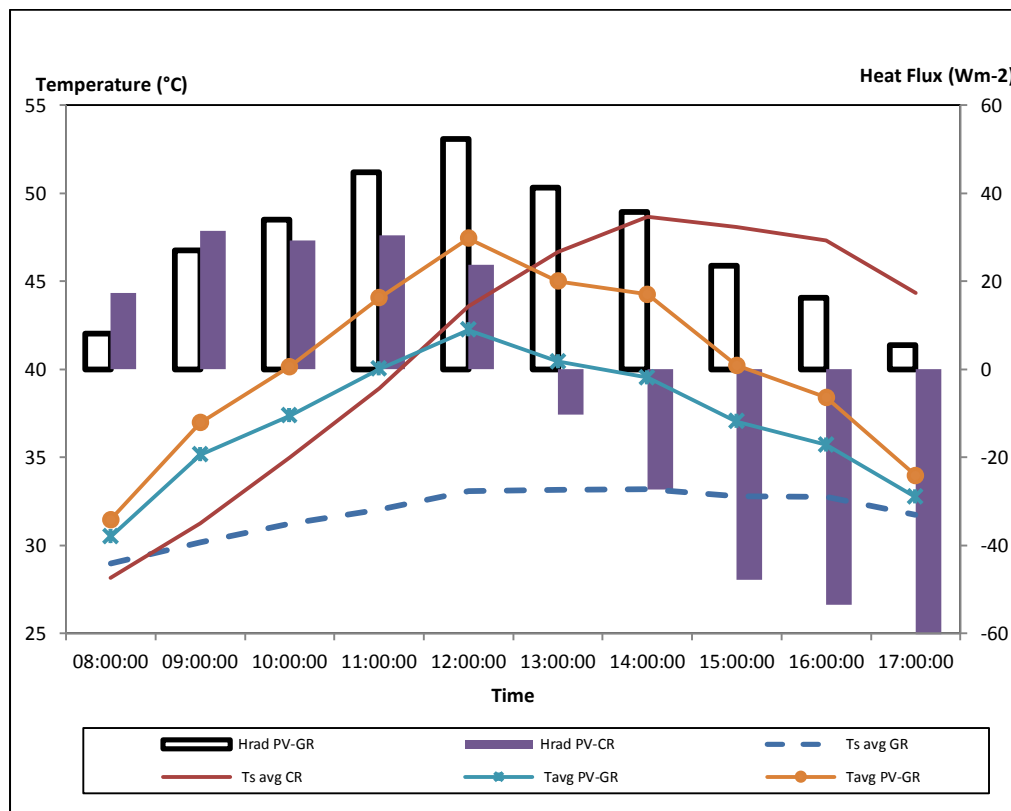
Figure 8.4 Radiant heat transfer from the PV modules to the roof surfaces
Hrad PV-GR: Average radiant heat of the PV module over green roof
Hrad PV-CR: Average radiant heat of the PV module over concrete roof
Ts avg GR:Surface temperature of green roof
Ts avg CR: Surface temperature of concrete roof
Tavg PV-GR: Surface temperature of the PV module over green roof
Tavg PV-CR: Surface temperature of the PV module over concrete roof

Figure 8.4 shows the average radiant heat transfer from the PV modules to the concrete roof and to the green roof respectively. The radiant heat from the PV module to the green roof displays a positive flux for the whole day which reaches its peak at 52 Wm^{-2} at mid-day. The heat flux from the PV module to the concrete roof, in contrast, shows an inverse flow in the afternoon of up to 60 Wm^{-2}. From this figure, it can be derived that the inverse heat flux is caused by the substantial increase of the surface temperature which emits the radiant heat back towards the surroundings.

- **Convective Heat Analysis**

The Nusselt number is used to quantify the convective heat coefficient from the PV modules to their sublayers. Eq. 5.13 is used to estimate the covective heat flux.
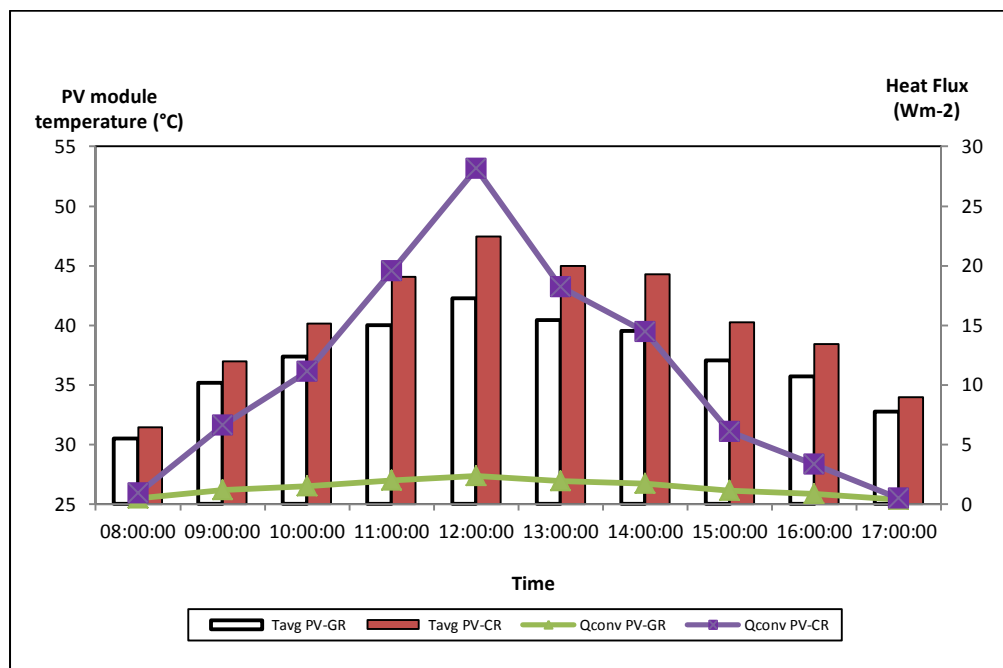
Figure 8.5 Convective heat transfer from the PV modules to the roof surfaces
Tavg PV-GR:Surface temperature of the PV module over green roof
Tavg PV-CR: Surface temperature of the PV module over concrete roof
Qconv PV-GR: Convective heat of the PV module over green roof
Qconv PV-CR: Convective of the PV module over concrete roof

173

Figure 8.5 shows that the convective heat flux between the PV module and the green roof is much lower than the convective heat flux between the PV module and the concrete roof. The difference can reach up to 28 Wm^{-2} or nearly 90% at mid-day. The average daytime reduction is 9.5 Wm^{-2} or 75%.

8.6.   Conclusion

The influence of the evapotranspiration of the green roof on PV module has been investigated through classifying the rate of evapotranspiration and the PV module temperature in the range of solar radiation (0 Wm^{-2} - >900 Wm^{-2}). Additionally, the effect of the reduced PV module temperature to the surrounding and to the ground surface were also investigated through radiant and convective heat analysis. The results can be concluded as follows:

- Based on the frequency of the solar radiation intensity with reference to Singapore climate, the effect of the green roof on PV module temperatures over a year is significant compared to the one over a concrete roof with the albedo lower than 1. The PV module temperature can be reduced between 4 °C and 5.5 °C for almost half of the year.

- The reduction of the PV module temperature is predominantly influenced by the evapotranspiration rate. The R-square resulted from the regression analysis is 0.97. In order to reduce the PV module temperature by 1 °C requires approximately 3.35×10^{-5} $kgm^{-2}s^{-1}$ of evapotranspiration rate or 82 Wm^{-2} of latent heat flux.

- The performance of the PV module can be increased around 2% in the high irradiance level (600 Wm^{-2} - >900 Wm^{-2}) for a monocrystalline silicon wafer-based PV module as used for the experiment.

- The lower PV module surface temperatures and the lower ambient temperature over the green roof lead to a reduction of its radiant and convective heat flux.

- The radiant heat of the PV module installed over the green roof to the sky can be reduced by 16% during mid-day and by 9% over the whole day. This shows that integrated PV over green roof can indeed reduce the infrared radiation to the surroundings.

- The convective heat flux over the integrated PV and green roof is also lower than over the concrete roof. The reduction can reach up to 38% at mid-day while the average daytime reduction is 34%.

- Since the surface temperature of the green roof is relatively constant during the day, the convection heat flux between the PV module and the green roof is much lower than the convective heat flux between the PV module and the concrete roof. The heat flux difference can be as high as 90% at mid-day and 75% over the whole day.

- An opposite trend occurrs on the radiant heat flux from the PV module to the concrete roof. There is an inverse flux in the afternoon which is caused by the increased temperature of the concrete roof. The radiant heat from PV module that absorbed by the concrete roof is hence emitted back to the surroundings once the heat capacity of the concrete roof is exceeded.

CHAPTER 9 SIMPLE LIFE CYCLE COST ANALYSIS OF THE PV MODULE INTEGRATED WITH GREEN ROOF IN SINGAPORE

9.1.   Introduction

As previously discussed that green roofs are beneficial to improve the PV module performance by reducing the module temperature. This chapter presents the economic impact of integrating PV module on a green roof top. The economics analysis considers the cost of both green roof and concrete roof. Hence the objective of this study is to analyse the life cycle cost (LCC) of PV modules when they are integrated with a green roof.

To facilitate those objectives, the Building Life Cycle Cost (BLCC) version 5, a product of U.S. Department of Energy, was used to analyse the life cycle cost of the PV systems installed over a green roof and a concrete roof. A PV system based on standard test conditions (STC) is used as the base case to quantify the impact of integrating PV module on green roof top. All the cost are projected into per kWp.

9.2.   Methodology

9.2.1.   Life cycle cost (LCC) analysis

The LCC analysis was conducted by using the software, namely Building Life Cycle Cost (BLCC) version 5. This software provides the economic analysis of a proposed capital investments and is particularly useful for evaluating the cost and benefits of energy conservation projects in buildings. Another advantage of this software is that it allows to evaluate two or more alternatives systems in terms of the lowest life-cycle cost and best economics in the long run.

The economic aspects required in the LCC are as follows:

1. Energy cost

2. Water cost

3. Capital component which includes: (a) investment cost, (b) replacement cost and (c) operating, maintenance and repairs, including annually and non-annually recurring cost.

9.2.2. Basic plan approach

The concept of the analysis is illustrated in Fig. 9.1. It can be seen from the diagram that the life cycle cost in this study considers the energy cost, the capital component cost of the PV systems and the water cost. The last cost was used only for the PV system integrated with green roof. Three parameters are used in the life cycle analysis are: (1) the service life, (2) the discount rate and (3) the inflation rate.
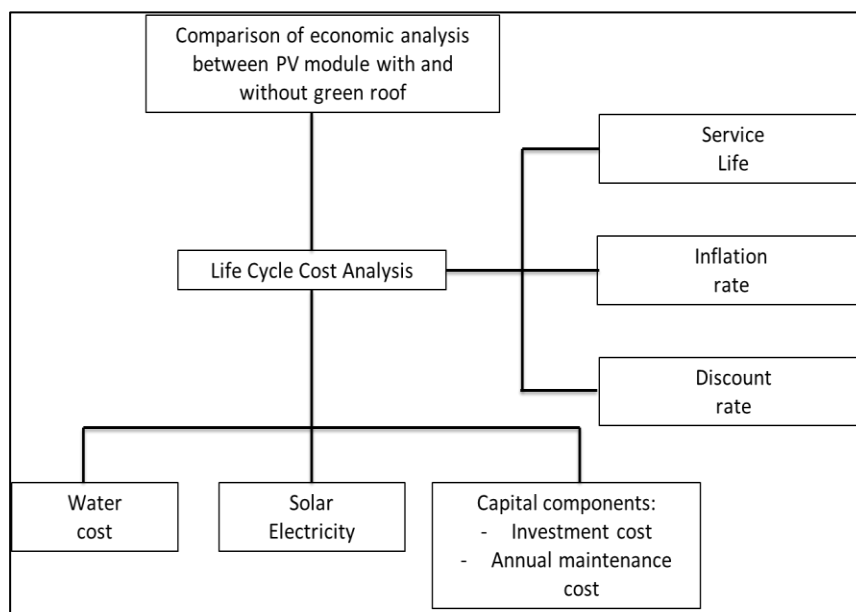
Figure 9.1 Basic plan approach

9.3. Data collection

9.3.1. Energy cost

The energy cost is determined by the loss of the PV energy yield resulting from the increase of the PV module temperature over the 25 $^{\circ}$C given by the standard test condition (STC). The electricity cost per kWh is defined as 26.06 S$-cents/kWh (Singapore Power, 2013). The investment cost for the PV systems includes solar panels, inverters, mounting structures and installation. The total investment cost for the PV systems for this study is based on price per Watt peak (S$/Wp). Watt peak is defined as the power at STC (solar irradiance of 1000 W/m^2, AM of 1.5 and temperature of 25°C).

9.3.2. The Operating & Maintenance cost

The cost for operation, maintenance and possible repairs are the annually recurring expenses for a PV system (Roy and Kabir, 2012). The cost also includes insurance. In general, the cost of running a solar PV system are very small, compared to conventional electricity generating technologies due to the fact that there are no fuel cost and no moving parts in a PV installation.

9.3.3. Parameters of LCC

9.3.3.1. Service life

The service life time in this study is based on the warranty released by the manufactures. In general, the warranty can be as long as 20-25 years. Hence, this study used 25 years as the service life.

9.3.3.2. Inflation rate

In general, the predictive inflation rate can be assumed as 4%. This assumption based on Fig. 9.2 which shows that the Singapore inflation rate within the last two years, 2011-2013, was around 4% on average.
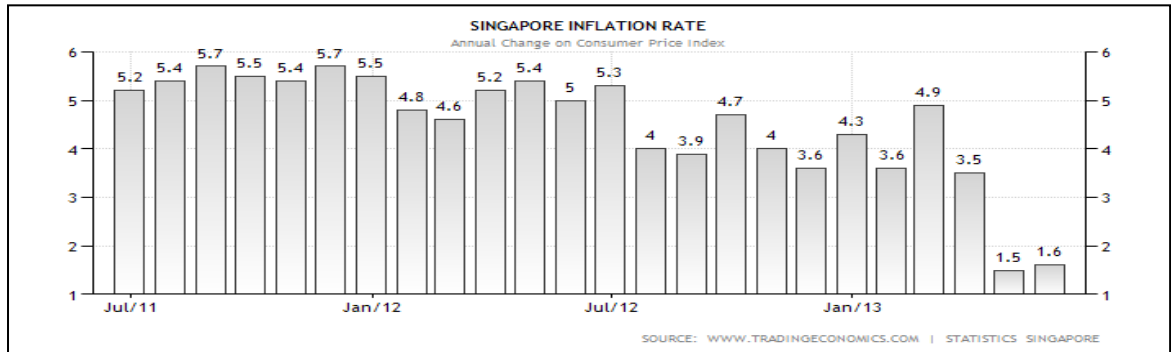
Figure 9.2 Singapore inflation rate between July 2011 and June 2013
Source: http://www.tradingeconomics.com

9.3.3.3. Discount rate

Table 9.1 Table of Prime Lending Rate for the past 10 years

Period	Prime Lending Rate
2003	5.3
2004	5.3
2005	5.3
2006	5.33
2007	5.33
2008	5.38
2009	5.38
2010	5.38
2011	5.38
2012	5.38

Source: Monetary Authority of Singapore

Discount rate is used to anticipate the escalating price over the system's life time and to calculate the so-called "present value". Table 9.1 lists the historical prime lending

rates, obtained from the Monetary Authority of Singapore.   The discount rate used for this study was 6% and hence takes a rather conservative approach.

9.4.   Analysis

This study used a monocrystalline silicon wafer-based PV technology with the specification: (1) 250 Wp, (2) the module efficiency is 15.4% and (3) the temperature coefficient is -0.45%C^{-1}. The total area of PV module is 1.6368 m^{-2}. The green roof area was defined as 2 m^2 or around 1.5 times of the area of the PV module, in order to provide a relatively homogeneous condition around the PV module. The area of the concrete roof is assumed to be the same as the area of the green roof.

9.4.1.   Specific annual energy production of the PV modules

Table 9.2 Energy yield of each PV module

Solar radiation (Wm^{-2})	PV module temperature over green roof (^{0}C)	PV module temperature over concrete roof (^{0}C)	PV module temperature reduction (^{0}C)	Energy yield of PV module over green roof (kWh/kWp)	Energy yield of PV module over concrete roof (kWh/kWp)	Expected energy yield (STC condition) (kWh/kWp)
0-100	27.3	28.10	0.80	52	52	52
101-200	30.4	31.70	1.30	108	108	111
201-300	32.2	33.80	1.60	147	146	152
301-400	34.5	36.60	2.10	165	164	172
401-500	36.4	38.40	2.00	155	154	163
501-600	38.2	40.80	2.60	156	154	165
601-700	40.7	44.40	3.70	160	157	171
701-800	42.4	46.60	4.20	191	187	207
801-900	46.5	51.60	5.10	186	181	206
900-1000	50.3	55.80	5.50	208	203	235
				1530	1505	1635

The irradiance data is provided by a single year measurement (2012) conducted by Solar Energy Research Institute of Singapore (SERIS) and it is adjusted with the data from Metonorm 7.0, where the annual total irradiance is 1623 kWh/m2.

The specific annual energy yield is the solar energy produced (Wh) relative to the installed watt peak (Wp). As previously stated in Chapter 2, the solar energy production is reduced when the module temperature increases. Hence, the annual operating energy yield of a PV module will be reduced accordingly. It should be emphasized that the amount of the specific annual energy yield only considers the effect of the PV module temperature; other factors such as the effect of inverter, cabling and soiling are considered identical for both systems and thus are not taken into account for the comparison.

Table 9.2 summarizes the operating energy yield of each PV module installed over the concrete roof and the green roof. It can be observed that there is a 7.9% reduction of the energy yield of the PV module over the concrete roof relative to STC conditions, while the reduction of the PV module over the green roof is only 6.1%. It means that the energy yield improves by 1.8% absolute because of the reduction the PV module temperature over the green roof. This improvement of the PV module performance is base for the following life cycle cost.

9.4.2. The component cost of LCC (Investment cost and Annual operating and maintenance).

In Singapore, the typical cost of installing a PV system is assumed to be S$ 2.5/Wp. The maintenance cost for the PV installation including the insurance fee is typically 2% of the total cost of the PV system.

This study defines the energy cost as the energy loss of each PV module compared to the module performance at STC (Table 9.2), hence, the cost of energy is the

difference between the expected energy yield, measured at STC (Standard Test Condition), and the actual energy production of each PV module in operation.

Table 9.3 Component cost of LCC of PV system with and without green roof

PV system over concrete roof		PV system over green roof	
Total investment of PV systems (S$2.5/Wp)	S$ 625.00	Total investment of PV systems (S$2.5/Wp)	S$ 625.00
Annual maintenance and insurance of the PV systems	S$ 12.50	Annual maintenance and insurance of the PV systems	S$ 12.50
Expected annual energy yield	1635 kWh/kWp	Expected annual energy yield	1635 kWh/kWp
Operating annual energy production	1505 kWh/kWp	Operating annual energy production	1535 kWh/kWp
Annual energy lost	130 kWh/kWp	Annual energy lost	105 kWh/kWp
Total investment of the concrete roof	-	Total investment of green roof systems (2 m^2)	S$ 200.00
Annual maintenance of the concrete roof	-	Annual maintenance of the green roof (2 m^2)	S$ 2.00
Annual irrigation cost	-	Annual irrigation cost (2 m^2)	S$ 2.53
Re-roofing for the concrete roof after 10 years (year 10, 15 and 20) (2 m^2)	S$ 432.00	Replanting at year 15 (2 m^2)	S$ 60.00

The cost of the green roof is defined as S$ 200.00 per square meter, and the cost of water, according to the national water agency (PUB), is S$1.17 for the water usage between 0 – 40 m^3 per month. The selected plants (*Complaya trilobata*) needs 3 liter

per m^2 per day or 1.08 m^3 per m^2 per year. As for the maintenance, since the green roof type is the extensive green roof, therefore, the maintenance is minimal. According to Wong et al (2003b) the maintenance, such as pruning, can be done twice a month. This study, therefore, assumes the maintenance cost to be 1% of the total cost of the green roof systems. The non-annually maintenance for green roof, such as replanting, is considered in year 15 only. This assumption is made based on the previous studies showing Singapore's climate is well-suited for plant growth and re-planting is barely required (Wong et al, 2003b). On the other hand, the exposed roof needs to be maintained more often. According to the same study, Wong et al (2003b) stated that the exposed roof probably requires re-roofing after 10 years of service and from then onwards repeatedly every 5 years. The cost of re-roofing is approximately S\$ 72.00 per square meter. Table 9.3 presents the summary of the component cost of LCC for each PV system.

9.5. Life cycle cost comparison

Table 9.4 summarizes the LCC of each PV modules. It can be seen that, the LCC of the PV module over the green roof is reduced to S\$1,310.00 per kWp from S\$1,412.00 per kWp, or there is a 7.2 % improvement of the LCC for 25 years life service. Given the uncertainties in the measured data and the assumptions, this improvement is significant.

Table 9.4 Summary of results of LCC analysis for PV modules

	PV over concrete roof	PV over green roof
Initial cost	S\$ 625.00	S\$ 825.00
Energy cost	S\$ 320.00	S\$ 269.00
LCC	S\$ 1,412.00	S\$ 1,310.00

Table 9.5 shows the present value and annual value of each PV systems. It can also be stated that the annual value of the PV module over the green roof increased by 7.4% compare to that of the PV module over the concrete roof.

Table 9.5 Present and annual value of the PV modules

PV over concrete roof			PV over green roof		
	Present Value	Annual Value		Present Value	Annual Value
Initial Cost	S$ 625.00	S$ 49.00	Initial Cost	S$ 825	S$ 65.00
Energy consumption cost	S$ 320	S$ 26.00	Energy consumption cost	S$ 269	S$ 21.00
Non-annually cost	S$ 319.00	S$ 23.00	Non-annually cost	S$ 44.00	S$ 3.00
Annually maintenance and insurance cost	S$ 148.00	S$ 12.00	Annually maintenance and insurance cost	S$ 172.00	S$ 13.00
Total life cycle cost	S$ 1,412.00	S$ 110.00	Total life cycle cost	S$ 1,310.00	S$ 102.00

9.6. Conclusion

An economic analysis, which focuses on the comparison of life cycle cost analysis between two PV systems which are installed over different roof top material (green roof and concrete roof), has been conducted. The PV system is a monocrystalline based solar cell with the efficiency of 15.4% and the temperature coefficient of -0.45%/K. Based on the results, there are some important findings:

-   The life cycle cost of the PV system over the green roof is 7.2% lower than the one over the concrete roof, over its life service (25 years).

-   A 7.4% improvement of the annual system value as compared to the 1.8% improvement of the annual energy gain demonstrates that PV system integrated with the green roof is relatively cost effective, despite the additional cost of the green roof.

CHAPTER 10 CONCLUDING REMARKS

10.1. Conclusion

The main objective of this study was to investigate the cooling effect of the evapotranspiration process (the combination of evaporation of water and transpiration of plants) on the temperature of photovoltaic (PV) module that is mounted over a green roof and to evaluate the improvement of its performance, particularly in the tropical climate of Singapore. The other objectives were to develop a prediction model for the evapotranspiration rate for a small green roof and for the dynamic change of the PV module temperature affected by the evapotranspiration process. In order to facilitate those objectives, a field measurement has been conducted by deploying two identical PV modules made of polycrystalline silicon where one of them was mounted over a concrete roof and one over a green roof. The one over the concrete roof was the reference to evaluate the cooling effect of the green roof on the PV module temperature. Furthermore, in order to quantify that cooling effect, the energy balance principle was applied to calculate the incoming and outgoing energy in the system.

The results from the field measurements have shown that the green roof with its evapotranspiration process can indeed reduce the PV module temperature. A significant reduction occurs in clear days, where the solar radiation intensity ranges between 600 Wm^{-2} and >900 Wm^{-2}. The PV module temperature over the green roof then is reduced between 3.7 ^{o}C and 5.5 ^{o}C. At the lower intensities, 200 Wm^{-2} to 500 Wm^{-2}, the reduction is between 1 ^{o}C and 2.5 ^{o}C. The higher reduction of the PV module temperature on clear day is caused by roof top material (here: concrete and plants) that behave differently in response to the solar radiation. Concrete roof,

which has low albedo (0.05-0.10), absorb almost 90% of the solar radiation, resulting in high surface temperatures (50 $^{\circ}$C in noon time) and a strong radiation heat back to the environment, which leads to the ambient temperatures of around 35 $^{\circ}$C. This high surface and ambient temperature then also expose to the PV module high radiant and convective heat. In contrast, the plants of the green roof have higher albedo (0.20-0.25) and are engaged in the evapotranspiration process. Therefore, the plants absorb 10% less solar radiation compared to the concrete material and use this energy for the evapotranspiration process in which water is converted into vapor. This process leads to a much lower surface temperature (32 – 35 $^{\circ}$C) and consequently resulting in a lower heat reflection to the environment. The ambient temperature above the green roof is hence reduced to 32 $^{\circ}$C, effectively reducing the radiant and convective heat exposure to the PV module. In consequence, the heat absorption of the PV module is lowered and due to a lower negative temperature effect, the efficiency of the PV module improved. As such, the performance ratio of the PV module over the green roof could be improved by 2% under clear and intermediate sky condition, while, under overcast sky conditions the ratio is below 1%. These results provide valuable evidence that green roofs are beneficial to the performance of PV module in tropical climates despites its climate with constantly high humidity close to the water vapor saturation level and low wind speed.

In order to predict the evapotranspiration rate of the green roof, the variables which include net radiation, soil heat flux, ambient temperature and relative humidity at 6 cm above green roof and air temperature have been proven to be the significant factor for the evapotranspiration rate. The adjusted R-square for the final regression is above 0.9 with the RMSD of $5.74\text{x}10^{-6}$ kgm^{-2}s^{-1}. Additionally, this study has also determined the relevant Priestley Taylor coefficient (1.22) and the canopy conductance for the Penman Monteith equation (20) as a mean to calculate the

evapotranspiration rate of the selected plants (*Complaya trilobata* or Weedelia, familia of Aesteraceae). The average evapotranspiration rate is 7.1×10^{-5} kgm^2s^{-1}. This result indicate that this selected plants needs to be watered frequently with 3 kilograms or approximately 3 liters of water per m^2 per day to allow for a proper and constant evapotranspiration process, otherwise the plants would be suffered from dry soil or withering. Furthermore, the finding is also valuable for the actual implementation since the numerical model only requires weather data. Complex input parameter such as the plants resistance to the heat or aerodynamic resistance can be ignored as long as the soil condition is rich with water and the conditions over the green roof is homogeneous.

In terms of the numerical model for predicting the dynamic changes of the PV module temperature influenced by the evapotranspiration process of the green roof top, the prediction model consist of: (1) absorbed solar radiation which is determined by the direct and reflected solar radiation, the long wave radiation from the sky and the green roof and the convective heat from the green roof, (2) the emitted solar radiation which is determined by the long wave radiation of the PV module to the sky and to the green roof and the convective heat from the PV module to the environment above and below the module, (3) the heat mass transfer from the PV module to the cavity between the PV module and the green roof, (4) the latent heat flux from the green roof as a result of the evapotranspiration process and (5) the electricity generation of PV module. The results show that the prediction model is in a well agreement with the field measurement. The determinant value (R^2) is above 0.9 for clear and overcast sky condition, while on intermediate days the R^2 is still 0.8. It implies that the numerical model could not fully capture the environmental condition under intermediate sky conditions. This result could be a valuable contribution for developer or system designers to predict the electrical generation improvement by applying a green roof as a sub layer roof underneath the PV system installation.

10.2. Limitations and recommendations of future studies.

The results of this work have shown the benefits of a green roof on the performance of a PV module, however, there are some limitations to this experimental study which could be further developed in future studies:

- Firstly: plants variety. Each type of plants has its own resistance to heat so that the evapotranspiration rate can be difference for each of them. The experiments here only used one type of vegetation: *Complaya trilobata*. An extended environmental study on green roofs with more variation of plants is recommended though to investigate the level of ambient temperature changes over different plants and how much the impact on the PV module is in reality.

- Secondly, this study is an experimental based study using a small green roof and one single PV module. Scaling-up the experiment to a complete roof top PV system with green roof underneath would result in more reliable data for the prediction model for a large scale effect.

- Thirdly, it may be worthwhile to investigate the effect of the higher humidity levels around the irrigated green roof on the life time and degradation of the PV modules.

BIBLIOGRAPHY

Amarakoon et.al., 2000, Estimating daytime latent heat flux and evapotranspiration in Jamaica, *Agricultural and forest meteorology*, Vol.102, pp 113-124.

Anderson, Bruce (1977), *Solar energy: fundamentals in building design*, Total Environmental Action, McGraw-Hill Book Company, New York.

Allen et.al., 2011, Evapotranspiration information reporting: I. Factors governing measurement accuracy, *Water management*, Vol.98, pp 899-920

Allen et al., 1998, *Crop evapotranspiration - Guidelines for computing crop water requirements,* FAO - Food and Agriculture Organization of the United Nations, Rome.

Allen, R. G., et al., 1991, Environmental requirements for lysimeters. pp. 170-181 in Allen, R. G., Howell, T. A., Pruitt, W. O., Walter, LA., and Jensen, M. E. (Editors), Lysimeters for Evapotranspiration and Environmental Measurements, *Proceedings of the ASCE International Symposium on Lysimetry*, Honolulu, HA, ASCE, New York, NY.

Amy, E.B., 2009, Thermal aspects of c-Si photovoltaic module energy rating, *Solar energy*, Vol. 83, pp. 1452-1433.

Agricultural Production and Externalities Simulation (2009): http://www.apesimulator.org/help/models/evapotranspiration/Soil_heat_flux.html

Bramson, M.A., 1968, Infrared radiation, *New York: Plenum Press*, in Jones, G.H., et.al., 2002, Radiation measurement for plants ecophysiology, *Journal of experimental botany*, Vol. 54, pp. 879-889

Brinkworth, B.J., 2000, A procedure for the routine calculation of laminar free and mixed convection in inclined ducts, *International Journal of Heat and Fluid Flow*, vol. 21, pp. 456-462

Brinkworth, B.J., et al., 1997, Thermal regulation of photovoltaic cladding, Solar Energy, Vol. 61, pp. 169-178.

Chauliaguet C. et al., (1979*), Solar Energy in Building*, John Wiley&Sons, Chichester. Solar technologies for buildings / Ursula Eicker

Chalabi, H and Brongersma, M.L., (2013), Plasmonics: Harvest season for hot electrons, *Journal of Nature Nanotechnology*, Vol. 8., pg. 229-230.

Chow, T.T., 2005, A review on photovoltaic/thermal hybrid solar technology, Applied Energy, Vol. 87, pp. 365-379

Chen, Y., and Wong, N.Y., 2006, Thermal benefits of city parks, *Environmental and Buildings*, vol. 38, pp. 105-120

Clarke, J.A, et.al., (1996), *Photovoltaic-Integrated Building Facades*, Energy Systems, Research Unit, University of Strathclyde, Glosgow, Scotland.

Cohen, Y., et al., 1988, Calibrated heat pulse method for determining water uptake in cotton, *Agron*, J. 80, pp. 398–402.

Dehghani Sanij, H. et.al., (2004), Assessment of evapotranpiration estimation models for use in semi-arid environments, *Agricultural water management*, Vol 64, pp.91-106.

Davis, M.W., Fanney, H.A., 2001, Prediction of Building Integrated Photovoltaic Cell Temperatures, *Solar Energy Engineering*, special Issue: Thermochemical Processing, Vol. 123, pp. 200-210.

Ding, R., et.al., 2013, Evapotranspiration measurement and estimation using modified Priestly-Taylor model in irrigated maize field with muching, *Agricultural and Forest Meteorology*, Vol. 168, pp. 140-148.

Duffie, A.J.,Beckman, W.A., 2006, *Solar engineering of thermal processes*.; Wiley: Hoboken, New Jersey.

Dugas,W.A and Bland, W.L, 1989, The accuracy of evaporation measurements from small lysimeters, *Agricultural and Forest Meteology*, Vol46, pp.119-129.

Dugas et al., 1991, Bowen ratio, eddy correlation, and portable chamber measurements of sensible and latent heat flux over irrigated spring wheat, *Agricultural and Forest meteorology*, Vol. 56, pp.1-20.

Evans, D.L., 1981, Simplified method for predicting photovoltaic array output, *Solar Energy*, Vol. 27, pp. 555-560.

Feng, C., et.al., 2010, Theoretical and experimental analysis of the energy balance of extensive green roofs, *Energy and Buildings*, Vol.42, pp. 959-965.

Flint, L.A and Childs, W.S., 1991, Use of the Priestley-Taylor evaporation equation for soil water limited conditions in a small forest clearcut, *Agricultural and Forest Meteorology*, Vol. 56, pp. 247-260.

Food and Agricultural Organisation (FAO) Document Respiratory, Chapter 2-FAO Penman Monteith Equation, http://www.fao.org/docrep/x0490e/x0490e06.htm

Fredlund, D.G and Rahardjo, H, (1993), *Soil mechanics for unsaturated soils*, New York: Wiley.

Frilling, N., et.al., 2009, Modeling the heat dynamics of building integrated and ventilated photovoltaics modules, Energy and Buildings,Vol.41, pp. 1051-1057.

Fuchs,M and Pieri, P., 1990, Comparison of bowen ratio and aerodynamic estimates of evapotranspiration, *Agricultural and Forest Meteorology*, Vo. 49, pp 243-256.

Garcia, M.C. and Balenzateguie, J.L., 2004, Estimation of photovoltaic yearly temperature and performance based on Nominal Operating Cell Temperature calculation, *Renewable Energy*, Vol. 29, pp. 1997-2010.

Grattan,S.R, 1988, New Crop coefficients estimate water use of vegetables, row crops, *California Agriculture*, Vol.52(1):16-21. DOI: 10.3733/ca.v052n01p16

Grebet, P., Cuenca R.H., 1991. History of Lysimeter Design and Effects of Environmental Disturbances, *Lysimeters for Evapotranspiration and Environmental Measurements, American Society of Civil Engineers Irrigation and Drainage Division Symposium, Honolulu*, Hawaii. pp. 10 - 18.

Grime, V.L., et al., 1995, Including the heat storage term in sap flow measurements with the stem heat balance method. Agric, *Forest Meteorology*, Vol. 74, pp. 1–25.

Gunston, H and Batchelor, C.H., 1983, A comparison of the Priestly-Taylor and Penman Methods for estimating reference crop evapotranspiration in tropical countries, *Argricultural Water Management*, Vol. 6, pp 65-77.

Hasan, M.A., Sumathy, K., 2010, Photovoltaic thermal module concepts and their performance analysis: A review, *Renewable and Sustainable Energy Reviews*, Vol. 14, pp. 1845-1859.

Hanlin, A.L., Stein, J.S., 2012, Improvement and validation of a transient model of photovoltaic module temperature, http://energy.sandia.gov/wp/wp-content/gallery/uploads/Luketa-Hanlin_WREF_Final_Paper_SAND2012-4307C.pdf

Heilman, J.L. and Brittin, C.L., 1989, Fetch requirements for Bowen Ratio measurements of latent and sensible heat flux, *Agricultural and Forest Meteorology*, Vol.44, pp. 261-273.

Huang et al., 2011, Solar cell junction temperature measurement of PV module, *Solar Energy*, vol. 85, pp. 388-392

Howell, T.A., Jensen, M.E., 1991, History of lysimeter design and use for evapotranspiration measurements, In Proc.of ASCE International Symposium on Lysimeter, Honolulu, HI, July 23-25, pp. 1-9.

Ichidah, K, et.al., 2009, Impact of environment factors on solar cell parameters of a-Si ‖μc- Si photovoltaic modules, *Solar Energy Materials and Solar Cells*, vol. 93,pp. 879-883.

Incropera, F.P and De Witt, P.D, (2002), *Fundamentals of heat and mass transfer* (5th ed). New York: John Wiley & Sons.

Itier, et al., 1994, Downwind evolution of scalar fluxes and surface resistance under condition of local advection. Part I: a reappraisal of boundary conditions, Agricultural and Forest Meteorology, Vol. 71, pp. 211-225.

Jayarama, P.R., 2010, Science and Technology of Photovoltaics, 2nd Edition, BS Publications, India

Jones, A.D. and Underwook, C.P., 2001, A thermal model for photovoltaic systems, *Solar Energy*, Vol. 70, pp. 349-359.

Jones, H.G.,(1992), *Plants and microclimate, A quantitative approach to environmental plant physiology* (2nd ed). Cambridge University Press.

Jones, H.G., et al., 2002. Radiation measurement for plant ecophysiology, *Experimental Botany*, Vol. 54, pp. 879-889

Kato, T., et.al., 2004, Estimation of evapotranspiration, transpiration ratio and water-use efficiency from a sparse canopy using a compartment model, *Agricultural water management*, Vol. 65, pp. 173-191.

King, D.L.,et.al, (1997), *Temperature coefficient for PV modules and arrays: measurement methods, difficulties and results*, 26th IEEE Photovoltaic specialist conference, California.

Kim, J.P. et al., (2011), Numerical analysis on the thermal characteristics of photovoltaic module with ambient temperature variation, *Solar Energy Materials & Solar Cells*, vol.95, pp. 404-407.

Kirkham, M.B., 2005, Chapter 26- Potential evapotranspiration, *Principles of soil and plant water relations*, pp. 455-468.

Kohler, M., et.al., 2002, Photovoltaic Panels on Greened Roofs: Positive Interaction Between Two Elements of Sustainability Architecture, *World Climate and Energy Event*, RIO 02, pp. 151-158.

Kohler, M., 2006, Long-term vegetation research on two extensive green roofs in Berlin, *Urban Habitats*, Vol.4, Number 1 ISSN 1541-7115

Krauter, S., (2004), Development of an integrated solar home system, SEMS 2004;82:119-30. In Journal of Renewable and Sustainable Energy Reviews (Zondag, 2008), Vol.12 pg. 891-959.

Krauter, S. , 2006, *Solar electric power generation – photovoltaic energy systems: modeling of optical and thermal performance, electrical yield, energy balance, effect on reduction of greenhouse gas emission.*; Springer: Berlin-New York.

Lasnier, F and Ang, T.G., (1990), *Photovoltaic Engineering Handbook*; Adam Hilger Publishing: New York.

Leod, et.al., 2004, Evaluation of an enclosed portable chamber to measure crop and pasture actual evapotranspiration at small scale, *Agricultural Water Management*, Vol. 67, pp. 15-34.

Lhomme, J.P., 1997, A theoretical basis for the Priestley Taylor coefficient, *Boundary-Layer Meteorology*, Vol. 42, pp. 179-191.

Li, L., et al., 2011, Modelling evapotranspiration in a Central Asian desert ecosystem, Journal of Ecological Modelling, Vol. 222, pp. 3680-3691.

Makrides, G,et.al, 2009, Temperature behaviour of different photovoltaic systems installed in Cyprus and Germany, *Solar Energy Materials & Solar Cells*, 93, 1095-1099

Mattei, M., et al., 2006, Calculation of the polycrystalline PV module temperature using a simple method of energy balance, *Renewable Energy*, Vol.31, pp.553-567.

Mavromatakis, F.,et.al., 2010, Modeling the photovoltaic potential of a site, *Renewable energy*, Vol.35, pp. 1387-1390.

McJannet, et al., 1996, *Soil and litter evaporation beneath re-growth and old-growth mountain ash forest*, Cooperative Research Centre for Catchment Hydrology, Clayton, Vic.

McLeod, et al., 2004, Evaluation of an enclosed portable chamber to measure crop and pasture actual evapotranspiration at small scale, *Agricultural Water Management*, Vol 67, pp. 15-34.

Meissner, R, Seyfarth, M, 2004, Measuring water and solute balance with new lysimeter techniques, Proceeding SuperSoil 2004: 3rd Australian New Zealand Soils Conference, University of Sydney, Australia.

Menesses-Rodriguez,D, et.al, 2005, Photovoltaic solar cells performance at elevated temperatures, *Solar Energy,* 78, pp. 243-250.

Minemoto,T., et.al., 2007, Impact of spectral irradiance distribution and temperature on the outdoor performance of amorphous Si photovoltaic modules, *Solar Energy Materials and Solar Cells*, Vol.91, pp. 919-923.

Moller, H.J., 1993, *Semiconductors for solar cells*, Artech House, Inc, Norwood, USA.

Moshfegh,B., Sandberg,M., 1998, Flow and heat transfer in the air gap behind photovoltaics panels, Renewable & Sustainable Energy Reviews, Vol. 2, pp. 287-301 (1998)

Nagae,S,et-all, 2006, Evaluation of the impact of solar spectrum and temperature variations on output power of silicon-based photovoltaic modules, *Solar Energy Materials and Solar Cells*, Vol.90, pp. 3568-3575.

Naveed et al., 2006, Effect of unglazed transpired collector on the performance of a polycrystalline silicone photovoltaic module. In Journal of Renewable and Sustainable Energy Reviews (Zondag, 2008), Vol.12 pp. 891-959.

Nichols, J., et al., 2004. Comparison of evaporation estimation methods for a riparian area,*UHR Technical Report No. 436*. College of Engineering, University of Iowa, USA.

Nobre, A., et.al.,2012, High performing PV systems for tropical regions-optimization of systems performance, *Proc. of 27th European Photovoltaic Solar Energy Conference Germany, pp. 3763-3769, doi: 10.4229/27thEUPVSEC2012-5CO.6.2.*

Notton, G., Cristofari, C., Mattei, M., Poggi, P., 2005. Modelling of a double-glass photovoltaic module using finite differences. AppliedThermal Engineering 25, 2854–2877.

Panofsky H.A., and Townsend A.A., 1964: Change of terrain roughness and the wind profile, *Q.J.R. Meteorol. Soc*., Vol. 90, pp. 147–155.

Photon International. 2004, *Market survey on solar modules*, p. 46-55 in Mattei et al., (2006) Calculation of the polycrystalline PV module temperature using a simple method of energy balance. *Renewable Energy*, 31, 553-567.

Park, K.E., et.al., 2009, Analysis of thermal and electrical performance of semi-transparent photovoltaic (PV) module, *Energy*, Vol.30, pp.1-7.

Pauliukonis, N and Schneider, R, 2001, Temporal patterns in evpotranspiration from lysimeter with three common wetland plant species in the eastern United States, *Aquatic Botany*, Vol 71, pp. 35-46.

Penman, H.L., 1948, Natural evaporation from open water, bare soil and grass, *Proceeding of the Royal Society*, London A, vol. 93, pp 120-145.

Pereira, A.R., 2004, The Priestley-Taylor parameter and the decoupling factor for estimating reference evapotranspiration, *Agricultural and Forest Meteorology*, Vol. 125, pp 305-313.

Priestley, C.H. B. and Taylor, R. J., 1972, On the Assessment of Surface Heat Flux and Evaporation Using Large-Scale Parameters. *Mon. Wea. Rev.*, **100**, 81–92. doi: http://dx.doi.org/10.1175/1520-0493(1972)100<0081:OTAOSH>2.3.CO;2

Rana,G and Katerji, N, 2000, Measurement and estimation of actual evapotranspiration in the field under Mediterranean climate : A review, *European Journal of Agronomy*, Vol.13, pp. 125-153.

Reicosky, D.C., et.al., 1983, Comparison of alfalfa evapotranspiration measured by a weighing lysimeter and a portable chamber, *Agricultural Meteorology*, Vol. 28, pp. 205-211.

Reicosky, D.C., Peters, D.P., 1977, A portable chamber for rapid evapotranspiration measurements on field plots, Agronomy Journal, Vol. 69, pp. 729-732.

Reindl, T. et.al., 2012, Investigation of the Performance of Commercial Photovoltaic Modules under Tropical Conditions, *Japanese Journal of Applied Physics*, Vol. 51, 10NF11.

Roy, A and Kabir, A, 2012, Relative life cycle economic analysis of stand-alone solar PV and fossil fuel powered systems in Bangladesh with regard to load demand and market controlling factors, *Renewable and Sustainable Energy Reviews*, Vol. 16 pp. 4629-4637

Sabounchi, 1998, Effect of ambient temperature on the demand energy of solar cells at different inclinations, *Renewable Energy*, Vol. 14, pg. 149-155.

Sailor, D.J., 2008, A green roof model for building energy simulations programs, *Energy and Buildings*, Vol. 40, pp 1466-1478

Saly, V, 2000, Chapter 437-Testing of Photovoltaic modules and encapsulations at elevated voltage, temperature and humidity, *World Renewable Energy Congress VI*, pp. 2053-2056.

Santbergen, R and Zolingen, R.J.C.,2008, The absorption factor of crystalline silicon PV cells: A numerical and experimental study, *Solar energy materials and solar cells*, Vol. 92, pp. 432-444.

Sashua-Bar, L and Milo.E.H., 2002, Quantitative Evaluation of The Effects of Built-Up Geometry and Trees on Diurnal Air Temperature in Canyon-Type Courtyards, *Advance in Building Technology*, Vol. 2, pp.1493-1500.

Sashua-Bar, L., et.al., 2006, Integrated thermal effects of generic built forms and vegetation on the UCL microclimate, *Building and Environment* , 41, pp. 343-354.

Sashua-Bar, L., et all, 2009, The cooling efficiency of urban landscape strategies in a hot dry climate, *Landscape and Urban Planning,* Vol. 92, pp. 179-186.

Scherba, et.al., 2011, Modeling impacts of roof reflectivity, integrated photovoltaic panels and green roof systems on sensible heat flux into the urban environment, *Building and Environment*, Vol. 46, pp. 2542-2551

Sharma, K.V., et.al, 1995, Photovoltaic technology: basic concepts, sizing of a stand alone photovoltaic system for domestic applications and preliminary economic analysis, *Energy conversion Management*, Vol.36, pp. 161-174.

Singh, P., et.al., 2008, Temperature dependence of I-V characteristics and performance parameters of silicon solar cell, *Solar Energy Materials & Solar Cells*, Vol. 92, pp. 1611-1616.

Skoplaki, E and Palyvos, J.A., 2008, A simple correlation for the operating temperature of photovoltaic modules of arbitrary mounting, *Solar Energy Materials & Solar Cells*, Vol. 92, pp 1393-1402.

Skoplaki, E and Palyvos, J.A., 2009, On the temperature dependence of photovoltaic module electrical performance: A review of efficiency/power correlations, *Solar Energy*, Vol. 83, pp. 614-624.

Smithson, P., et.al., (2002), *Fundamentals of the physical environment* (3rd ed), Routledge: New York, 2002.

Stannard, D.I., 1988, *Use of a hemispherical chamber for measurement of evapotranspiration*, Open-File Report, pp. 88-452, United State Geological Survey, Denver, CO

Summer, D.M. and Jacobs, J.M., 2005, Utility of Penman-Monteith, Priestley-Taylor, reference evapotranspiration, and pan evaporation methods to estimate pasture evapotranspiration, *Hydrology*, Vol. 308, pp. 81-104.

Swaine, D.J., (Ed), (1990), *Greenhouse and energy*, CSIRO Publications, East Melbourne, Australia.

Swibank, W.C., 1951, The measurement of the vertical transfer of heat, *Journal of Meteorology*, Vol. 8, pp. 135-145.

Tady, Y., et.al., 2008, Study on thermal performance of semi-transparent building-integrated photovoltaic glazings, *Energy and Buildings* , 40,pp 341-350.

Takakur, T, et.al., 2000, Cooling Effect of greenery cover over a building, *Energy and Building* , Vol.31 ,pp. 1-6.

Takebayasi, H and Moriyama, M., 2007, Surface heat budget on green roof and high reflection roof for mitigation of urban heat island, *Building and Environment*, Vol. 42, pp. 2971-2979.

Tang, R, et al., (2004), Estimates of clear night sky emissivity in Negev Highlands, Israel, Energy Conversion and Management, Vol. 45, pp. 1831-1843.

Tanner C B, 1960, Energy balance approach to evapotranspiration from crops, *Soil Science Society of America Journal*, Vol. 24, pp. 1-9

Tian, W.,et.al., 2007, Effect of building integrated photovoltaics on microclimate of urban canopy layer, *Building and Environment*, Vol.42, pp.1891-1901.

Todd, R.W., et.al., 2000, The bowen ratio-energy balance method for estimating latent heat flux of irrigated alfalfa evaluatedin a semi-arid, advective environment, *Agriculture and Forest Meteorology,* 103, pp.335-348.

Trambouze, W.,et.al., 1998, Comparison of methods for estimating actual evapotranspiration in a row-cropped vineyard, *Agricultural and Forest Meteorology*, Vol. 91, pp. 193-208.

Trinuruk, et.al, 2009, Estimating operating cell temperature of BIPV modules in Thailand, *Renewable Energy*, Vol.34,pp 2515-2523.

Uddin, J., et.al., 2013, Measurement of evapotranspiration during sprinkler irrigation using a precision energy budget (Bowen ratio, energy covariance) methodology, *Argricultural Water Management*, Vol. 116, pp 89-100

Wieringa, J., 1993, Representative roughness parameters for homogeneous terrain, *Boundary Layer Meteorology*, Vol. 63, pp. 323-363.

Wilson, B.K., et al, 2001, A comparison of methods for determining forest evapotranspiration and its components: sap-flow, soil water budget, eddy covariance and catchment water balance, *Agricultural and Forest Meteorology*, Vol. 106, pp 153-168.

Wittkopf, S.K., et.al., 2012, Analytical performance monitoring of a 142.5 kWp grid-connected rooftop BIPV system in Singapore, *Renewable Energy*, Vol. 47, pp 9-20.

Wong, N.H.,et.al, (2003a), Investigation of thermal benefits of rooftop garden in the tropical environment, *Building and Environment,* 38, pp. 267-270

Wong, N.H.,et.al, (2003b), Life cycle cost analysis of rooftop gardens in Singapore, *Building and environment*, Vol. 38, pp. 499-509.

Wong, N.H.,et.al., 2009, *Promoting Skyrise Greenery in Singapore's Public Housing*, International Green Building Conference 2009 Singapore.

Wong, N.H.,et.al, (2009), Thermal Evaluation of vertical greenery systems for building walls, *Building and Environment,* 45 (2010) 663-672.

Wong, N.H.,et.al, (2009), Energy simulation of vertical greenery systems, *Energy and Buildings,* vol. 41 (2009) 1401-1408.

Wong, N.H., et. al., (2011), Evaluation of the impact of the surrounding urban morphology on building energy consumption, *Solar Energy*, Vol 85, 57-71.

Wysocky and Rappaport, 1960, Effect of temperature on Photovoltaic solar energy conversion, *Journal of Applied Physics*, Vol. 31, pp.571, doi:10.1063/1.1735630

Yang, F, and Zhang W, 2009, Estimation of evapotranspiration with drainage lysimeters in the Taihang Mountain area, China, *Forestry Studies in China,* Vol.11, pp. 219-224.

Ye, Z., et al., 2013, On PV module temperatures in tropical regions, *Solar Energy*, Vol. 88, pp 80-87.

Yeh, G.T., and Butsaert, W.H., 1971, A solution for simultaneous turbulent heat and vapor transfer between a water surface and the atmosphere, *Boundary-Layer Meteorol*, vol. 2, pp. 64-82.

Young Yun,G, 2007, Design and overall energy performance of a ventilated phovoltaic facade, *Solar Energy*, Vol. 81, pp.383-394.

Yuki et al, 2009, Modeling of the I-V curves of the PV modules using linear interpolation / extrapolation, *Solar energy materials & solar cells*, Vol. 93, pp. 1070-1073.

Zhang, B., et al, 2008, Comparison of three evapotranspiation models to Bowen ratio-energy balance method for a vineyard in an arid desert region of northwest China, *Agricultural and Forest Meteorology*, Vol.148, pp.1629-1640.

Zhou, M.C., et al., (2006), Estimating potential evapotranspiration using Shuttleworth-Wallace model and NOAA-AVHRR NDVI data to feed a distributed hydrological model over the Mekong River basin, *Journal of Hydrology*, Vl. 327, pp. 151-173.

Zondag, H.A., 2008, Flat-plat PV-Thermal collectors and systems: A review, *Renewable and Sustainabl Energy Reviews*, vol. 12, pp. 891-959.

LIST OF PUBLICATION

Hendarti, R., Sun, W., Wittkopf, S., Wong, N.H., 2011. *A simulation study of thermal impact of greenery on PV roof top*, Proceedings of ISES: ISES Solar World Congres 2012: Rapid transition to a renewable energy world, Kassel-Germany, 28 Aug-2 Sept 2011.

Hendarti, R, Wong, N.H., Reindl, T., Tan, P.Y., Chan W.L., 2012, *Integrated Photovoltaic and greenery for roof top as a potential form for sustainable architecture element in the tropics*, Proceedings of Kalam-UTM Conference: Bridging the old and new toward future sustainable Built Environment, Johor-Malaysia, 5-7th November 2012.

Hendarti, R, Wong, N.H., Reindl, T., Tan, P.Y., Wittkopf, S., Chan W.L., 2012, *Integration of solar photovoltaic and green roofs in tropical climates*, Proceedings of 4th International Network for Tropical Architecture (INTA) 2012: Tropics 2050, National University of Singapore, Singapore, 12-14th December 2012.

GLOSSARY

Absorptance: The ratio of absorbed to incident solar radiation. Absorptance is the property of absorbing radiation possessed by all materials to varying extents.

Absorptivity: The ratio of the incident radiant energy absorbed by a surface to the total radiant energy falling on the surface.

Advection : The process whereby solutes are transported by the bulk mass of flowing fluid (Freeze and Cherry, 1979). See also convective transport.

Air mass (AM): The length of the path through the earth's atmosphere traversed by direct solar radiation, expressed as a multiple of the path length with the sun at zenith (overhead).

Ambient condition: The condition of the surroundings.

Albedo: The ratio of the light reflected by a surface to the light falling on it.

Azimuth: the angle between the south-north line at a given location and the projection of the earth-sun line in the horizontal plane.

Black body: An ideal surface that absorbs all the radiation incident on it an emits none; alternatively, a body that emits the maximum possible radiation at a given temperature.

Conduction: the heat transfer through matter by exchange of kinetic energy from particle to particle

Direct conversion: The conversion of sunlight directly into electric power, instead of collecting sunlight as heat and using the heat to produce power.

Direct radiation: The radiation from the sun received from a narrow solid angle measured from a point on the earth's surface.

Efficiency: The ratio of the measured of a desired effect to the measure of the input causing the effect, both expressed in the same units of measure.

Emittance: The ratio of radiation emitted by a real surface to the radiation emitted by a perfect radiator at the same temperature. Normal emittance is the value measured at 90° to the plane of the sample; hemispheric emittance is the total amount emitted in all directions.

Evaporation : Process by which liquid water is converted into water vapor.

Evaporation Pan : A pan used to hold water during observations for the determination of the quantity of evaporation at a given location. Such pans are of varying sizes and shapes, the most commonly used being circular or square.

Evaporation Rate : The quantity of water, expressed in terms of depth of liquid water, which is evaporated from a given surface per unit of time. It is usually expressed in inches depth, per day, month, or year.

Evapotranspiration: Combination of evaporation from free water surfaces and transpiration of water from plant surfaces to the atmosphere.

Band gap: The range of energy levels in a semiconductor forbidden to electrons; photons are readily absorbed if their energy exceeds the band gap. The electron states below the gap (in energy) constitute the valence band (normally filled); above the gap is the conduction band (normally empty) into which valence band electrons can be excited by light. Impurities and atomic displacements produce allowed energy states for electrons in the otherwise forbidden gap.

Emissivity: The property of emitting radiation

Incident angle: The angle between the direction of the sun and the perpendicular to the surface on which sunlight is falling.

Irradiation (irradiance): The radiant energy per unit area falling on a plane surface per unit time, normally stated in watts per square meter.

I-V curves: The current-voltage characteristic curves of a solar cell.

Kelvin temperature scale: A temperature scale whose degrees are equal to degrees on the Celsius scale but whose zero point is at the 'absolute zero' of temperature, at which all molecular motion ceases. On the Kelvin scale, the freezing point of water is 273 °K and the boiling point 373 °K.

Latitude: The angular distance North (+) or South (-) from the equator.

Laminar Flow: Streamline flow in which successive flow particles follow similar path lines and head loss varies with velocity to the first power.

Latent heat: The energy released by or absorbed from a substance during a phase change from a gas to a liquid or a solid or vice versa.

Local solar time: A system of astronomical time in which the sun always crosses the true north-south meridian at 1200 hours (noon). This system of time differs from local time according to longitude, time zone and equation of time.

Lysimeter : A device to measure the quantity or rate of downward water movement through a block of soil usually undisturbed, or to collect such percolated water for analysis.

n type: A semiconductor doped with impurities so as to have free electrons closer to the conduction band.

Nominal Operating PV Cell Temperature (NOCT): module temperature from which is used for a simple estimation of a module performance over a year under following condition: Irradiance on cell surface is 800 Wm^{-2}, air temperature is 20° C, wind velocity is 1 ms^{-1}, with the mounting is open back side.

Open-circuit voltage: Maximum voltage of a solar cell at which the electric current is zero.

Operating temperature: The temperature at which an electrical or mechanical device is working

Pay-back period: The length of time required to recover the investment of a project by benefits accruing from the investment; pay-back period is an incomplete economic index.

Photon: A quantum of electromagnetic radiation; its energy E_v is related to the frequency v of the radiation by the equation $E_v=h*v$ where h is Planck's constant.

Photovoltaic cell (solar cell): A semiconducting device that converts sunlight directly into electric power.

Photovoltaic effect: Direct conversion of sunlight into electricity by photo-sensitive semiconductor device.

p-n junction: A junction of dissimilar semiconductor materials, where electrons move from one type to another, under specific conditions.

Precipitation : As used in hydrology, precipitation is the discharge of water, in a liquid or solid state, out of the atmosphere, generally onto a land or water surface. It is the common process by which atmospheric water becomes surface, or subsurface water. The term "precipitation" is also commonly used to designate the quantity of water that is precipitated. Precipitation includes rainfall, snow, hail, and sleet, and is therefore a more general term than rainfall.

Present value: The value of a future cash flow discounted to the present; based on the premise that "a dollar today is worth more than a dollar received in the future by "virtue of the amount of interest (or return) that it earns.

P type: A semiconductor doped with impurities so as to have vacancies ("holes" close to the valence band).

Pyranometer: A solar radiometer that measures total diffuse and direct radiation.

Reflectivity (reflectance): The ratio of light reflected from a surface to the light falling on the surface. The reflectivity plus the absorptivity equals unity, since the incident sunlight is either reflected or absorbed.

Semiconductor: A material whose atomic structure is such that it has an electrical conductivity intermediate between an insulator, such as glass, and a metal such as copper. Its conductivity can be greatly influenced by the addition of minimal amounts of certain elements called doping agents. Depending on the agent, the doped semiconductor will have either an excess (n type) or deficiency (p type) of energy-conducting electrons.

Silicon cell: A photovoltaic cell made of silicon, as semiconductor.

Standard Test Conditions (STC). Solar panels in a flash tester in a room has been calibrated to deliver the equivalent of 1000 watts per square meter of sunlight intensity, hold a cell temperature of 25'C (77'F), and assume an air mass of 1.5.

Solar energy: the energy, in the form of radiation, emitted from the sun and generated by means of a fusion reaction within the sun.

Solar radiation: The radiant energy received from the sun both directly as a beam component and diffusely by scattering from the sky and reflection from the ground.

Specific heat capacity: The amount of heat required to raise the temperature of unit mass of material one degree, usually measured in British thermal units per pound per degree Fahrenheit or joules per kilogram per kelvin.

Spectral irradiance: The monochromatic irradiance eof a surface per unit band width at a particular wavelength. Units often in watts per square meter per nanometer band width.

Temperature, dry bulb: The temperature of the air as indicated by an ordinary thermometer.

Temperature, wet bulb: The temperature of the air as indicated by a thermometer whose bulb is surrounded by a wet gauze and past which air is blown rapidly. The difference between the wet-bulb and dry-bulb temperature is used to find the atmospheric humidity. When the atmosphere is completely saturated with water vapour (humidity of 100%), the wet bulb temperature equals the dry-bulb temperature.

Transpiration: Water discharged into the atmosphere from plant surfaces.

Infrared radiation: The electromagnetic radiation of wavelengths between 760nm and approximately 1μm.

Longwave radiation: The radiation originating from sources at terrestrial temperatures (e.g. ground and other terrestrial objects) and thus substantially all at wavelengths greater than 3 μm.

Radiant energy: Energy in the form of electromagnetic waves.

Radiant flux: Power emitted, transferred or received in the form of radiation.

Radiation: The physical process of emission or transfer of energy in the form of electromagnetic waves.

Sensible heat is the energy required to change the temperature of a substance with no phase change

Short-wave radiation: The radiation with wavelengths less than 3 μm.

Solar flux: The radiant flux originating from the sun.

Solar spectrum: The distribution by wavelength (or frequency) of electromagnetic radiation emitted from the sun.

Visible radiation: The radiation with wavelengths that stimulate the human optic nerves. Visible radiation lies approximately within a wavelength band from 380 to 760 nm.

Diffuse (solar) radiation: the downward scattered and reflected solar radiation incident upon a given plane surface.

Direct (solar) radiation: The radiation received from a solid angle centered on the sun's disc, on a given plane.

Global (solar) radiation: The sum of the direct and diffuse solar radiation incident upon a given plane.

Sky temperature: The atmospheric radiation received at a surface may be expressed in terms of an equivalent black-body radiation temperature, which is the sky temperature.

Watt peak (Wp): A unit used for the performance rating of PV modules and systems. A PV module rated at 1 Wp will deliver 1 W.

APPENDIX 1

PRELIMINARY RESULTS:

Comparison of PV modules temperature reduction at the back and front surface

A significant reduction occurs at the back surface of the PV module over the green roof on a clear day. The reduction can reach as much as 5° C at mid-day, while the average daytime reduction is between 2° C and 3° C. At the front surface of the PV modules, the temperature reduction was not significant with a relatively flat trend line at around 1° C. On cloudy days, the results show only a small reduction in the afternoon for both sides.

Weather conditions on cloudy and clear day during outdoor experiments

9th June 2012				17th June 2012			
Total hourly solar irradiation (Whm^{-2})	Sky Condition	Average wind speed (ms^{-1})	Average relative humidity (%)	Total hourly solar irradiation (Whm^{-2})	Sky Condition	Average wind speed (ms^{-1})	Average relative humidity (%)
2,060	Overcast (Cloudy day)	1.3	82.5	5,606	Clear	2.41	73.6
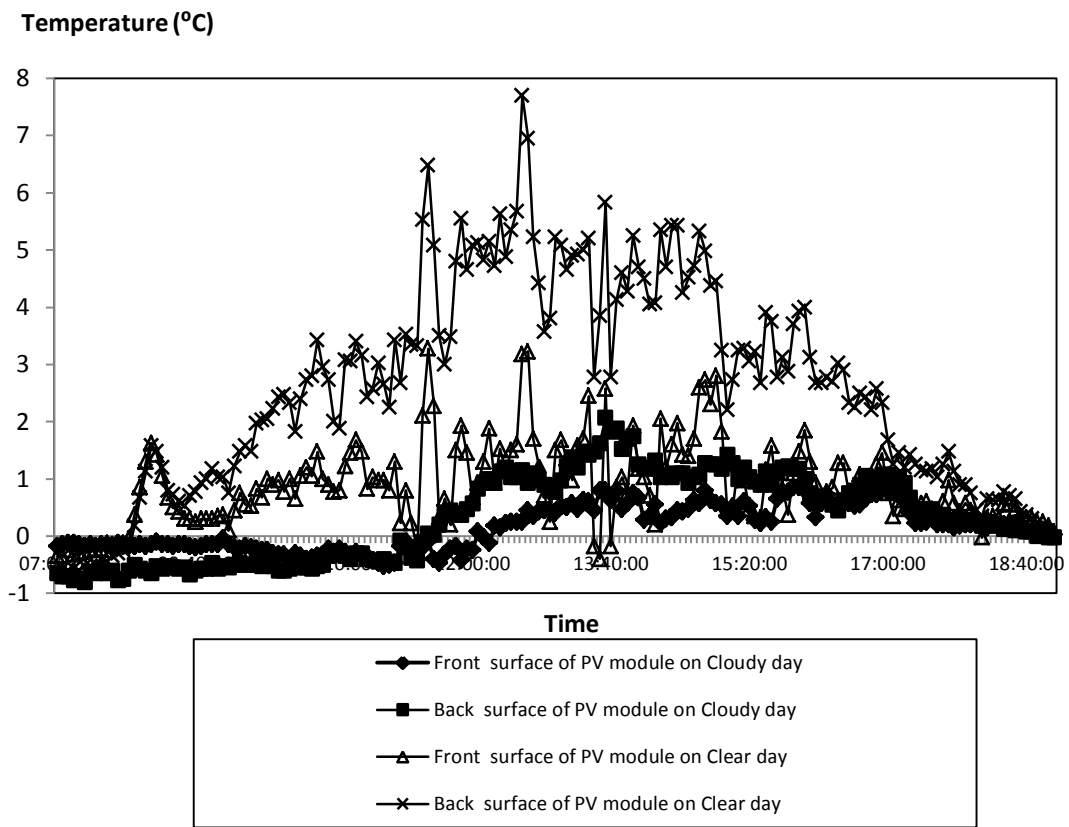
Temperature (°C)

Figure 1. PV surface temperature reductions at its front and back surface

APPENDIX 2

Measured data for PV module temperature numerical model

Signal	Symbol	Unit	Measurement
Sky temperature	T_{sky}	K	Derived from the air temperature
Irradiance	I	Wm^{-2}	Same elevation as the height of the PV module
Wind speed	V_w	ms^{-1}	2 m above the roof
PV module			
PV module temperature	T_{pv}	K	Derived from the back surface of the PV module
Ambient temperature between PV module and ground surface	T_{apvtop}	K	Derived from the air temperature, measured 2 m above the roof
Temperature difference between inlet and out let (T_{amb} outside-T_{amb} inside)	$T_{in} - T_{out}$	K	15 cm above the sub layer (ground)
PV power	P_{out}	Watt	Derived from the Eq.2.2
PV module area	A	m^2	
Green roof			
Plant surface temperature	T_{gr}	K	Space between the canopy and the soil
Ambient temperature between PV module and green roof	T_{apv-gr}	K	Measured at 12 cm above green roof
Concrete roof			
Concrete roof surface temperature	T_{cr}		
Ambient temperature between PV module and concrete roof	T_{apv_cr}		

APPENDIX 3

Variables and source for the predictive numerical models

Variables	Definition	Values	Source
α_{pv}	absorptance of PV module	0.9	Santbergen and Zolingen (2007)
α_{leaf}	absorptance of leaf	0.6	Jones, 1992
ρ_{leaf}	Reflectivity coefficient of leaf	0.3	Jones, 1992
ε_{sky}	Sky emissivity	1 = cloudy sky 0.9 = clear sky	Jones, 2001
ε_{leaf}	Leaf emissivity	0.98	Jones, 2002
$\varepsilon_{pvfront}$	PV front surface emissivity	0.9	Scherba et al, 2011
ε_{pvback}	PV back surface emissivity (the surface is made from a particular plastic with white color)	0.91	Scherba et al, 2011
f	Fraction of energy to air from PV module	0.25	Engineering documentation , EnergyPlus
ρ	Air density	1.190 kgm^{-3}	Fradlund and Rahardjo, 1993
m_{pv}	Module mass weight	1.2 kg	PV module data sheet
σ	Stefan-Boltzmann constant	2.67x10^{-8} Wm^{-2}K^{-4}	Jones, 1992

APPENDIX 4

Some temperature-dependent properties of air and water

Density of dry air (ρ_a), density of air saturated with water vapour (ρ_{as}), psychrometer constant ($\gamma = Pc_p/0.622\lambda$), latent heat vapourisation of water (λ), radiative resittance ($r_R = \rho c_p/4\varepsilon\sigma T^3$), the factor converting conductance in units of mm s^{-1} to mmol m^{-2} s^{-1} ($g/g = g^m/g = P/RT$) and kinematic viscosity of water (v). (At 100 kPa where appropriate).

T (°C)	ρ_a (kgm^{-3})	ρ_{as} (kgm^{-3})	γ (PaK^{-1})	λ (MJkg^{-1})	r_R (sm^{-1})	g/g $(\frac{mmol \cdot m^{-2} \cdot s^{-1}}{mm \cdot s^{-1}})$	v (mm^{2}s^{-1})
-5	1.3316	1.314	64.6	2.513	304	44.8	-
0	1.292	1.289	64.9	2.501	282	44.0	1.79
5	1.269	1.265	65.2	2.489	263	43.2	-
10	1.246	1.240	65.6	2.477	244	42.5	1.31
15	1.225	1.217	65.9	2.465	228	41.7	-
20	1.204	1.194	66.1	2.454	213	41.0	-1.01
25	1.183	1.169	66.5	2.442	199	40.3	-
30	1.164	1.145	66.8	2.430	186	39.7	0.80
35	1.146	1.121	67.2	2.418	174	39.0	-
40	1.128	1.096	67.5	2.406	164	38.4	0.66
45	1.110	1.068	67.8	2.394	154	37.8	-

APPENDIX 5

Temperature dependence of air humidity and associated quantities

Saturation water vapor pressure (e_s), saturation water vapor concentration (c_{sw}), slope of saturation (s) and the ratio of the increase of latent heat content to increase of sensible heat content of saturated air ($\varepsilon = s / \lambda$)

T (°C)	e_s (Pa)	c_{sw} (gm-3)	s (Pa°C-1)	ε	T (°C)	e_s (Pa)	c_{sw} (gm-3)	s (Pa°C-1)	ε
-5	421(402)[a]	3.41	32	0.50	20	2337	17.30	145	2.20
-4	455(437)[a]	3.66	34	0.53	21	2486	18.34	153	2.31
-3	490(476)[a]	3.93	37	0.57	22	2643	19.43	162	2.44
-2	528(517)[a]	4.22	39	0.60	23	2809	20.58	170	2.56
-1	568(562)[a]	4.52	42	0.65	24	2983	21.78	179	2.69
0	611	4.85	45	0.69	25	3167	23.05	189	2.84
1	657	5.19	48	0.74	26	3361	24.38	199	2.99
2	705	5.56	51	0.78	27	3565	25.78	210	3.15
3	758	5.95	54	0.83	28	3780	27.24	221	3.31
4	813	6.36	57	0.88	29	4005	28.78	232	3.48
5	872	6.79	61	0.94	30	4243	30.38	244	3.66
6	935	7.26	65	1.00	31	4493	32.07	257	3.84
7	1002	7.75	69	1.06	32	4755	33.83	269	4.02
8	1072	8.27	73	1.12	33	5031	35.86	283	4.22
9	1147	8.82	78	1.19	34	5320	37.61	297	4.43
10	1227	9.40	83	1.26	35	5624	39.63	312	4.65
11	1312	10.01	88	1.34	36	5942	41.75	327	4.86
12	1402	10.66	93	1.42	37	6276	43.96	343	5.09
13	1497	11.35	98	1.49	38	6626	46.26	357	5.33
14	1598	12.07	104	1.58	39	6993	48.67	376	5.58
15	1704	12.83	110	1.67	40	7378	51.19	394	5.84
16	1817	13.63	117	1.77	41	7780	53.82	413	6.11
17	1937	14.48	123	1.86	42	8202	56.56	432	6.39
18	2063	15.37	130	1.97	43	8642	59.41	452	6.68
19	2196	16.31	137	2.07	44	9103	62.39	473	6.98

PV module specification

Solartech Power, Inc.
SPECIFICATIONS

ELECTRICAL CHARACTERISITICS				
	SPM022P	SPM020P	SPM018P	SPM015P
Power at STC(Pm)	22W	20W	18W	15W
Maximum power voltage(Vpm)	18.1V	17.2V	16.5V	16.3V
Maximum power current(Ipm)	1.24A	1.17A	1.10A	0.93A
Open circuit voltage(Voc)	22.1V	21.7V	21.0V	20.7V
Short circuit current(Isc)	1.32A	1.25A	1.2A	1.1A
Tolerance	±5%	±5%	±5%	±5%
Module efficiency	10.9%	10.0%	8.9%	7.7%
Standard test conditions	Temperature 25℃, Irradiance 1000W/m², AM=1.5			
Maximum system voltage	1000V DC	Series fuse rating		10A
Temperature coefficient	Isc:0.05%/K	Voc:-0.36%/K	Pmax:-0.46%/K	

Specifications	
Cell	Multicrystalline silicon solar cell, (156mmx26mm)
No. of cell and connection	36(2x18)
Dimension	550mm (21.7in) x399mm(13.9in)x25mm(0.98in)
Weight	2.8KG

AMBIENT CONDITIONS	
Operating Temperature	-40℃ to +85℃
Storage Humidity	<90%

OUT PUT	
Type of output terminal	Junction box
Cable	Length 3000mm

OUTLINE DIMENSIONS

IV CURVES
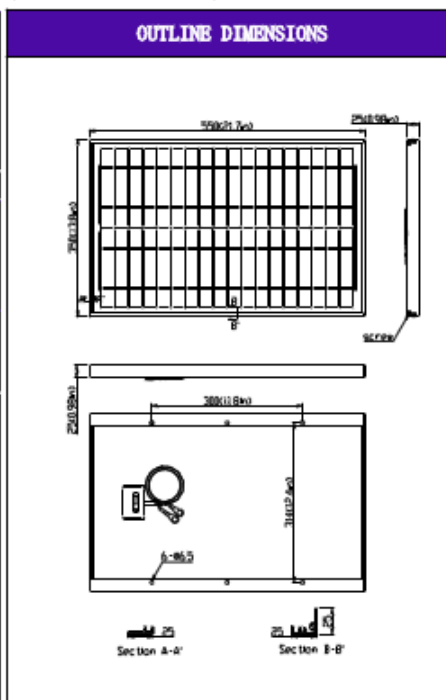
UL No.: E330673   TUV No.:0000022551   IEC No.:C1-ASN07001   ETL No.:4001057

IEC   CE   TÜV   c(UL)us 41WC   ETL Intertek

SOLAR DEPOT   800.822.4041   www.solardepot.com

DC Power Systems   (800) 987-6917   www.dcpower-systems.com

211

APPENDIX 7

Questions and Answers

The questions from the examiners with the corresponded answers are summarized in

the following table:

1   *What is the specification of the concrete roof, is it asphalt concrete or asphalt.*

The concrete roof is the asphalt concrete which contain of bitumen.

2   *In order to validate the numerical equation of the evapotranspiration rate, it is need to conduct an actual observation, such as water balance.*

Ideally the validation of the proposed numerical model should have been validated with that actual observation such as water balance. It is realize that there was a limitation in the equipment.

However, the proposed equation has been constructed from three equation models and has also been compared and the results showed a good agreement.

3   *Is a 2% increase of the PV performance is significant?*

A 2% increase of PV performance is significant. The PV module temperature can be reduced more than 5 ^{0}C without any improvement on its cell specification, but only with the improvement of the surrounding environment.

4   *Wouldn't this be within the margin of error?*

A 2% improvement on PV performance was the overall results, whereas the improvement can reach almost 3% on mid-day of a clear day. The energy yield of PV performance is derived from calculation not from measurement. These results were determined by the PV cell temperature reduction, and the reduction can be more 5 ^{0}C which is not in the range of the error margin.

5   *Why the same PV technology have different temperature coefficient and what is the significance of Table 2.1 ?*

Skoplaki and Palyvos (2008), stated that the temperature coefficient depends on the PV material and also the Temperature references.

The significance of this table is to give an illustration that beside outdoor condition; the PV cell specification made by the manufacture also contributes the electrical production of the PV module.

6   *Add the explanation of NOCT*

NOCT, which is usually available in the module's data sheet, is used to calculate PV module temperature by providing the ambient temperature and the amount of irradiance at other environmental conditions. Further details are explained in Chapter 2.2.2.

Provide more information of k

Another comparison study to investigate the impact of ambient temperatures on PV module temperatures in tropical Singapore is a study of is employing the "Ross coefficient", (*k*), by (Ye et al, (2013)). *k* is the coefficient that state the temperature rise above ambient with increasing irradiance (Ross, 1976) and the value is influenced by wind speed, less to wind speed direction and practically insensitive to the ambient temperature level (Griffith et al, 1981). Further details   are   provided   in Chapter 2.2.2.

8   *How much is the ambient temperature improvement on Chen and Wong Work ?*

According to Wong and Yu, the ambient temperature over green roof is lower of 2^0 C when it is compared to a concrete roof. This ambient temperature was measured at the height of 30 cm from the roof (Wong et al., 2003a)

9   *Did Chen and Wong study for green roof not green infrastructure ?*

The study conducted by Wong et al (2003a) was the study of the thermal benefit of the roof top garden.

10   *Dig deeper about the concept of resistance to transpiration especially that relate to stomatal conductance, role of photosynthesis mechanism (e.g. CAM/night-time photosynthesis for sedums.*

It is summarized from Jones (1992), the concept of resistance and conductance to evapotranspiration can be explained as follows:

The basic principle of evapotranspiration is equal to the total conductance between the evaporating sites and the bulk air and the difference of water vapor deficit between the pathway of the canopy and the bulk air.
Therefore, the transpiration is less when the canopy conductance value low. Furthermore, the canopy conductance affects the vapor pressure term and the effect is different between forest and short grass. The ET for forest is more sensitive to the vapor pressure difference, while short grass is more sensitive to the value of the net radiant. The value of the leaf conductance is strongly influenced by the growth conditions and the age of the leaf.

In terms of resistance, the soil resistance increase when its condition is lack of water. The soil evaporation depends on the wetness of the soil and plant cover. However, the soil water condition affects the physiological stress of the plants and resulted in the ET reduction because of the stomatal closure.

The stomatal aperture is affected by the environment, such as light, water status, humidity, temperature and carbons dioxide and other pollutant gasses.

The central role of the stomata is important in the process of regulating water vapor and CO_2 exchange. In terms of photosynthesis, there is a pigment near the stomata (located on the grana and stroma lamella membranes of the chloroplasts, that absorb the incoming solar radiation.

The stomata particularly for CAM plants works inversely as compared to C3 and C4 plants, where the stomata open during the night and open during the

213

day. Therefore, CAM has an advantageous for water conservation.

11 *Soil heat flux calculation.*

The soil heat flux can be calculated from the following equation:

$$G = \frac{k \times \Delta T}{x} \ [\text{Wm}^{-2}]$$

where, k is the soil conductivity, ΔT is the difference of the soil temperature whereas the first sensor was located on the soil surface and the second sensor was located around 50 mm down from the first sensor.

Therefore the distance (x) was defined as 50 mm. The soil was constructed from the non-organic soilless volcanic ejecta substrate which is mixed with sand, whereas the soil conductivity for volcanic rocks with the porosity of between 50 and 60% is between 0.3 and 0.6 $\text{Wm}^{-1}\text{K}^{-1}$ (Clauser and Huenges, 1995), and as for the moist sand is $0.25 - 2.00 \ \text{Wm}^{-1}\text{K}^{-1}$. Therefore the soil conductivity for the proposed numerical model was defined as 0.45 $\text{Wm}^{-1}\text{K}^{-1}$.

12 *In lit review the lower Ta and Rh are measured at 30 cm above the canopy. Why in the experiment reduced it to 6 cm*

The height of the measurement is reduced because the area of green roof is much smaller than the one on the literature review. This height is assumed to be within the equilibrium zone. Please also see Fig. 6.2 about the equilibrium layer.

13 *What % of data was used to validate the model ?*

The validation used 35% data which are collected from June to October.

14 *Does this imply that the model is not accurate under high advection?*

Yes the model would not be accurate when there is a high advection heat. The amount of latent heat flux could exceed the net radiant heat flux

15 *How this affect the annual results projection*

The model is used best for hourly calculation. The value of each component is the hourly averaged value. The study did not cover the annual results projection.

16 *why the results of PM equation is generally underestimate the BREB calculation?*

As seen on Table 4.5, in general the PM equation underestimates the ET rate as compared to the other two equation models. A well summarized made by Zhang et al (2008) from some studies (Kato et al., 2004; Stannard, 1993, Jarvis, 1976 and Shuttleworth and Wallace, 1985) that the possible reason for ET rate underestimated by PM model is generally caused by a high soil water content

with a sparse canopy, so that it may decrease the soil surface resistance below the canopy resistance.

On the other words, the surface canopy resistance will comprise the effect of soil evaporation. In contrast, the results of PM calculation is generally overestimate as compared to BREB in and advective regime (Zhang et al., 2008). The dryness over the soil surface leads to a higher soil surface resistance to the canopy resistance, because the reduction of the wet area

17 *Coefficient of heat transfer used for the equation may not be appropriate.*

The suggested heat convection coefficient has been adopted and also the calculation has been revised whereas the results were improved.

Details on the convective heat coefficient are provided in Chapter 5.3.1.

18 *What is the basis for the statement that "PV module power output is influenced by PV module temperature above 30 ^{0}C?.*

When we refer to the Temperature reference (*Tr*), the power output works optimal in environment within temperature of 25 ^{0}C, and when the cell temperature increases the performance reduces. In the experiment it was observed that a significant reduction of PV performance occurred after the cell temperature exceeded 30 ^{0}C.

19 *Does the weather station include wind direction*

The weather station is also equipped with wind direction. In general the wind direction showed between 135 and 194. Because there is a roof top of building on the north side. However, this roof top does not block the sunlight. The distance between the building block and the experiment is around 3 meters.

20 *Are the Temp sensors shield*

Yes it does.

21 *Section 7.4.1.2 ...is it 15 cm ?*

The ambient temperature over concrete roof was measured at 15 cm above the roof top, while the ambient temperature over green roof was measured at 12 cm above the green roof canopy.

22 *Provide the initial measurement*

The initial measurement details are provided in Chapter 7.4.2.2.

23 *PV module performance increase of 2% is a result of unimpeded evapotranspiration achieved by flooding the green roof.*
How do you done any sensitivity analysis to the test the impact of evapotranspiration process heat removal on the module performance.

It has been stated in some researches that it is rather difficult to differentiate between evaporation and transpiration. Here, the calculation also does not differentiate those aspects.

In order to compare with other equation models, I have done sensitivity analysis

to determine the most suitable PT coefficient (4.8.2) and the canopy conductance (4.8.1).

24 *A short chapter about minimum size – of needed research installation – explain that this size was following normal installation and it was big enough to get sufficient numbers.*

Refer to Chapter 5.5.

25 *The examiner would like to hear some words, how to integrate PV-systems into modern architecture in dense cities in future?*
PV systems on roofs are one way- what about integration into the facade – as windows shade-systems.

In my opinion, the main concern of using PV technology is to get maximum sunlight in which this requirement should always be fulfilled all the time.

Moreover, this requirement should also be applied in designing and planning a building. Therefore, the sun direction over a place is certainly become the main requirement to determine the PV module orientation.

In regards to modern architecture in dense cities in the future, shading from the neighboring building is the main issues. So that, there some alternatives application of PV technology for buildings:

- Locate the PV module at the height which free from shading. The structure can be a free standing structure, separate from the main structure of the building.

- As for the new building, BIPV can be a solution but the height of building should be at least has the same height as the neighboring building to avoid shading from other buildings.

However, those two alternatives could also have some drawbacks in the future, because the neighboring buildings are possible to elevate their height.

Currently there is a new concept of integrating PV module to a city by applying ICT or Information and Communication Technology, which is called "smart grid". It is used to provide the flow of energy in a network and in order to control the networking for the "smart grid", Power Line Communication (PLC) is deployed. This concept is promising because it can control the use of energy.

In terms of the integration into the façade, the application depends on the local condition. For tropical region, this integration may not be a good choice. Because the sun circulate perpendicular the ground surface.

Chapter 9:

From examiner 1:

A few caveats for LCC:

a). would you need to add space between panels so that plants would have access to sunlight and precipitation ? Even with some space between panels might the aggregate performance be less than that of the case of the isolated panel?

b). you mention that shading was not accounted for. You should comment on this risk and the maintenance cost associated with avoiding this scenario.

Answer:

This simulation is only illustrated the LCC comparison using a single PV module and a small green area, whereas the area of green roof is accounted also for a single PV module. Therefore, I understand that in a real PV systems application, it will deploy more PV modules and need spaces in between panels and also the possibility of shading. In consequences, the calculation of LCC can be more complex.

Therefore, I might adopt the statement from the 3rd examiner that to make a LCC comparison, it should be seen as case by case. Ideally, the steps before calculating the LCC, there are some steps which in my opinion should be conducted first. They are as follows:
-        To concept the PV systems application and transferred it into a planned drawing.
-        The planned drawing includes the area and material of the PV systems, the ground surface and the dimensions.
-        Simulate the concept in terms of shading possibility. In my opinion, for tropical region, the shading could be less because the mounting position is almost horizontal, only 10 degree inclination maximum.
-        However, some spaces between them are still needed for air circulation and as a way for receiving sunlight and precipitation if the green roof is used for the sub layer. The space should be arranged effectively and it can be done by simulation.

From examiner 2:

Question:

The module cost could have been omitted from the analysis using the same logic used in the section 9.4.2., Par. 2. However, you have under estimated the maintenance costs of a green roof. The experiments are based on a tray system which has to be replaced at 6-7 year intervals, while 10% of the plants also have to be replaced.

The module cost is already included in the 2.5 S\$. It is true that my experiment used a green roof module system which should be changed in 6-7 years. The use of this type of green roof is just for the experiment not for a permanent green roof, which is more appropriate to use a common green roof. I also would like to adopt the statement from the 3rd examiner, that the main consideration is to use a roof material which has a long maintenance intervals as well as the type of green roof which could help to lesser the running cost and indeed reduce the overall LCC.

From examiner 3:

If a few percentages of savings are worth to install it on green roofs, has to be answered for each project individually. As I understand it for the tropics – one main benefit is to extend the maintenance intervals of the roof materials – this helps to lower the running cost and it is one of the main costly factors on the overall LCC of the installation.

I agree that to define the LCC, it has to be answered case by case and cannot justify generally. In regards to my simulation, the LCC comparison is to illustrate that even the improvement of PV module performance is relatively small, but it can improves the LCC quite significant. Additionally, there are more benefit of the green roof application such as it reduces CO_2 and lead to a healthier environment.

Indeed, what I would like to highlight that the PV cell temperature can be reduced green roof underneath to more than 5 ^{0}C in mid-day under high solar radiation. This results approve that green roof has a substantial benefit to PV modules.